

EXPERIMENTAL INVESTIGATION OF THE SETTLING VELOCITY OF SPHERICAL  
PARTICLES IN VISCOELASTIC FLUIDS

by

Sumanth Kumar Arnipally

A thesis submitted in partial fulfillment of the requirements for the degree of

Master of Science

in

Petroleum Engineering

Department of Civil and Environmental Engineering  
University of Alberta

© Sumanth Kumar Arnipally, 2017

## ABSTRACT

Knowledge of settling behavior of particles in various types of fluids is indispensable to design and optimize numerous industrial operations such as cuttings transport in oil and gas well drilling, proppant transport in hydraulic fracturing operations, and so on.

Most of the models developed so far were to predict settling velocity of particles in either Newtonian or purely viscous non-Newtonian shear thinning fluids where there were no considerations of the fluid elasticity effect. Therefore, these models are not suitable for settling velocity prediction when the process involves fluids of viscoelastic nature such as drilling and hydraulic fracturing fluids.

The main objective of this study is, therefore, set to determine how the fluid shear viscosity and the elasticity would influence the particle settling velocity and even more so to answer the question of which one of these two rheological properties is more dominant in controlling the particle settling velocity when viscoelastic drilling fluids are used.

The settling velocities of the spherical particles (diameters: 1.18, 1.5, 2 and 3mm) in partially hydrolyzed polyacrylamide (HPAM) polymer fluids were measured by using Particle Image Shadowgraph (PIS) technique. Two sets of test fluids were formulated by mixing three different grades of HPAM (molecular weights of 500,000; 8,000,000; and 20,000,000) at polymer concentrations 0.09%, 0.05% and 0.03% wt. The shear viscosity and elasticity characteristics of test fluids were determined by performing shear viscosity and frequency sweep oscillatory measurements, respectively. The first set of fluids had almost identical shear viscosity characteristics while showing significantly different elastic properties. The second set of fluids had similar elastic properties but different shear viscosity characteristics.

Experimental results showed that: (i) When the fluids having similar shear viscosity profile were used, the settling velocity of spherical particles decreased significantly with the increasing fluid elasticity. Comparison of the experimental results against the values calculated from the model developed for predicting the settling velocity of spherical particles in power law (visco-elastic) fluids have shown that the settling velocity values can be 14 to 50 times over-estimated if the effect of the elasticity is not considered; (ii) At constant elasticity, the settling velocity of spherical particles also decreased significantly when the fluid shear viscosity was increased; (iii) The spherical particles settling velocity increased pronouncedly as their diameter increased from 1.18mm to 3mm. But the magnitude of the increase in settling velocity with the increasing particle diameter is less for the samples having higher elasticity and similar shear viscosity characteristics.

A follow up experimental study has been conducted to understand the reasons behind why the settling velocity of the particles decrease with the increasing fluid elasticity. In this case, the main objectives were: (i) to investigate the fluid flow field behind the settling particle by using particle image velocity (PIV) technique; (ii) to understand the changes caused by the elasticity of the fluid on the flow field past the settling particle; (iii) more specifically, to determine how the fluid velocity profile and the resultant drag forces acting on the settling particle change with the increasing fluid elasticity.

Two sets of viscoelastic fluids were formulated by mixing three different grades of partially hydrolyzed polyacrylamide (MW of 500,000; 8,000,000; and 20,000,000) at polymer concentrations of 0.09%wt and 0.1%wt. The viscoelastic fluids were formulated in such a way that they had almost identical shear viscosity but significantly different elastic properties. The fluid flow field (i.e. near particle velocity profile) behind the settling particle was determined by using the PIV technique.

The results of the PIV measurements demonstrated that negative wake was present in viscoelastic fluids. However, the stagnation point (the point at which fluid velocity becomes zero and above that the fluid starts moving in the opposite direction to the particle movement) was closer to the particle settling in the higher elasticity fluid than that in the lower elasticity fluid.

The velocity of the fluid in the recirculation region was higher for the flow of the fluid with higher elasticity. Therefore, the presence of stronger negative wake having fast moving fluid in reverse direction nearer to the settling particle could possibly create higher drag forces (acting in the direction against the particle movement), which would affect the settling velocity of the particle.

## **PREFACE**

Chapter 4 of the thesis is partially based on two papers. The results and discussion part of Group-A test fluids is based on the paper that has been presented as Sumanth Kumar Arnipally and Ergun Kuru, “Effect of Elastic Properties of the Fluid on the Particle Settling Velocity” at ASME 36th International Conference on Ocean, Offshore and Arctic Engineering, OMAE, Trondheim, Norway on June 25-30, 2017. The results and discussion part of Group-B test fluids is based on the paper that has been submitted as Sumanth Kumar Arnipally and Ergun Kuru, “Settling Velocity of Particles in Viscoelastic Fluids: A Comparison of the Shear Viscosity vs Elasticity Effect” with paper number SPE-187255-MS for presentation at the 2017 SPE Annual Technical Conference and Exhibition to be held in San Antonio, Texas, 9-11 October 2017. This paper has also been submitted to SPE Journal for review and possible publication. I was responsible for data collection, analysis and manuscript composition. Dr. Ergun Kuru was the supervisory author and responsible for the manuscript revisions.

## ACKNOWLEDGEMENTS

I take the great pleasure in admitting my deep sense of gratitude to my supervisor, **Dr. Ergun Kuru** who offered his wholehearted support and guidance for research throughout my Masters. His encouragement, motivation, and suggestions in my pursuit of knowledge have been exceptional. I shall forever be indebted to him without whose guidance and assistance, this thesis would not have been possible.

I would also like to express my sincere gratitude to **Mr. Todd Kinnee**, for his technical advice and his help in obtaining necessary materials required for the study. I would like to thank **Dr. Zhenghe Xu** for permitting me to use the rheometer in his laboratory. Special thanks to Majid Bizhani and Doszhan Mamedulanov for helping me with the experimental setup and conducting experiments in the lab.

I shall be eternally grateful to my mother, father, brother Sudhir and other family members in India for their constant love and encouragement. Very special thanks to my dearest friends Sowmya, Sai Ravi Teja, Venkateswara Rao and Dr. Moe Piniseti for their love and moral support.

This research is financially supported through the funds available from Natural Sciences and Engineering Research Council of Canada (NSERC RGPIN-2016-04647 KURU and NSERC RGPIN 238623 KURU). I would also like to thank SNF Floerger Company for providing us polymers at free of cost.

Last but not least, I shall be thankful to my God Almighty for blessing me with the necessary strength, knowledge and aptitude to complete this study successfully. This accomplishment would not have been possible without his blessings.

# TABLE OF CONTENTS

Chapter 1: Introduction.....	1
1.1 Overview .....	2
1.2 Problem Statement .....	3
1.3 Objectives and Scope of the Current Study .....	6
1.4 Contributions of the Current Study .....	7
1.5 Structure of the Thesis.....	9
1.6 References .....	11
Chapter 2: Literature Review.....	14
2.1 Background .....	15
2.2 Fluids and their Rheological Properties .....	16
2.2.1 Shear stress.....	16
2.2.2 Shear rate .....	17
2.2.3 Viscosity .....	17
2.2.4 Newtonian and Non-Newtonian fluids .....	17
2.2.5 Power-law fluids .....	19
2.2.6 Viscoelastic fluids.....	21
2.2.7 Influence of the average molecular weight and the molecular weight distribution on the rheological properties of polymer solutions.....	25
2.3 Particle Settling Behavior in Various Types of Fluids.....	26

2.3.1	Settling velocity of particles in Newtonian fluid .....	26
2.3.2	Settling velocity of particles in shear thinning fluid.....	29
2.3.3	Settling velocity of particles in viscoelastic fluids .....	31
2.4	References .....	35
Chapter 3: Experimental Program .....		41
3.1	Materials.....	42
3.1.1	Glass spheres.....	42
3.1.2	HPAM polymers .....	43
3.2	Compositions of the HPAM Polymer Test Fluids .....	44
3.2.1	Test fluids of Group-A.....	45
3.2.2	Test fluids of Group-B .....	46
3.3	Mixing Procedure Followed to Prepare HPAM Test Fluids .....	47
3.4	Characterization of Test Fluids .....	49
3.4.1	Density measurements .....	49
3.4.2	Rheometers used for rheological measurements.....	49
3.4.3	Rheological measurements performed.....	51
3.5	Particle Image Shadowgraph (PIS) Technique and its Experimental Setup .....	53
3.5.1	PIS technique .....	53
3.5.2	PIS experimental setup and its components.....	54
3.5.3	Camera calibration procedure .....	59

3.6	Procedure to Measure Particle Settling Velocity .....	61
3.7	Verification of PIS Measurements .....	65
3.8	Sources of Errors and Precautions to be Followed to Avoid the Errors .....	67
3.8.1	Fluid preparation and its rheology measurements .....	68
3.8.2	PIS experimental setup and procedure.....	68
3.9	References .....	70
Chapter 4: Experimental Investigation of Particle Settling Velocity in Viscoelastic Polymer Fluids Using Particle Image Shadowgraph Technique.' .....		
4.1	Experimental Results of Group-A Test Fluids.....	74
4.1.1	Density measurements of Group-A test fluids.....	75
4.1.2	Rheological characterization of Group-A test fluids .....	75
4.1.3	Settling velocity measurements of particles in Group-A test fluids .....	79
4.2	Experimental Results of Group-B Test Fluids .....	83
4.2.1	Density measurements of Group-B test fluids .....	84
4.2.2	Rheological characterization of Group-B test fluids .....	84
4.2.3	Settling velocity measurements of particles in Group-B test fluids .....	91
4.3	Conclusions .....	103
4.4	Appendix .....	105
4.4.1	Settling velocity in Group-A fluids as per Shah et al. model .....	105
4.4.2	Settling velocity in Set-I of Group-B test fluids as per Shah et al. model.....	105

4.5	References .....	106
Chapter 5: Experimental Investigation of Flow Field Past a Spherical Particle Settling in Viscoelastic Fluids using Particle Image Velocimetry technique..... 108		
5.1	Materials and Methods .....	109
5.1.1	Test fluids and their rheological measurements.....	109
5.1.2	Particle Image Velocimetry (PIV) Technique .....	110
5.1.3	PIV Experimental Setup .....	111
5.1.4	Experimental procedure to investigate the fluid flow field by PIV technique .....	114
5.1.5	PIS experimental setup and experimental procedure.....	117
5.2	Results and Discussions .....	117
5.2.1	Test fluids characterizations .....	117
5.2.2	PIV results.....	120
5.3	Conclusions .....	125
5.4	References .....	126
Chapter 6: Analyses of the Dimensionless Parameters Affecting Particle Settling Velocity in Viscoelastic Fluids .....		
6.1	Analyses of Parameters Affecting the Shear Rates Induced by the Settling Particle ..	129
6.2	Analyses of Dimensionless Parameters Affecting the Particle Settling Velocity .....	133
6.3	Analyses of Dimensionless Parameters Affecting Drag Coefficient and Drag Correction Factor .....	135

6.4	References .....	139
Chapter 7:	Conclusions and Recommendations For Future Work .....	142
7.1	Conclusions .....	143
7.2	Recommendations for Future Work.....	147
Bibliography.....		149

## LIST OF FIGURES

Figure 2-1. Schematic picture of shear flow [2] .....	16
Figure 2-2. Schematic diagram of shear stress versus shear rate of Newtonian and non-Newtonian fluids [3].....	18
Figure 2-3. Schematic diagram of viscosity versus shear rate of shear thinning and shear thickening fluids [4].....	19
Figure 2-4. Schematic diagram of viscosity versus shear rate of various models [2] .....	21
Figure 2-5. Schematic representation of (a) Maxwell model and (b) Kelvin-Voigt model [2] ....	23
Figure 2-6. Oscillatory frequency sweep of a polymer solution [12] .....	24
Figure 2-7. Schematic of forces acting on a settling particle in a Newtonian fluid.....	27
Figure 3-1. The primary chain structure of polyacrylamide and partially hydrolyzed polyacrylamide [2] .....	43
Figure 3-2. Classification of the test fluids used in the present study .....	45
Figure 3-3. Equipment used: (a) Magnetic stirrer (b) Overhead mixer .....	48
Figure 3-4. Bohlin rheometer.....	50
Figure 3-5. AR G2 rheometer with concentric cylinder (cup and bob) geometry .....	51
Figure 3-6. Schematic diagram of particle image shadowgraph experimental setup .....	55
Figure 3-7. Nd:YAG laser from New Wave Research .....	56
Figure 3-8. Picture of (a) diffuser and (b) illumination high efficiency diffuser.....	56
Figure 3-9. Lavision image intense double framed camera with 12x Navitar lens .....	57
Figure 3-10. Schematic of the particle velocity calculation [14].....	59
Figure 3-11. Calibration sheet used to calibrate the camera .....	60
Figure 3-12. Image scaling process in Davis 8.3 software .....	61

Figure 3-13. Image of a particle in focus as appeared on the Davis 8.3 screen.....	63
Figure 3-14. Experimental image after processing in Davis 8.3 software.....	64
Figure 3-15. Experimental values of $C_D$ plotted on universal drag coefficient versus particle Reynolds number ( $Re_p$ ) curve.....	67
Figure 4-1. Shear stress versus shear rate profiles of all the test fluids of Group-A .....	76
Figure 4-2. Shear viscosity versus shear rate profiles of all the test fluids of Group-A .....	76
Figure 4-3. Oscillatory frequency sweep data of all the test fluids of Group-A.....	78
Figure 4-4. Settling velocity of 2mm glass spheres versus the relaxation time of the test fluids of Group-A. ....	80
Figure 4-5. Comparison of the measured settling velocity values of 2mm particles in all test fluids of Group-A to the velocity values calculated from Shah et al. [5] model. ....	81
Figure 4-6. Ratio of the settling velocity of 2mm particles in the inelastic fluid to that of the ones in the elastic fluid as a function of the relaxation time of the fluid. ....	82
Figure 4-7. Shear stress versus shear rate profiles of Set-I test fluids of Group-B.....	85
Figure 4-8. Shear viscosity versus shear rate profiles of Set-I test fluids of Group-B .....	85
Figure 4-9. Oscillatory frequency sweep data for Set-I test fluids of Group-B.....	86
Figure 4-10. Shear stress versus shear rate profiles of Set-II test fluids of Group-B .....	88
Figure 4-11. Shear viscosity versus shear rate profiles of Set-II test fluids of Group-B.....	88
Figure 4-12. Oscillatory frequency sweep data of Set-II test fluids of Group-B.....	90
Figure 4-13. Settling velocity of glass spheres of 2mm diameter versus relaxation time of the Set-I test fluids having similar viscosity but different elasticity. ....	92
Figure 4-14. Over-estimation of settling velocities if the effect of elasticity is not considered. ..	94

Figure 4-15. Settling velocity of glass spheres of 2mm diameter versus apparent shear viscosity of the Set-II test fluids of Group-B. ....	96
Figure 4-16. Settling velocity of glass spheres of 2mm diameter in the Set-II test fluids of Group-B having similar elasticity ( $\lambda = 12$ s) and different consistency index (K). ....	97
Figure 4-17. Settling velocity versus diameter of glass spheres in (a) Set-I test fluids having a similar shear viscosity ( $K= 0.26$ Pa.s <sup>n</sup> and $n=0.35$ ) but different elasticity and (b) Set-II test fluids having similar elasticity ( $\lambda = 12$ s) but different shear viscosity. ....	101
Figure 5-1. The schematic diagram of the PIV experimental setup used to visualize the fluid flow field past the settling spherical particle.....	111
Figure 5-2. The PIV post processing schematic to determine instantaneous velocity [7].....	113
Figure 5-3. Calibration sheet used to calibrate the camera.....	114
Figure 5-4. The captured PIV image of a settling particle in the test fluid containing tracer particles .....	116
Figure 5-5. Shear stress versus shear rate profiles of test fluids A-1 and A-4.....	117
Figure 5-6. Shear viscosity versus shear rate profiles of test fluids A-1 and A-4 .....	117
Figure 5-7. Oscillatory frequency sweep data of fluid A-1 .....	119
Figure 5-8. Oscillatory frequency sweep data of fluid A-4 .....	119
Figure 5-9. Velocity field around and past the settling particle in the test fluid A-1 .....	120
Figure 5-10. Velocity field around and past the settling particle in the test fluid A-4 .....	121
Figure 5-11. Velocity profiles of the fluid A-1 and fluid A-4 along the streamline past the settling particle.....	123
Figure 6-1. Shear rate profiles versus the relaxation time in fluids having $K=0.53$ Pa.s <sup>n</sup> & $n=0.38$ and $K=0.26$ Pa.s <sup>n</sup> & $n=0.35$ .....	131

Figure 6-2. Shear rate profiles versus the apparent viscosity of fluids having $\lambda=12$ s .....	132
Figure 6-3. Shear rate profiles versus the particle diameters in fluids having $K=0.26$ Pa.s <sup>n</sup> , $n=0.35$ and relaxation time 12, 50 and 110 s .....	133
Figure 6-4. Experimental settling velocity values versus $Wi/Re$ .....	134
Figure 6-5. Drag coefficient profile versus $Wi/Re$ ratio .....	136
Figure 6-6. Drag correction factor profile versus Weissenberg number .....	139

## LIST OF TABLES

Table 3-1. Details of the diameters of glass spheres specified by manufacturer .....	42
Table 3-2. HPAM grades along with their SNF batch lot number and average molecular weight values .....	44
Table 3-3. Polymer blend composition details of Group-A test fluids .....	46
Table 3-4. Polymer blend composition details of the test fluids in Set-I of Group-B .....	46
Table 3-5. Polymer blend composition details of the test fluids in Set-II of Group-B.....	47
Table 3-6. Comparison of the manufacturer specified diameter versus the measured diameters of glass spheres.....	65
Table 3-7. Comparison of the measured settling velocity values versus the values reported by Shahi [9].....	66
Table 4-1. Polymer blend composition details of Group-A test fluids .....	74
Table 4-2. Densities of Group-A test fluids.....	75
Table 4-3. Power law parameters K & n for the test fluids of Group-A.....	76
Table 4-4. Longest relaxation times of the test fluids of Group-A.....	78
Table 4-5. Settling velocities of 2mm diameter spherical particles in the test fluids of Group-A	79
Table 4-6. Polymer blend composition details of the test fluids in Set-I of Group-B .....	83
Table 4-7. Polymer blend composition details of the test fluids in Set-II of Group-B.....	83
Table 4-8. Densities of Group-B (Set-I and Set-II) test fluids.....	84
Table 4-9. Power law parameters K & n for Set-I test fluids of Group-B.....	85
Table 4-10. Longest relaxation times of the Set-I test fluids of Group-B .....	87
Table 4-11. Power law parameters of K & n of the Set-II test fluids .....	89
Table 4-12. Longest relaxation times of Set-II test fluids of Group-B.....	90

Table 4-13. Settling velocities of spherical particles of diameter 2 mm in Set-I test fluids of $K=0.26$ Pa.s <sup>n</sup> & $n=0.35$ .....	91
Table 4-14. Settling velocities of spherical particles of 2 mm diameter in Set-II test fluids along with apparent shear viscosities and other rheological properties (K, n).....	95
Table 4-15. Settling velocities of spherical particles of various diameters in Set-I test fluids with different elasticity and similar shear viscosity ( $K= 0.26$ Pa.s <sup>n</sup> and $n=0.35$ ) .....	98
Table 4-16. Settling velocities of spherical particles of various diameters in Set-II test fluids with different shear viscosities and similar elasticity ( $\lambda = 12$ s).....	99
Table 4-17. Increase factor of settling velocities of glass spheres in Set-I and Set- II test fluids .....	101
Table 5-1. Polymer blend composition details of the test fluids.....	110
Table 5-2. Power law parameters K & n for the test fluids A-1 & A-4.....	118
Table 5-3. Longest relaxation times of the test fluids A-1 & A-4 .....	119
Table 5-4. Settling velocities of 2mm diameter spherical particles in the test fluids .....	123
Table 6-1. Compiled data of experimentally measured settling velocity and calculated shear rates along with fluid properties .....	130

## NOMENCLATURE

$\tau$	=	Shear stress, Pa
$F_s$	=	Shear force parallel to surface, N
$A_s$	=	Surface area, m <sup>2</sup>
$\dot{\gamma}$	=	Shear rate, s <sup>-1</sup>
$V$	=	Velocity of the fluid, m/s
$h$	=	Distance between the two layers, m
$\mu$	=	Viscosity of the fluid, Pa.s
$\eta_0, \mu_0$	=	Zero shear viscosity, Pa.s
$\eta_\infty$	=	Infinite shear viscosity, Pa.s
$C$	=	Cross time constant, s
$m$	=	Cross rate constant, dimensionless
$\gamma$	=	Shear strain
$G$	=	Young's modulus, Pa
$M_{w,B}$	=	Average molecular weight of the polymer blend, g/gmol
$\beta$	=	Experimental constant
$\omega_i$	=	Weight fraction of polymer grade i
$M_{w,i}$	=	Molecular weight of polymer grade i, g/gmol
$M_w$	=	Weighted average molecular weight, g/gmol
$M_n$	=	Number average molecular weight, g/gmol

$I$	=	Polydispersity index
$C_D$	=	Drag coefficient
$g$	=	Acceleration due to gravity, m/s <sup>2</sup>
$D_s$	=	Diameter of the sphere, m
$\rho_s$	=	Density of sphere, kg/m <sup>3</sup>
$\rho_f$	=	Density of fluid, kg/m <sup>3</sup>
$V_s$	=	Settling velocity, m/s
$Re_p$	=	Particle Reynolds number
$D_p$	=	Characteristic length of a particle, m
$\mu_f$	=	Viscosity of a fluid, kg/m.s
$K$	=	Flow consistency index, Pa.sn
$n$	=	Flow behavior index
$G'$	=	Elastic modulus, Pa
$G''$	=	Viscous modulus, Pa
$G^*$	=	Complex modulus, Pa
$\omega$	=	Angular frequency, rad/s
$\delta$	=	Phase angle, degrees
$\lambda$	=	Relaxation time, s
$\mu_a$	=	Apparent shear viscosity, Pa.s
$A, B$	=	Two model constants

$C_{D_{VE}}$	=	Drag coefficient of viscoelastic fluid
$C_{D_{INVE}}$	=	Drag coefficient of visco-inelastic fluid
$Re_{PL}$	=	Particle Reynolds number
$Wi$	=	Weissenberg number
$V_{elastic}$	=	Settling velocity in viscoelastic fluid, m/s
$V_{Inelastic}$	=	Settling velocity in visco-inelastic fluid, m/s
$a$	=	Radius of the spherical particle, m
$R$	=	Radius of the fluid particle column, m
$K$	=	Drag correction factor

# **CHAPTER 1: INTRODUCTION**

## 1.1 OVERVIEW

Suspensions of solid particles in liquids are commonly encountered in a wide range of industrial applications. In petroleum industry, for instance, proppants are transported by suspending them in fracturing fluids for hydraulic fracturing process and the cuttings are conveyed to the surface by suspending them in a drilling fluid in drilling operations,. Similarly in chemical industries, solid particles are dealt in processes such as mineral transportation, solid separations, suspension of abrasive particles in surfactant formulations, solid-liquid mixing, paint and pigmentation and so on. Suspension of particles in liquids are, therefore, handled extensively to meet the ever increasing requirements of industrial applications.

However, handling the solid particles in liquids has always been a challenge. So information about the fluid particle system plays an essential role to improve the efficiency of industrial process. Settling velocity is a principal parameter to consider when the behavior of particles in any fluids is studied. When a particle is falling freely in a fluid due to gravity, it achieves a constant velocity once the equilibrium is attained and that velocity is termed as the terminal velocity or the settling velocity [1]. To study the settling behavior of particles in fluids, determining the settling velocity of a particle in stagnant fluids of various types such as Newtonian and non-Newtonian becomes the starting point. When the settling velocity of particles in a fluid is higher, it means that they settle at faster rate when suspended in the fluid, which is undesirable. Henceforth, a good understanding of the settling behavior and the settling velocity of particles in various types of fluids becomes the significant interest for the industries. Also it becomes imperative to reduce the settling velocity of particles in fluids to design optimum hydraulic program for cuttings transportation in the drilling, proppant transportation in the hydraulic fracturing operations, pipeline transportation of slurries and many more applications.

## 1.2 PROBLEM STATEMENT

Most of the fluids encountered in the industrial applications tend to have both the shear thinning and the viscoelastic properties. A shear-thinning characteristic indicates that the fluid viscosity decreases with the increasing shear rate. A viscoelastic fluid demonstrates both viscous and elastic behavior under deformation.

In oil and gas well drilling operations, one of the primary functions of a drilling fluid is to transport drilled cuttings to the surface. The drilled cuttings tend to settle because of their own weight often creating a difficult problem to handle particularly when drilling the high inclination and horizontal wells. Having appropriate suspension properties in the drilling fluid would abate the settling of the drill cuttings.

The shear thinning is a desirable fluid property because when the fluid is pumped down the drill pipes and through the bit nozzles, the effective fluid viscosity decreases thereby lowering the power requirements of the pump [2]. Viscoelasticity is also a desirable property because it is reported that the drilling fluids that possess viscoelastic properties would strongly impact the gel strength, barite sag, cuttings transport, filtration loss characteristics of the drilling fluids [3]. Likewise, in hydraulic fracturing, for effective proppant transport and to avoid their premature settling, hydraulic fracturing fluids are advised to have viscoelasticity [4, 5]. Therefore, knowledge of the particle settling behavior and the particle settling velocity in viscoelastic shear thinning fluids is indispensable to optimize the properties of these industrial fluids.

Empirical correlations are commonly used to predict the settling velocity of particles in various types of fluids encountered in industrial processes as the analytical solutions of the problem are difficult to obtain.

The settling velocity of the particles,  $V_s$ , can be calculated if the drag coefficient,  $C_D$ , and the respective particle Reynolds number are known. The pioneering work of Stokes [6] provided one of the first correlation between the drag coefficient ( $C_D$ ) and the particle Reynolds number ( $Re_p$ ) as shown in Equation 1-1 to Equation 1-3. Stokes model is given for the particle settling in a Newtonian fluid in the creeping flow regime ( $Re_p < 1$ ). The Stokes model thereafter formed the basis for further investigations in various types of complex fluids.

$$C_D = \frac{24}{Re_p} \quad \text{Equation 1-1}$$

$$Re_p = \frac{D_p V_s \rho_f}{\mu_f} \quad \text{Equation 1-2}$$

$$V_s = \frac{(\rho_s - \rho_f) g D_s^2}{18 \mu_f} \quad \text{Equation 1-3}$$

The Stokes model has been generally modified to predict the settling velocity of particles in non-Newtonian shear thinning fluids by introducing apparent shear viscosity instead of Newtonian fluid viscosity term in Equation 1-2 and Equation 1-3 [7-10].

Apparent viscosity is the viscosity of the fluid at the respective shear rates induced by the settling particles. However, most of these models were valid only for the purely viscous non-Newtonian shear thinning fluids where the effect of the fluid elasticity was not taken into consideration in these models. Therefore, these models are not suitable for settling velocity prediction when the process involves fluids of viscoelastic nature such as drilling and fracturing fluids.

Several research studies were done in the past to understand the settling behavior of particles in viscoelastic fluids and also in the Boger fluids (i.e. elastic fluids of constant viscosity). For instance, Acharya et al. [11, 12] after working with the shear thinning viscoelastic polymer solutions, reported the drag reduction at high Reynolds numbers [11]. Chhabra et al. [13] studied the settling behavior of particles in the Boger fluids and reported the drag coefficient diminution at high values of the Weissenberg number. The Weissenberg number is a product of relaxation time and shear rate, and it is used as a measure of fluid elasticity. Acharya [14, 15] conducted settling experiments using viscoelastic fracturing fluids and indicated that at the low Reynolds number flow regime, settling velocities of the proppants were controlled by the fluid viscosity rather than by the fluid elasticity whereas at the intermediate Reynolds number flow regime, settling velocities were amplified because of the fluid elasticity. On the other hand, Van den Brule et al. [16] observed a noticeable decrease in particle settling velocity due to the fluid elasticity in the highly elastic shear thinning fluids. Walters and Tanner [17] subsequently noticed that for a particle settling in the Boger fluids, the elasticity caused the drag decline at low Weissenberg numbers and the drag improvement at higher Weissenberg numbers.

These studies already noticed that the fluid elasticity has an effect on the settling velocities of particles. The experimentally measured values of the particle velocities from those studies, however, were not in agreement with the theoretically predicted values [18]. It was later stated by Chhabra [18] that this deviation was caused due to the fact that the experimental values of particle velocities had both viscoelasticity and shear thinning effects in consideration whereas the theoretical models had only included viscoelasticity effect without considering the effects of shear thinning characteristics of the fluid [18]. Chhabra [18] also commented that it is difficult to integrate both the viscoelasticity and the shear thinning effects in the theoretical models. This is

because their individual influences on the particle settling velocity are not known conclusively since no study in the literature disengaged the effects.

To design better drilling fluids or hydraulic fracturing fluids and optimize the settling velocities of particles in them, one should be in cognizance of the individual effects of fluid elasticity and the non-Newtonian shear viscosity. There was no previous research found in the literature investigating individual effects of fluid elasticity and the non-Newtonian shear viscosity on the particle settling velocity by disassociating them from each other. Therefore, in this study effects of the shear viscosity and the elasticity on the particle settling velocity examined separately by decoupling them from one another. The focus of the current study is to investigate the individual effect of the elasticity on settling velocity of particles in viscoelastic fluids and to determine the most governing factor between the fluid elasticity and the shear viscosity to regulate the settling velocity of the particles in viscoelastic fluids.

### **1.3 OBJECTIVES AND SCOPE OF THE CURRENT STUDY**

The major objectives of this research study are:

- To conduct experiments to measure settling velocity of particles in viscoelastic fluids using particle image shadowgraph (PIS) technique.
- To investigate the effect of the fluid elastic properties on the settling velocity of the spherical particles in viscoelastic polymer fluids by decoupling the effect of the elasticity from effect of the shear viscosity.
- To determine the most prominent factor between the fluid elasticity and the fluid shear viscosity to govern the particle settling velocity reduction in viscoelastic fluids.

- To investigate the fluid flow field behind the settling particle by using particle image velocity (PIV) technique.
- To understand the changes caused by the elasticity of the fluid on the flow field past the settling particle.
- More specifically, to determine how the fluid velocity profile and the resultant drag forces acting on the settling particle change with the increasing fluid elasticity.

Following specific tasks were completed to accomplish the above mentioned objectives.

- To prepare polymer fluids by mixing three different grades of partially hydrolyzed polyacrylamide (HPAM) polymer so that the test fluids should possess similar shear thinning viscosity but significantly different elasticity.
- To design and commission the Particle Image Shadowgraph (PIS) experimental setup for measuring the settling velocities of particles in various fluids. The experimental setup is calibrated by measuring the settling velocities of spheres in water.
- To design and commission the Particle Image Velocimetry (PIV) experimental setup to determine the flow field past the settling sphere in viscoelastic fluids.

#### **1.4 CONTRIBUTIONS OF THE CURRENT STUDY**

The key contributions of the current study are as follows:

- In the first phase of research study, the HPAM polymer blends were formulated such a way that they have the same average molecular weight but varying molecular weight distribution. By doing this, we have developed the aqueous solutions of these polymer blends which have similar shear thinning viscosity properties but significantly different elastic properties.

- In the second phase, an experimental setup to measure the settling velocities of the spherical particles were designed and commissioned. To measure the velocities, Particle Image Shadowgraph (PIS) technique was utilized.
- In the next and essential phase of this research study, the settling velocities of the spherical particles were measured in the aqueous solutions of HPAM polymer blends having similar shear thinning viscosity properties but significantly different elastic properties. By doing this, we have determined the individual effect of elasticity on the settling velocity of particles by decoupling it from the effect of shear viscosity.
- Later, the most prominent factor between the fluid elasticity and the fluid shear viscosity was determined to govern the particle settling velocity reduction in viscoelastic polymer solutions. By conducting experiments under controlled conditions, for the first time in the literature, we were able to quantify the individual effects of fluid shear viscosity and elasticity on the particle settling velocity.
- In the next phase, changes caused by the elasticity in the flow field past the settling particle in the viscoelastic fluid were investigated. Using Particle Image Velocimetry (PIV) technique, we have proven that the negative wakes exists in the flow field past the settling particle.
- Lastly, the dimensionless parameters such as Weissenberg number, Reynolds number, drag coefficient, drag corrections etc. were calculated from the experimental results to determine their effect on the settling velocity of particles and also the functional relationships among these dimensionless parameters were analyzed further.

## 1.5 STRUCTURE OF THE THESIS

In this thesis, I have reported the results of an experimental investigation in which the settling velocities measurements of the spherical particles in viscoelastic fluids were conducted.

- **Chapter 1: Introduction**

- This chapter provides an overview of the research study. It summarizes the research background, problem statement along with the objectives and the scope of the current work, contributions from this study and the structure of the thesis.

- **Chapter 2: Literature Review**

- The purpose of this chapter is to provide a comprehensive review of the concepts of the rheology of fluids and the research work done in the past to understand the settling behavior and settling velocities of the particles in several types of complex fluids.

- **Chapter 3: Experimental Program**

- This chapter describes the methodology followed in the present study to prepare the test fluids of required viscoelastic characteristics. It also explains the Particle Image Shadowgraph (PIS) experimental setup details, its working principles, and the methodology followed to measure the settling velocities of particles in various polymer solutions by PIS technique. The calibration of the experimental set up is also presented in this chapter.

- **Chapter 4: Experimental Investigation of Particle Settling Velocity in Viscoelastic Polymer Fluids Using Particle Image Shadowgraph Technique**

- This chapter provides the results of the experimental measurements performed to investigate the effect of elastic properties of the fluids on the particle settling velocity. It also contains the results of the comparative study that is performed to determine the

prominent factor between the fluid shear viscosity and the fluid elasticity that governs the particles settling velocity reduction in viscoelastic polymer solutions.

- **Chapter 5: Experimental Investigation of Flow Field Past the Settling Sphere in a Viscoelastic Fluid Using Particle Image Velocimetry Technique**
  - This chapter comprises of the results of Particle Image Velocimetry (PIV) experimental study that is done to investigate the near particle velocity profile measured as the particle settles through the viscoelastic fluid.
- **Chapter 6: Analyses of the Dimensionless Parameters Affecting Particle Settling Velocity in Viscoelastic Fluids**
  - This chapter provides the details of dimensionless parameters such as drag corrector factors, Weissenberg numbers, Reynold's numbers, etc. that are determined from the experimentally measured values of particle settling velocities in viscoelastic fluids. It also discusses the functional relationship between those parameters
- **Chapter 7: Conclusions and Recommendations.**
  - This chapter summarizes the conclusions of the research work as well as recommendations for future works.

## 1.6 REFERENCES

- [1] McCabe, W.L., Smith, J.C. and Harriott, P. 2004. *Unit Operations of Chemical Engineering*, New York: McGraw-Hill.
- [2] Caenn, R., Darley, H.C.H. and Gray, G.R. 2011. Introduction to Drilling Fluids. In *Composition and Properties of Drilling and Completion Fluids*, 6th edition, Chap. 1, 1-37. Boston: Gulf Professional Publishing.
- [3] Bui, B., Saasen, A., Maxey, J., Ozbayoglu, M.E., Miska, S.Z., Yu, M. and Takach, N.E. 2012. Viscoelastic Properties of Oil-Based Drilling Fluids. *Annual Transactions of the Nordic Rheology Society* **20**: 33-48.
- [4] Gomaa, A.M., Gupta, D.V.S.V. and Carman, P.S. 2015. Proppant Transport? Viscosity Is Not All It's Cracked up to Be. Presented at SPE Hydraulic Fracturing Technology Conference, 3-5 February., The Woodlands, Texas, USA., 2015/2/3/. SPE-173323-MS. <http://dx.doi.org/10.2118/173323-MS>.
- [5] Hu, Y.T., Chung, H. and Maxey, J.E. 2015. What is More Important for Proppant Transport, Viscosity or Elasticity? Presented at SPE Hydraulic Fracturing Technology Conference, 3-5 February., The Woodlands, Texas, USA 2015/2/3/. SPE-173339-MS. <http://dx.doi.org/10.2118/173339-MS>.
- [6] Stokes, G.G. 1851. *On the Effect of the Internal Friction of Fluids on the Motion of Pendulums*: Pitt Press.
- [7] Chien, S.F. 1972. Annular Velocity for Rotary Drilling Operations. *International Journal of Rock Mechanics and Mining Sciences & Geomechanics Abstracts* **9** (3): 403-416. [http://dx.doi.org/10.1016/0148-9062\(72\)90005-8](http://dx.doi.org/10.1016/0148-9062(72)90005-8).
- [8] Lali, A.M., Khare, A.S., Joshi, J.B. and Nigam, K.D.P. 1989. Behaviour of Solid Particles in Viscous Non-Newtonian Solutions: Settling Velocity, Wall Effects and Bed Expansion in Solid-Liquid Fluidized Beds. *Powder Technology* **57** (1): 39-50. [http://dx.doi.org/10.1016/0032-5910\(89\)80102-0](http://dx.doi.org/10.1016/0032-5910(89)80102-0).

- [9] Miura, H., Takahashi, T., Ichikawa, J. and Kawase, Y. 2001. Bed Expansion in Liquid–Solid Two-Phase Fluidized Beds with Newtonian and Non-Newtonian Fluids over the Wide Range of Reynolds Numbers. *Powder Technology* **117** (3): 239-246. [http://dx.doi.org/10.1016/S0032-5910\(00\)00375-2](http://dx.doi.org/10.1016/S0032-5910(00)00375-2).
- [10] Moore, P.L. 1974. *Drilling Practices Manual*, Tulsa, Oklahoma, USA: Petroleum Publishing Company.
- [11] Acharya, A., Mashelkar, R.A. and Ulbrecht, J. 1976. Flow of Inelastic and Viscoelastic Fluids Past a Sphere. Part II: Anomalous Separation in the Viscoelastic Fluid Flow. *Rheologica Acta* **15** (9): 471-478. <http://dx.doi.org/10.1007/bf01530349>.
- [12] Acharya, A., Mashelkar, R.A. and Ulbrecht, J. 1976. Flow of Inelastic and Viscoelastic Fluids Past a Sphere. Part I. Drag Coefficient in Creeping and Boundary-Layer Flows. *Rheologica Acta* **15** (9): 454-470. <http://dx.doi.org/10.1007/bf01530348>.
- [13] Chhabra, R.P., Uhlherr, P.H.T. and Boger, D.V. 1980. The Influence of Fluid Elasticity on the Drag Coefficient for Creeping Flow around a Sphere. *Journal of Non-Newtonian Fluid Mechanics* **6** (3): 187-199. [http://dx.doi.org/10.1016/0377-0257\(80\)80002-4](http://dx.doi.org/10.1016/0377-0257(80)80002-4).
- [14] Acharya, A.R. 1988. Viscoelasticity of Crosslinked Fracturing Fluids and Proppant Transport. *SPE Production Engineering* **3**: 483-488. SPE-15937-PA. <http://dx.doi.org/10.2118/15937-PA>.
- [15] Acharya, A.R. 1986. Particle Transport in Viscous and Viscoelastic Fracturing Fluids. *SPE Production Engineering* **1** (02). SPE-13179-PA. <http://dx.doi.org/10.2118/13179-PA>.
- [16] Van den Brule, B.H.A.A. and Gheissary, G. 1993. Effects of Fluid Elasticity on the Static and Dynamic Settling of a Spherical Particle. *Journal of Non-Newtonian Fluid Mechanics* **49** (1): 123-132. [http://dx.doi.org/10.1016/0377-0257\(93\)85026-7](http://dx.doi.org/10.1016/0377-0257(93)85026-7).
- [17] Walters, K. and Tanner, R. 1992. The Motion of a Sphere through an Elastic Fluid. In *Transport Processes in Bubbles, Drops and Particles*, ed. Chhabra, R. and De Kee, D., Chap. 3. New York: Hemisphere.

- [18] Chhabra, R.P. 2007. *Bubbles, Drops, and Particles in Non-Newtonian Fluids, Second Edition*: CRC Press, Taylor & Francis Group.

## **CHAPTER 2: LITERATURE REVIEW**

The purpose of this chapter is to provide a comprehensive review of the concepts of the rheology of fluids and the research work done in the past to understand the settling behavior and settling velocities of the particles in several types of complex fluids that are encountered in chemical and petroleum industries. A short background description of the practical importance to appreciate the particle settling behavior in drilling fluid is also provided.

## **2.1 BACKGROUND**

In oil and gas well drilling operation, drilling fluid is circulated in the wellbore to expedite the drilling process. This fluid has several functions such as removal of solids particles from the wellbore, drill bit lubrication, providing support to the drill pipe/bit, etc. Among all these functions, removing the drill cuttings or solid particles from the wellbore and maintain them in suspension in the borehole when there is no fluid flow is the primary role of the drilling fluid [1].

Due to their weight, these drilling cuttings and solid particles from the wellbore tend to settle down in the borehole. This problem of settling needs to be addressed in vertical, inclined and horizontal wells. To avoid the particles from settling and maintain them in suspension, the drilling fluid should possess certain rheological properties such as viscosity, yield stress, gel strength and physical properties such as density [1]. The settling of the drilling cuttings can be controlled by reducing their settling velocities in the fluid. The drilling fluids may exhibit various types of rheological behaviors such as Newtonian, non-Newtonian (shear thinning, Bingham plastic, yield power law, viscoelastic), etc. and understanding the settling motion and velocities of the drilling cuttings in these various types of complex and structured drilling fluids is challenging. However, examining the simpler case of motion of a single particle in these complex fluids will be instructive to secure an insight of this phenomenon. Therefore, one must have proper knowledge about the particle settling behavior and estimation of the particles settling velocities in the different

kinds of fluids before designing the drilling fluid to maximize its efficiency of cuttings transportation. Extensive research has already been done in the past to study and understand the settling behavior and the settling velocities of particles in various types of fluids. This chapter is dedicated to reviewing some of these relevant literature work.

## 2.2 FLUIDS AND THEIR RHEOLOGICAL PROPERTIES

Aqueous solutions of polymers exhibit various kinds of rheological behaviors depending upon the nature of the polymer. A summary of the rheology concepts and rheological properties of various fluids is presented in the following subsections to aid the interpretation of the behavior of polymer solutions.

### 2.2.1 Shear stress

Shear flow is the movement of fluid layers in such way that they slide over each other [2]. Shear stress is defined as the shear force acting per unit area and denoted by  $\tau$ . The shear force always acts in the direction parallel to the surface plane [3]. For instance, as shown in **Figure 2-1**, if  $F_s$  is the shear force acting parallel to the surface of area  $A_s$  then the shear stress is given by Equation 2-1 [2]. In SI system, it is given in units of Pascal, Pa, the unit is the same as that of pressure.

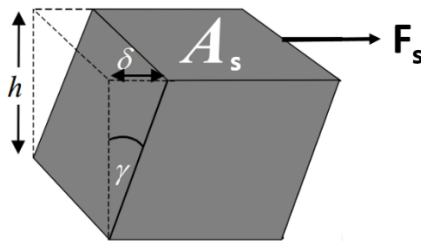


**Figure 2-1. Schematic picture of shear flow [2]**

$$\tau = \frac{F_s}{A_s} \quad \text{Equation 2-1}$$

### 2.2.2 Shear rate

In **Figure 2-1**, the velocity of the layers that are sliding over each other will be different, and it increases proportionally with regard to the layer below it [2]. Shear rate is defined as the velocity gradient between the layers in the direction perpendicular to the flow. If  $V$  is the velocity of the top layer and  $h$  is the distance between the layers, then the shear rate is given by Equation 2-2 [2]. Shear rate is also known as strain rate and denoted by  $\dot{\gamma}$ . In SI system, it is given in units of  $s^{-1}$ .

$$\dot{\gamma} = \frac{V}{h} \quad \text{Equation 2-2}$$

### 2.2.3 Viscosity

The resistance offered by the fluid to the forces in shear flow is defined as the viscosity and it is denoted by  $\mu$ . For a Newtonian fluid experiencing shear stress of  $\tau$ , Pa and shear rate of  $\dot{\gamma}$ ,  $s^{-1}$ , the viscosity ( $\mu$ ) of the fluid is given by the Newton's law as shown in Equation 2-3. In SI system, it is given in units of Pa.s. Viscosity is a function of both temperature and pressure.

$$\tau = \mu \dot{\gamma} \quad \text{Equation 2-3}$$

### 2.2.4 Newtonian and Non-Newtonian fluids

Fluids are classified depending upon the relationship between the shear stress and shear rate. If shear stress is linearly proportional to shear rate as shown in Equation 2-3, such fluids are

called Newtonian fluids [3]. If they are not linearly related, then those fluids are called non-Newtonian fluids [3]. Typically, polymer solutions are characterized as non-Newtonian fluids.

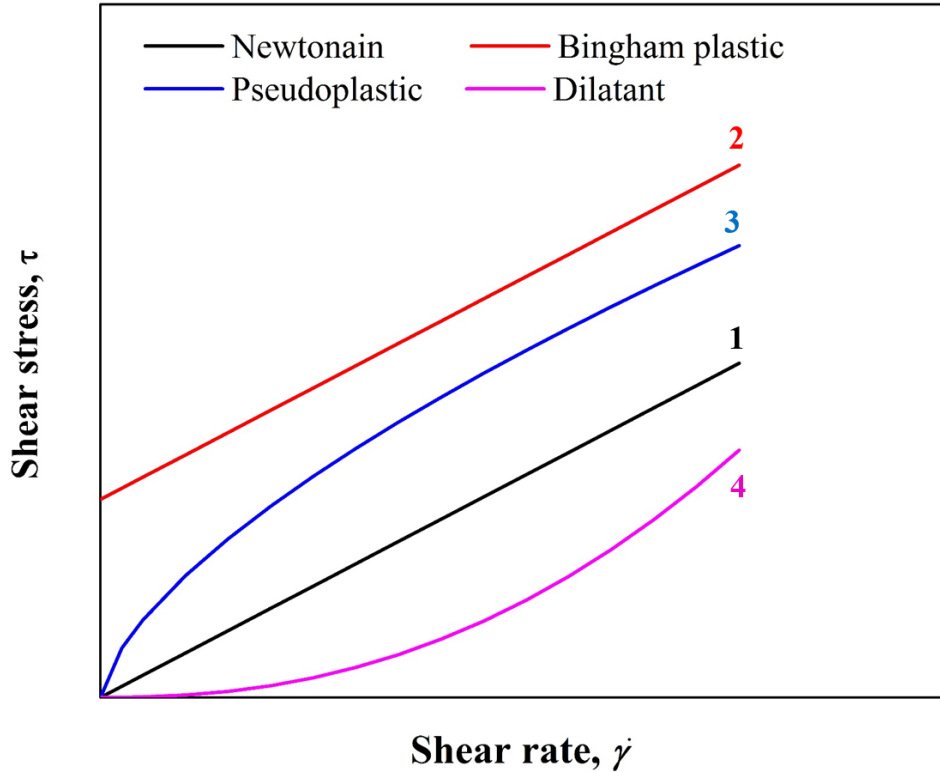


**Figure 2-2. Schematic diagram of shear stress versus shear rate of Newtonian and non-Newtonian fluids [3]**

**Figure 2-2** describes the shear stress to the shear rate relationship curves for various types of fluids [3]. The linear relationship between shear stress and shear rate is demonstrated as curve 1 by Newtonian fluids [3]. If the fluid requires minimum or threshold stress to flow and then exhibits linear relationship as shown by curve 2, such fluids are called Bingham plastics [3]. If the relationship curve is concave downwards so that the slope of the curve 3 (i.e. viscosity of fluid) decreases with shear rate, such fluids are called pseudoplastics or shear thinning fluids [3]. If the curve is concave upwards so that the slope of the curve (i.e. viscosity of fluid) increases with the shear rate as shown by curve 4, such fluids are called dilatant or shear thickening fluids [3].

### 2.2.5 Power-law fluids

The shear thinning and shear thickening fluids behavior can be represented by a power law relationship between shear stress and shear rate as shown in Equation 2-4, where K is the consistency index, Pa.s<sup>n</sup> and n is the flow behavior or power law index. For these fluids, the viscosity of the fluids is a function of shear rate. Therefore, the apparent viscosity ( $\mu_a$ ) of the fluid is measured at appropriate shear rates as shown in Equation 2-5. For shear thinning fluids, n is lower than 1 and for shear thickening fluids n is higher than 1. The viscosity behaviors of the shear thinning and the shear thickening fluids in comparison to Newtonian fluids with respect to shear rates are given in **Figure 2-3**. In general, polymer solutions behavior can be reflected by power law model.

$$\tau = K\dot{\gamma}^n \quad \text{Equation 2-4}$$

$$\mu_a = K\dot{\gamma}^{n-1} \quad \text{Equation 2-5}$$

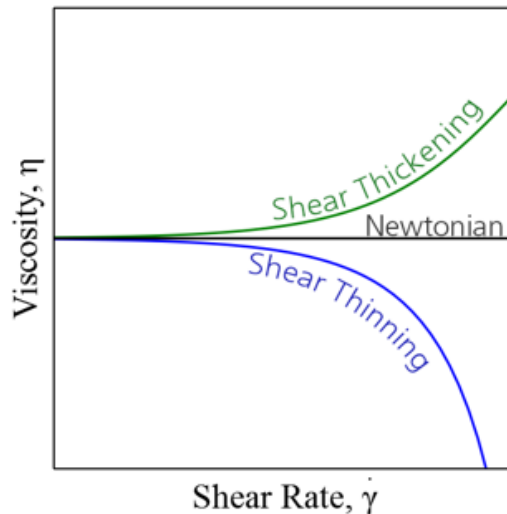


**Figure 2-3. Schematic diagram of viscosity versus shear rate of shear thinning and shear thickening fluids [4]**

For shear thinning fluids, few other models such as Cross [5], Sisko [6] take into account the plateau regions of viscosity at low and high shear rates, as shown in **Figure 2-4** [2]. The equation forms of Cross model and Sisko model are given by Equation 2-6 and Equation 2-7 respectively.

$$\frac{\eta - \eta_{\infty}}{\eta_o - \eta_{\infty}} = \frac{1}{1 + (C\dot{\gamma})^m} \quad \text{Equation 2-6}$$

$$\eta = \eta_{\infty} + \frac{\eta_o - \eta_{\infty}}{1 + (C\dot{\gamma})^m} \quad \text{Equation 2-7}$$

where  $\eta_o, \eta_{\infty}$  are the asymptote values of viscosity at zero and infinite shear rates, C is the cross time constant and m is the cross rate constant.

Though these models give more satisfactory results, for most of the fluids, the measurement shear rate range would be too low or too high to pick up the higher shear rate or lower shear rate plateau regions [2]. That's why power law model is used most widely to describe the non-Newtonian behavior of polymer solutions. In addition, power law model requires only two parameters whereas other models such as Cross and Sisko models require four parameters.

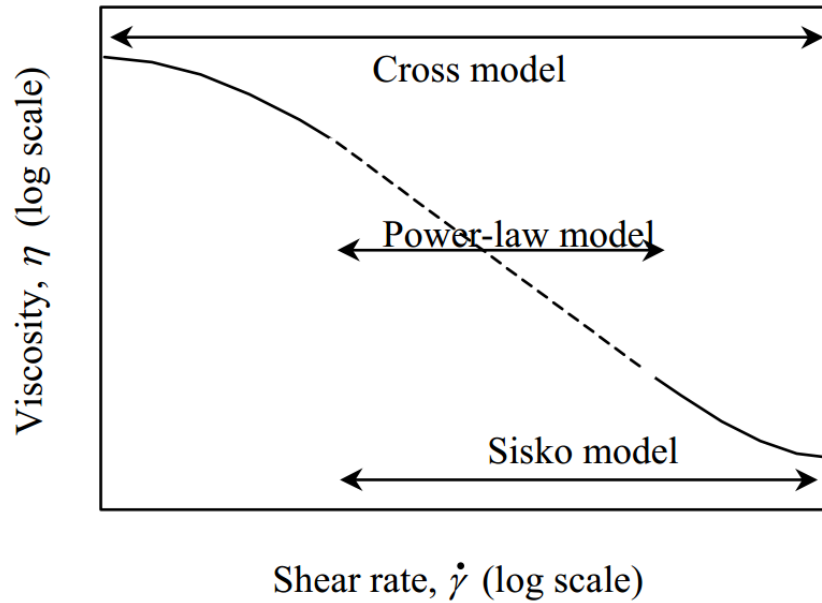


**Figure 2-4. Schematic diagram of viscosity versus shear rate of various models [2]**

### 2.2.6 Viscoelastic fluids

Viscoelastic fluids are the type of non-Newtonian fluids that exhibit viscoelasticity property. Viscoelasticity is the material property to demonstrate both viscous and elastic properties during deformation [7]. The elastic property is the material ability to regain its shape to the original when the deforming forces are removed [8]. For an ideal solid, the linear relationship between the stress ( $\tau$ ) and the strain ( $\gamma$ ) is given by Hooke's law [2] as shown in Equation 2-8, where  $G$  is young's modulus.

$$\tau = G\gamma \quad \text{Equation 2-8}$$

The viscous property is the material ability to dissipate the energy of deformation [8]. For an ideal liquid, the linear relationship between shear stress ( $\tau$ ) and shear rate ( $\dot{\gamma}$  or  $\frac{d\gamma}{dt}$ ) is given by Newton's law that is shown in Equation 2-3.

Between the elastic and the viscous properties, the type of response displayed by the fluid depends upon the experimental time scale compared to the material time scale [7]. For example, if the experimental time scale is longer, the fluid behaves viscous instead of elastic and if the experimental time scale is shorter, the fluid behaves elastic instead of viscous [7].

The viscoelastic behavior of the materials can be better explained by using simple mechanical models that consist of spring and dashpot to denote linear elastic and viscous elements respectively. Since spring obeys Hooke's law and dashpot obeys Newton's law, the combination of these two are used in the mechanical models to represent viscoelasticity [2]. As shown in **Figure 2-5**, when a spring and a dashpot are connected in series, it represents simple viscoelastic liquid and such combination is called Maxwell model, whereas when they are connected in parallel, it represents simple viscoelastic solid and such combination is called Kelvin-Voigt model [2]. The Maxwell model is the most basic and simple mechanical model. The series of combinations of spring and dashpot models are considered to represent the realistic viscoelastic liquids. Later on many mechanical models such as Rouse model [9], Zimm models [10] were developed for various polymer systems [11].

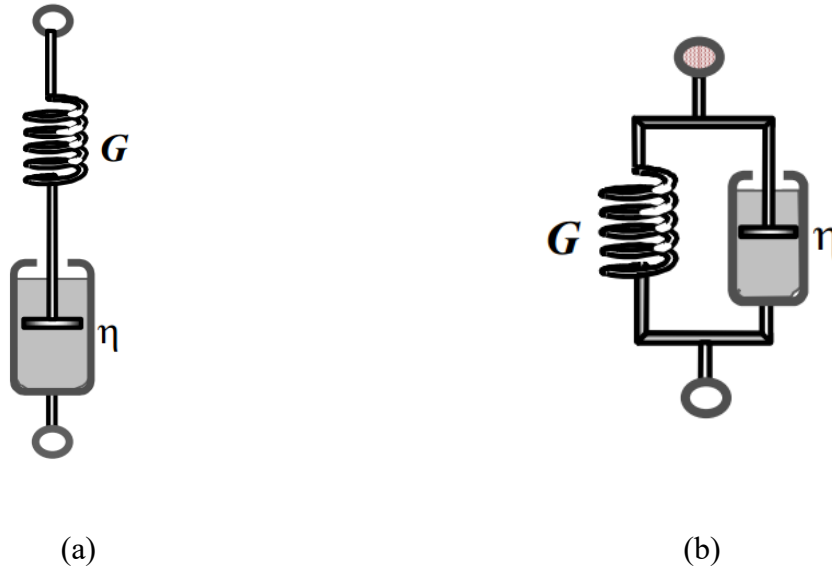


**Figure 2-5. Schematic representation of (a) Maxwell model and (b) Kelvin-Voigt model [2]**

The simplified Maxwell model that consists of one spring and one dashpot is given by Equation 2-9 and Equation 2-10 where  $G'$  and  $G''$  represent the storage modulus and the loss modulus at a particular frequency respectively,  $\omega$  is frequency,  $G$  is the spring modulus and  $\lambda$  is the relaxation time. The storage modulus denotes the solid-like behavior of the material, and the loss modulus denotes the liquid-like behavior of the material when a sinusoidal form of deformation is applied. The storage modulus will be in phase whereas the loss modulus will be out of phase by  $\frac{\pi}{2}$  with the applied frequency,  $\omega$  [2].

$$G' = \frac{G(\omega\lambda)^2}{1 + (\omega\lambda)^2} \quad \text{Equation 2-9}$$

$$G'' = \frac{G\omega\lambda}{1 + (\omega\lambda)^2} \quad \text{Equation 2-10}$$

From Equation 2-9 and Equation 2-10, it can be noticed that  $G'$  and  $G''$  are functions of angular frequency. Experimentally, the relationship of  $G'$  and  $G''$  with respect to angular frequency can be measured by performing oscillatory frequency sweep test. The oscillatory frequency sweep of a polymer solution for illustration purpose is provided in **Figure 2-6** [12]. As shown in **Figure 2-6**, at lower frequencies, when the experimental time scale is longer, the loss modulus is greater than the storage modulus and as the frequency increases, the storage modulus increases at higher rate than the increase in loss modulus. Eventually, at higher frequencies, when the experimental time scale is shorter, the storage modulus becomes greater than the loss modulus. The frequency at which  $G'$  and  $G''$  becomes equal has a significance, and that frequency is called cross over frequency. The inverse of the crossover frequency provides the longest relaxation time of the material [13, 14]. The physical importance of relaxation time is that it is the time needed for any deformed material to regain its original structure and elasticity of a material can be quantified by its relaxation time [8].

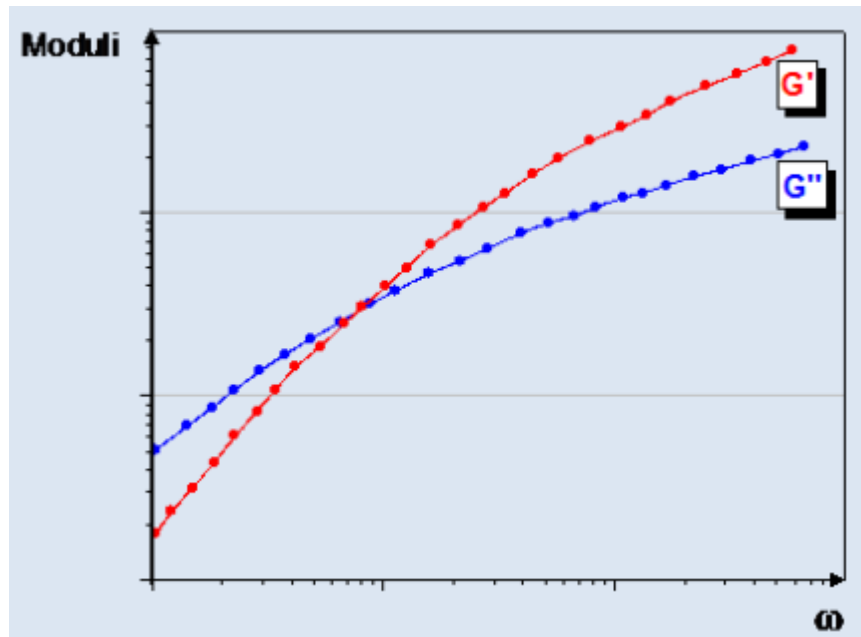


**Figure 2-6. Oscillatory frequency sweep of a polymer solution [12]**

### 2.2.7 Influence of the average molecular weight and the molecular weight distribution on the rheological properties of polymer solutions

Parameters such as the average molecular weight and the molecular weight distribution influence the rheological properties of the polymer solutions. For instance, the zero shear viscosity is strongly influenced by the average molecular weight [15] and the longest relaxation time is known to be affected by the molecular weight distribution [16-19]. Ferry [15] provided a relationship between zero shear viscosity ( $\mu_0$ ) and the average molecular ( $M_w$ ) weight as shown in Equation 2-11, where  $K$  is the constant that is dependent upon polymer type and temperature, and  $\beta$  is the experimental constant.

$$\mu_0 = KM_w^\beta \quad \text{Equation 2-11}$$

Zang [20] provided a relationship to determine the weight-average molecular weight of a polymer mixture ( $M_{w,B}$ ) as shown in Equation 2-12, where  $M_{w,i}$  is the weight-average molecular weight of  $i^{\text{th}}$  polymer and  $\omega_i$  is the weight fraction of  $i^{\text{th}}$  polymer in the polymer mixture.

$$M_{w,B} = \sum_{i=1}^n \omega_i M_{w,i} \quad \text{Equation 2-12}$$

Dehghanpour [16, 21] worked with polyethyloxide (PEO) solutions to investigate viscoelastic properties of polymer fluids, and in his study, he prepared aqueous solutions of PEO polymer mixtures based on the Equation 2-11. However, the average molecular weights of the polymer blends were noticed to deviate from the ones given by Equation 2-12. Therefore, he proposed Equation 2-13 to determine the average molecular weight of any polymer blend. He also observed that similar shear viscosity behavior was exhibited by the polymer solutions having similar average molecular weight [16, 21].

$$M_{w,B} = \prod_{i=1}^n M_{w,i}^{\omega_i} \quad \text{Equation 2-13}$$

Polydispersity index is used to describe the effect of molecular weight distribution on the rheological properties of the polymer solutions. The polydispersity index (I) is the ratio of the weight-average molecular weight ( $M_w$ ) to number-average molecular weight ( $M_n$ ), and it is given by the Equation 2-14 [20].

$$I = \frac{M_w}{M_n} = \left( \sum_{i=1}^n \omega_i M_{w,i} \right) \times \left( \sum_{i=1}^n \frac{\omega_i}{M_{w,i}} \right) \quad \text{Equation 2-14}$$

Equation 2-13 and Equation 2-14 are widely used in the past to determine the average molecular weight and the molecular weight distribution of the polymer blends. Dehghanpour [16, 21] and others [16, 21-27] showed that the polymer solutions having similar average molecular weight but different molecular weight distribution exhibited similar shear viscosity but different elastic behaviors.

## 2.3 PARTICLE SETTLING BEHAVIOR IN VARIOUS TYPES OF FLUIDS

A brief description of the literature available on the settling behavior of the particles in various types of fluids such as Newtonian, shear thinning, Boger and viscoelastic fluids is provided here in this section.

### 2.3.1 Settling velocity of particles in Newtonian fluid

The traditional understanding of settling behavior of a spherical particle in Newtonian fluid formed the basis for further investigations in all other types of fluids. When a particle is settling in a Newtonian fluid, three forces (i.e. force due to gravity ( $F_G$ ), force due to buoyancy ( $F_B$ ) and drag force ( $F_D$ )) act upon the particle [3]. The gravity force is an external force that acts downwards, the buoyancy force acts in the opposite direction to gravity, and the drag force tries to oppose the

particle movement. The schematic of the forces and their directions on a settling spherical particle are shown in **Figure 2-7**.

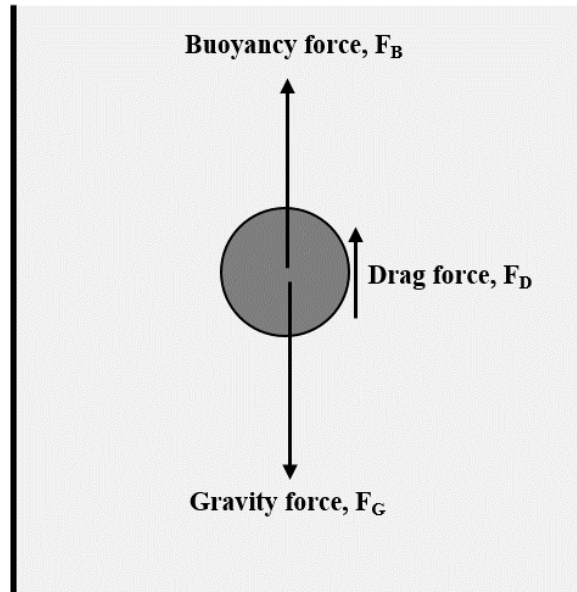


**Figure 2-7. Schematic of forces acting on a settling particle in a Newtonian fluid**

When the particle starts settling down, initially the velocity of the particle will be very high. Due to opposing forces that are acting upwards, the velocity decreases gradually. When the equilibrium stage is reached, downward acting forces will be equal to upward acting forces. So the net acceleration of the settling particle becomes zero thereby it attains a constant velocity of settling [3]. The terminal settling velocity is the constant velocity attained by a settling particle due to gravity in a fluid medium when all the forces on the particle are in equilibrium [3].

For a solid spherical particle of diameter  $D_s$  and density  $\rho_s$  settling in a Newtonian fluid of density  $\rho_f$ , the relation between the constant settling velocity ( $V_s$ ) attained at equilibrium and the drag coefficient ( $C_D$ ) is given by Equation 2-15[3]. The drag coefficient is the ratio of drag force on the settling particle to the product of a characteristic area of the particle and the kinetic energy

per unit volume. The flow regime in which the motion of the particle lies is obtained by calculating particle Reynolds number ( $Re_p$ ) using Equation 2-16 [3] where  $D_p$  is the characteristic length.

$$C_D = \frac{4gD_s(\rho_s - \rho_f)}{3\rho_f V_s^2} \quad \text{Equation 2-15}$$

$$Re_p = \frac{D_p V_s \rho_f}{\mu_f} \quad \text{Equation 2-16}$$

From Equation 2-15 and Equation 2-16, it can be noted that in addition to the particle characteristics, the properties of the fluid system (such as viscosity, density, etc.) also affect the settling velocities of the particles [3]. Also, walls of the fluid container in which the particle is settling will have an effect on the particle settling velocity. If the particle is at a larger distance from the container wall or other particles, i.e. if the particle settling is not affected by them, then it is called as free particle settling [3]. If the solid particle motion is hampered by the other particles or by the nearby wall, then it is called hindered particle settling [3]. The drag coefficient ( $C_D$ ) for hindered settling is likely to be greater than that for free settling, in other words, the particle settling velocity will be lower in the hindered settling.

Particle Reynolds number (which is a function of settling velocity) determines the flow regime in which the particle motion lies and the drag coefficient is highly dependent upon the flow regime so it is a function of particle Reynolds number. The particles settling velocity can easily be back calculated once the drag coefficient for a particular particle Reynolds number is determined. That is why substantial attention was given to develop a correlation between drag coefficient and particle Reynolds number to understand the particle settling behavior at wide flow regimes. The classical work by Stokes et al. [28], analyzing the behavior of settling sphere in a Newtonian fluid,

provided a correlation between drag coefficient ( $C_D$ ) and Reynolds number at creep flow regime ( $Re_p < 1$ ) as shown in Equation 2-17 [3].

$$C_D = \frac{24}{Re_p} \quad \text{Equation 2-17}$$

Later on, among several studies were performed by the researchers, works by Clift et al.[29], Khan & Richardson [30], Flemmer & Banks [31], Turton & Levenspiel [32] and Heider & Levenspiel [33] are worth mentioning to understand the spherical particle settling behavior and calculate sphere settling velocities in Newtonian fluids at different flow regimes.

### 2.3.2 Settling velocity of particles in shear thinning fluid.

The fluids encountered in the industrial applications are non-Newtonian in nature. Estimating the fluid rheological properties at the suitable shear rate is the primary obstacle to accurately predict the settling velocity of the particle in the non-Newtonian fluid. Most of the work done previously was related to shear thinning fluids. Shear thinning is the fluid's property indicating that fluid viscosity decreases with the increasing shear rate. So the fluid viscosity experienced by the particle in the course of settling will be different from the zero shear viscosity of the fluid (i.e. the fluid viscosity when it is un-sheared). Settling of a spherical particle in a shear thinning fluid is commonly studied by using apparent viscosity term to calculate the particle Reynolds number. An example of such shear thinning fluid is the one whose shear stress and shear rate relationship can be described by power law as shown in Equation 2-18 [3].

$$\tau = K \dot{\gamma}^n \quad \text{Equation 2-18}$$

So, the particle Reynolds number for the shear thinning power law type fluids can be evaluated by using Equation 2-19 [34], which is obtained by introducing the apparent viscosity term in Equation 2-16.

$$\text{Re}_p = \frac{D_p V_s \rho_f}{K'} \quad \text{Equation 2-19}$$

However, investigators found out that flow behavior index of the power law fluid ( $n$ ) showed an extra dependence on drag coefficient even after modifying particle Reynolds number using the apparent viscosity [35]. For instance, after conducting settling experiments with fluids such as hydroxyethyl cellulose (HEC), carboxymethyl cellulose (CMC) and polyethylene oxide (PEO), Dallon [36] developed an empirical correlation between spherical particle drag coefficients and Reynolds number of the non-Newtonian fluid [35]. Prakash [37] after experimentation with carboxymethyl cellulose solutions and Peden & Luo [38] with carboxymethyl cellulose and hydroxyl ethyl cellulose solutions, they individually reported that flow behavior index of a power law fluid had an effect on the motion of spheres [35].

Chhabra [39], on the other hand, after reviewing the experimental literature data, stated that the relation between drag coefficient and Reynolds numbers for the power law fluids could be represented by the Newtonian standard drag curve with an average deviation of 30%. But the relevant data from the petroleum field was not taken into account during this study.

### **2.3.2.1 Model for predicting settling velocity of particle in power law visco-inelastic fluid**

Later on, after reanalyzing several previously performed studies, Shah et al. [35] developed a different model to predict the settling velocity of a spherical particle in visco-inelastic power law fluids. He employed the two constants ( $A, B$ ) as a function of power-law flow behavior index ( $n$ ) in the correlation of drag coefficient with the particle Reynolds number. The Shah et al. [35] model

is valid for fluids having flow behavior index values in the range of 0.28-1.0 and the particle Reynolds number values in the range of 0.001-1000. The procedure to calculate the settling velocity of a spherical particle in visco-inelastic power law fluid according to Shah et al. [35] is as follows:

$$\begin{aligned} \text{Step-1:} \quad A &= 6.9148n^2 - 24.838n + 22.642 \\ B &= -0.5067n^2 + 1.3234n - 0.1744 \end{aligned}$$

$$\text{Step-2:} \quad (C_D^{2-n} \text{Re}^2)^{\frac{1}{2}} = \left( \frac{13.08^{2-n} d_p^{n+2} \rho_f^n (\rho_p - \rho_f)^{2-n}}{2^{2(n-1)} K^2} \right)^{\frac{1}{2}}$$

$$\text{Step-3:} \quad \text{Re} = \left( \frac{(C_D^{2-n} \text{Re}^2)^{\frac{1}{2}}}{A} \right)^{\frac{1}{B}}$$

$$\text{Step-4:} \quad V_s = \left( \frac{2^{n-1} K \text{Re}}{d_p^n \rho_f} \right)^{\frac{1}{2-n}}$$

### 2.3.3 Settling velocity of particles in viscoelastic fluids

In the recent decades, usage of viscoelastic fluids for the industrial applications has been in improved demand. Therefore, this increased usage made researchers to study the particle motion in the viscoelastic fluids. Typically, three types of viscoelastic fluids have been investigated in the literature[40]. They are: a) Boger fluids (elastic fluids of non-shear thinning or constant viscosity); b) Shear thinning viscoelastic fluids and; c) Drag reducing fluids. Various theoretical and experimental studies were implemented to understand the particle settling motion in these viscoelastic fluids. These studies tried to measure either drag force on the particle or particles settling velocity in the fluids. The drag force and settling velocity are inversely related to each

other. Higher the drag force, lower the settling velocity and vice versa. Some of the major contributions and observations of those studies are discussed here.

The elastic fluids of almost constant viscosity were first developed by Boger [41] in 1977 by mixing a small quantity of polyacrylamide in Newtonian corn syrup of greater viscosity containing water in little quantity. Later on, other elastic fluids of constant viscosity were prepared by different procedures. These fluids were proven to demonstrate almost constant viscosity but variable first normal stress differences ( $N_1$ ) at a limited range of shear rates [40]. Initially, experiments of particle settling in these Boger fluids had inconsistent outcomes. To quote a few, Chhabra et al.[42] performed sphere settling tests in glucose-based Boger fluids and reported that the drag reduction with the rise in fluid elastic property (defined in terms of Weissenberg number). The Weissenberg number is the product of the shear rate and the relaxation time of the fluid.

On the contrary, experimental studies with polyisobutylene in polybutene based Boger fluids by Chmielewski et al. [43] and Tirtaatmadja et al. [44] witnessed drag enhancement as the Weissenberg number was increased. All the above-mentioned studies had almost insignificant wall effects on the settling particle. Later on, Walters and Tanner [45] hypothesized that for Boger fluids, the drag reduction happens until a certain value of the Weissenberg number, beyond which the drag increases along with the Weissenberg number; this behavior was further substantiated by Degand and Walters [46]. Also Jones et al.[47] performed experiments with Boger fluids by varying the sphere to the cylinder tube diameter and showed that wall effects had a considerable impact on the drag intensification with respect to the Weissenberg number.

Shear thinning viscoelastic fluids are the fluids that possess both shear thinning and viscoelastic behaviors. Observations from the experimental studies of particle motion in shear thinning viscoelastic fluids were contradictory. It was reported by Chhabra [40] that few studies

observed the drag reduction due to viscoelastic nature of the fluids, whereas some other studies stated that shear thinning effects outweighed the viscoelastic effects. For instance, in 1976, Acharya et al. [48, 49] conducted particle settling experiments in shear thinning viscoelastic polymer solutions of carboxymethyl cellulose, polyacrylamide, polyethylene oxide, hydroxyethyl cellulose and observed a decrease in drag at higher Reynolds numbers [48]. He developed an empirical equation considering the effect of viscoelasticity on drag coefficient as shown in Equation 2-20 [49].

$$C_{D_{VE}} = C_{D_{INVE}} \{1 - \alpha(\text{Re}_{PL} \text{Wi})^\beta\} \quad \text{Equation 2-20}$$

Where  $C_{D_{VE}}$  is the drag coefficient of viscoelastic fluid;  $C_{D_{INVE}}$  is the drag coefficient of visco-inelastic fluid;  $\text{Re}_{PL}$  is the particle Reynolds number;  $\text{Wi}$  is the Weissenberg number;  $\alpha$  and  $\beta$  are the constants used whose values after linear regression analysis found to be 0.18 and 0.19 respectively [49]. In 1988, when Acharya [50] worked with uncrosslinked and crosslinked fracturing fluids, he observed that the proppant particles settling velocities in the creeping flow range were controlled by fluid's viscosity parameters but not by fluid's elasticity, and proppant velocities were increased due to fluid's elasticity at intermediate Reynolds number flow range.

Conversely, measurements of drag on particles in 2% solution of polyacrylamide by Broadbent and Mena [51] and measurements of drag around a spherical obstacle in a flow of polyethylene oxide solution by Sigli and Coutanceau [52] demonstrated a drag decline in the creeping flow range. On the other hand, Brule et al. [53] conducted settling experiments with a spherical particle in highly elastic shear thinning fluid prepared by dissolving polyacrylamide in glucose syrup having 21% of water and observed a pronounced decrease in the particle terminal velocity due to increase in the elasticity.

The studies cited above proved the point that the experimental observations of viscoelasticity influence on the particle settling show contradictory results and not converging well. Furthermore it was summarized in the review by Chhabra [40] that as per theoretical studies at low values of the Weissenberg number, no deviation from its Newtonian value is expected in drag caused by viscoelasticity, however, drag enhancement from its Newtonian value might result at moderate values of Weissenberg number ( $Wi$  nearly 2-3) beyond which the drag values are not available. It shows that the results of experimental studies of particle settling in shear thinning viscoelastic fluids were not in greater agreement with the theoretically predicted results. The possible reason for this conflicting observations could be because the experimentally measured velocities of particle had both viscoelasticity and shear thinning effects in consideration, whereas, the theoretical models had only viscoelasticity effect without considering the shear thinning behavioral effects of the fluid [40]. Chhabra [40] also commented that it is difficult to integrate both the viscoelasticity and the shear thinning effects in the theoretical models. This is because their individual influences on the particle settling velocity are not known conclusively since no study in the literature disengaged the effects.

To sum it up, none of the studies mentioned above seemed to be conducted in a controlled way to dissociate the effects of the shear thinning viscosity and the elasticity of the fluid. In this regard, the primary intention of the current research study is to investigate the sole influence of fluid elasticity on particle settling velocity by conducting experiments in the controlled manner of upholding the fluid shear thinning viscosity constant and also to identify the governing parameter between the two to optimize the settling velocity of the particle.

## 2.4 REFERENCES

- [1] Fink, J.K. 2015. Drilling Fluids In *Water-Based Chemicals and Technology for Drilling, Completion, and Workover Fluids*, Chap. 2, 5-114. Boston: Gulf Professional Publishing.
- [2] Barnes, H.A. 2000. *A Handbook of Elementary Rheology*, Aberystwyth: University of Wales, Institute of Non-Newtonian Fluid Mechanics.
- [3] McCabe, W.L., Smith, J.C. and Harriott, P. 2004. *Unit Operations of Chemical Engineering*, New York: McGraw-Hill.
- [4] RheoSense. 2016. Viscosity of Newtonian and Non-Newtonian Fluids, <http://www.rheosense.com/applications/viscosity/newtonian-non-newtonian> (accessed on 20th June 2017).
- [5] Cross, M.M. 1965. Rheology of Non-Newtonian Fluids: A New Flow Equation for Pseudoplastic Systems. *Journal of colloid science* **20** (5): 417-437.
- [6] Sisko, A. 1958. The Flow of Lubricating Greases. *Industrial & Engineering Chemistry* **50** (12): 1789-1792.
- [7] Barnes, H.A., Hutton, J.F. and Walters, K. 1989. *An Introduction to Rheology*, Amsterdam: Elsevier.
- [8] Choi, S.K. 2008. *pH Sensitive Polymers for Novel Conformance Control and Polymer Flooding Applications*. PhD Thesis, University of Texas, , Austin.
- [9] Rouse Jr, P.E. 1953. A Theory of the Linear Viscoelastic Properties of Dilute Solutions of Coiling Polymers. *The Journal of Chemical Physics* **21** (7): 1272-1280. <http://dx.doi.org/10.1063/1.1699180>.
- [10] Zimm, B.H. 1956. Dynamics of Polymer Molecules in Dilute Solution: Viscoelasticity, Flow Birefringence and Dielectric Loss. *The Journal of Chemical Physics* **24** (2): 269-278. <http://dx.doi.org/10.1063/1.1742462>.

- [11] Macosko, C. 1994. *Rheology: Principles, Measurements and Applications*, New York: Wiley-VCH.
- [12] WEE-Solve. Oscillatory Test: Frequency Sweep, <http://www.wee-solve.de/en/frequency-sweep.html> (accessed on 20th June 2017).
- [13] Larson, R.G. 1998. *The Structure and Rheology of Complex Fluids*, New York: Oxford University Press.
- [14] Sunthar, P. 2010. Polymer Rheology. In *Rheology of Complex Fluids*, 171-191. Springer New York.
- [15] Ferry, J.D. 1980. *Viscoelastic Properties of Polymers*, 3rd. edition, New York: Wiley.
- [16] Dehghanpour Hossein Abadi, H. 2008. *Investigation of Viscoelastic Properties of Polymer Based Fluids as a Possible Mechanism of Internal Filter Cake Formation*. Masters, University of Alberta, Edmonton, Canada (Fall 2008).
- [17] Liu, Y., Shaw, M.T. and Tuminello, W.H. 1998. Obtaining Molecular-Weight Distribution Information from the Viscosity Data of Linear Polymer Melts. *Journal of Rheology* **42** (3): 453-476. <http://dx.doi.org/10.1122/1.550951>.
- [18] Shaw, M.T. and Tuminello, W.H. 1994. A Closer Look at the MWD-Viscosity Transform. *Polymer Engineering & Science* **34** (2): 159-165. <http://dx.doi.org/10.1002/pen.760340213>.
- [19] Wulf, K. 1987. Fließverhalten Von Stoffen Und Stoffgemischen. Hg. Von W.-M. Kulicke. Isbn 3-85738-115-4. Basel/Heidelberg/New York: Hüthig Und Wepf Verlag 1986. 487 S., Geb. Dm 168,-. *Acta Polymerica* **38** (8): 507-507. <http://dx.doi.org/10.1002/actp.1987.010380817>.
- [20] Zang, Y.H., Muller, R. and Froelich, D. 1987. Influence of Molecular Weight Distribution on Viscoelastic Constants of Polymer Melts in the Terminal Zone. New Blending Law and Comparison with Experimental Data. *Polymer* **28** (9): 1577-1582. [http://dx.doi.org/10.1016/0032-3861\(87\)90362-4](http://dx.doi.org/10.1016/0032-3861(87)90362-4).

- [21] Dehghanpour, H. and Kuru, E. 2011. Effect of Viscoelasticity on the Filtration Loss Characteristics of Aqueous Polymer Solutions. *Journal of Petroleum Science and Engineering* **76** (1–2): 12-20. <http://dx.doi.org/10.1016/j.petrol.2010.12.005>.
- [22] Doda, A. 2014. *Effect of Viscoelasticity and Alkali on Heavy Oil Eor Performance Using Hpam, 'Aa-Nvp' Co- and Cross-Linked Polymers*. Masters Thesis, University of Alberta, Edmonton, Canada (Spring 2014).
- [23] Urbissinova, T. 2010. *Experimental Investigation of the Effect of Elasticity on the Sweep Efficiency in Viscoelastic Polymer Flooding Operations*. Masters Thesis, University of Alberta, Edmonton, Canada (Fall 2010).
- [24] Urbissinova, T.S., Trivedi, J. and Kuru, E. 2010. Effect of Elasticity During Viscoelastic Polymer Flooding: A Possible Mechanism of Increasing the Sweep Efficiency. *Journal of Canadian Petroleum Technology* **49** (12): 49-56. SPE-133471-PA. <http://dx.doi.org/10.2118/133471-PA>.
- [25] Veerabhadrapa, S.K. 2012. *Study of Effects of Polymer Elasticity on Enhanced Oil Recovery by Core Flooding and Visualization Experiments*. Masters Thesis, University of Alberta, Edmonton, Canada (Fall 2012).
- [26] Veerabhadrapa, S.K., Doda, A., Trivedi, J.J. and Kuru, E. 2013. On the Effect of Polymer Elasticity on Secondary and Tertiary Oil Recovery. *Industrial & Engineering Chemistry Research* **52** (51): 18421-18428. <http://dx.doi.org/10.1021/ie4026456>.
- [27] Veerabhadrapa, S.K., Trivedi, J.J. and Kuru, E. 2013. Visual Confirmation of the Elasticity Dependence of Unstable Secondary Polymer Floods. *Industrial & Engineering Chemistry Research* **52** (18): 6234-6241. <http://dx.doi.org/10.1021/ie303241b>.
- [28] Stokes, G.G. 1851. *On the Effect of the Internal Friction of Fluids on the Motion of Pendulums*: Pitt Press.
- [29] Clift, R., Grace, J. and Weber, M. 1978. *Bubbles, Drops and Particles*, Academic Press, New York.

- [30] Khan, A.R. and Richardson, J.F. 1987. The Resistance to Motion of a Solid Sphere in a Fluid. *Chemical Engineering Communications* **62** (1-6): 135-150. <http://dx.doi.org/10.1080/00986448708912056>.
- [31] Flemmer, R.L.C. and Banks, C.L. 1986. On the Drag Coefficient of a Sphere. *Powder Technology* **48** (3): 217-221. [http://dx.doi.org/10.1016/0032-5910\(86\)80044-4](http://dx.doi.org/10.1016/0032-5910(86)80044-4).
- [32] Turton, R. and Levenspiel, O. 1986. A Short Note on the Drag Correlation for Spheres. *Powder Technology* **47** (1): 83-86. [http://dx.doi.org/10.1016/0032-5910\(86\)80012-2](http://dx.doi.org/10.1016/0032-5910(86)80012-2).
- [33] Haider, A. and Levenspiel, O. 1989. Drag Coefficient and Terminal Velocity of Spherical and Nonspherical Particles. *Powder Technology* **58** (1): 63-70. [http://dx.doi.org/10.1016/0032-5910\(89\)80008-7](http://dx.doi.org/10.1016/0032-5910(89)80008-7).
- [34] Lali, A.M., Khare, A.S., Joshi, J.B. and Nigam, K.D.P. 1989. Behaviour of Solid Particles in Viscous Non-Newtonian Solutions: Settling Velocity, Wall Effects and Bed Expansion in Solid-Liquid Fluidized Beds. *Powder Technology* **57** (1): 39-50. [http://dx.doi.org/10.1016/0032-5910\(89\)80102-0](http://dx.doi.org/10.1016/0032-5910(89)80102-0).
- [35] Shah, S.N., El Fadili, Y. and Chhabra, R.P. 2007. New Model for Single Spherical Particle Settling Velocity in Power Law (Visco-Inelastic) Fluids. *International Journal of Multiphase Flow* **33** (1): 51-66. <http://dx.doi.org/10.1016/j.ijmultiphaseflow.2006.06.006>.
- [36] Dallon, D.S. 1967. *A Drag-Coefficient Correlation for Spheres Settling in Ellis Fluids*. Ph. D Thesis, University of Utah, Salt Lake City, UT.
- [37] Prakash, S. 1983. Experimental Evaluation of Terminal Velocity in Non-Newtonian Fluids in the Turbulent Region. *Chem. Eng* **25**: 1-4.
- [38] Peden, J.M. and Luo, Y. 1987. Settling Velocity of Various Shaped Particles in Drilling and Fracturing Fluids. *SPE Drilling Engineering* **2** (04): 337-343.
- [39] Chhabra, R.P. 1990. Motion of Spheres in Power Law (Viscoelastic) Fluids at Intermediate Reynolds Numbers: A Unified Approach. *Chemical Engineering and*

- Processing: Process Intensification* **28** (2): 89-94. [http://dx.doi.org/10.1016/0255-2701\(90\)80004-O](http://dx.doi.org/10.1016/0255-2701(90)80004-O).
- [40] Chhabra, R.P. 2007. *Bubbles, Drops, and Particles in Non-Newtonian Fluids, Second Edition*: CRC Press, Taylor & Francis Group.
- [41] Boger, D.V. 1977. A Highly Elastic Constant-Viscosity Fluid. *Journal of Non-Newtonian Fluid Mechanics* **3** (1): 87-91. [http://dx.doi.org/10.1016/0377-0257\(77\)80014-1](http://dx.doi.org/10.1016/0377-0257(77)80014-1).
- [42] Chhabra, R.P., Uhlherr, P.H.T. and Boger, D.V. 1980. The Influence of Fluid Elasticity on the Drag Coefficient for Creeping Flow around a Sphere. *Journal of Non-Newtonian Fluid Mechanics* **6** (3): 187-199. [http://dx.doi.org/10.1016/0377-0257\(80\)80002-4](http://dx.doi.org/10.1016/0377-0257(80)80002-4).
- [43] Chmielewski, C., Nichols, K.L. and Jayaraman, K. 1990. A Comparison of the Drag Coefficients of Spheres Translating in Corn-Syrup-Based and Polybutene-Based Boger Fluids. *Journal of Non-Newtonian Fluid Mechanics* **35** (1): 37-49. [http://dx.doi.org/10.1016/0377-0257\(90\)85071-6](http://dx.doi.org/10.1016/0377-0257(90)85071-6).
- [44] Tirtaatmadja, V., Uhlherr, P.H.T. and Sridhar, T. 1990. Creeping Motion of Spheres in Fluid M1. *Journal of Non-Newtonian Fluid Mechanics* **35** (2): 327-337. [http://dx.doi.org/10.1016/0377-0257\(90\)85057-6](http://dx.doi.org/10.1016/0377-0257(90)85057-6).
- [45] Walters, K. and Tanner, R. 1992. The Motion of a Sphere through an Elastic Fluid. In *Transport Processes in Bubbles, Drops and Particles*, ed. Chhabra, R. and De Kee, D., Chap. 3. New York: Hemisphere.
- [46] Degand, E. and Walters, K. 1995. On the Motion of a Sphere Falling through an Elastic Liquid Contained in a Tightly-Fitting Cylindrical Container. *Journal of Non-Newtonian Fluid Mechanics* **57** (1): 103-115. [http://dx.doi.org/10.1016/0377-0257\(94\)01298-V](http://dx.doi.org/10.1016/0377-0257(94)01298-V).
- [47] Jones, W.M., Price, A.H. and Walters, K. 1994. The Motion of a Sphere Falling under Gravity in a Constant-Viscosity Elastic Liquid. *Journal of Non-Newtonian Fluid Mechanics* **53**: 175-196. [http://dx.doi.org/10.1016/0377-0257\(94\)85048-8](http://dx.doi.org/10.1016/0377-0257(94)85048-8).

- [48] Acharya, A., Mashelkar, R.A. and Ulbrecht, J. 1976. Flow of Inelastic and Viscoelastic Fluids Past a Sphere. Part II: Anomalous Separation in the Viscoelastic Fluid Flow. *Rheologica Acta* **15** (9): 471-478. <http://dx.doi.org/10.1007/bf01530349>.
- [49] Acharya, A., Mashelkar, R.A. and Ulbrecht, J. 1976. Flow of Inelastic and Viscoelastic Fluids Past a Sphere. Part I. Drag Coefficient in Creeping and Boundary-Layer Flows. *Rheologica Acta* **15** (9): 454-470. <http://dx.doi.org/10.1007/bf01530348>.
- [50] Acharya, A.R. 1988. Viscoelasticity of Crosslinked Fracturing Fluids and Proppant Transport. *SPE Production Engineering* **3**: 483-488. SPE-15937-PA. <http://dx.doi.org/10.2118/15937-PA>.
- [51] Broadbent, J.M. and Mena, B. 1974. Slow Flow of an Elastico-Viscous Fluid Past Cylinders and Spheres. *The Chemical Engineering Journal* **8** (1): 11-19. [http://dx.doi.org/10.1016/0300-9467\(74\)80014-6](http://dx.doi.org/10.1016/0300-9467(74)80014-6).
- [52] Sigli, D. and Coutanceau, M. 1977. Effect of Finite Boundaries on the Slow Laminar Isothermal Flow of a Viscoelastic Fluid around a Spherical Obstacle. *Journal of Non-Newtonian Fluid Mechanics* **2** (1): 1-21. [http://dx.doi.org/10.1016/0377-0257\(77\)80029-3](http://dx.doi.org/10.1016/0377-0257(77)80029-3).
- [53] Van den Brule, B.H.A.A. and Gheissary, G. 1993. Effects of Fluid Elasticity on the Static and Dynamic Settling of a Spherical Particle. *Journal of Non-Newtonian Fluid Mechanics* **49** (1): 123-132. [http://dx.doi.org/10.1016/0377-0257\(93\)85026-7](http://dx.doi.org/10.1016/0377-0257(93)85026-7).

## **CHAPTER 3: EXPERIMENTAL PROGRAM**

This chapter comprises of: (1) the description of materials used in the current experimental study. (2) The method to prepare test fluids of aqueous Partially Hydrolyzed Polyacrylamide (HPAM) polymer solutions. (3) The description of rheometers used in the current study and the rheological measurements performed to characterize the test fluids of HPAM polymer. (4) The description of experimental setup and procedure to measure settling velocities of particles in the test fluids using Particle Image Shadowgraph (PIS) technique. (5) The methodology followed to validate the PIS measurements. (6) Sources of errors in the experimental setup & procedure and precautions to avoid them.

### 3.1 MATERIALS

The description of various materials that were used in the course of study is provided in this subsection.

#### 3.1.1 Glass spheres

In the present study, glass spheres were used as the particles to perform settling velocity measurements. For this purpose, glass spheres of four different diameters were used. These glass spheres were acquired from Corposular’s Glass Spacers Millibeads. The dimensions and shape of these glass spheres were of high precision, and the specific gravity of these spheres was 2.51. The diameters of these glass spheres specified by the manufacturer are given in **Table 3-1**.

**Table 3-1. Details of the diameters of glass spheres specified by manufacturer**

<b>Diameter specified by manufacturer (mm)</b>	
0.71 ± 0.02	1.5± 0.03
1.18± 0.02	2.00± 0.04

### 3.1.2 HPAM polymers

Partially hydrolyzed polyacrylamide (HPAM) was the polymer used in the present study. It is a product of copolymerization between the monomers of acrylamide and acrylic acid [1]. As shown in **Figure 3-1**, HPAM is the straight chain polymer of partially hydrolyzed acrylamide monomers [2]. Its degree of hydrolysis provides the fraction of this polymer chain that has been hydrolyzed. The degree of hydrolysis affects the physical properties of the polymer such as stability, hardness sensitivity, solubility, etc. [2]. The average molecular weight of this polymer is typically in the range of 2 to 20 million.

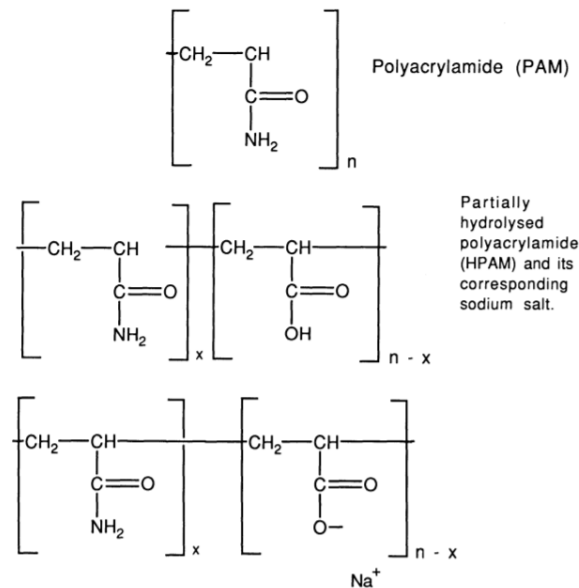


**Figure 3-1. The primary chain structure of polyacrylamide and partially hydrolyzed polyacrylamide [2]**

Three different grades of HPAM polymers of various molecular weights were used to prepare the test fluids of the present study. These HPAM polymers were water soluble anionic polymers with 25-30% of the degree of hydrolysis. These polymers were supplied in the form of odorless white granular powder by SNF Floerger Company. The details of HPAM polymers used in this study are provided in **Table 3-2**.

**Table 3-2. HPAM grades along with their SNF batch lot number and average molecular weight values**

<b>HPAM grade</b>	<b>Batch lot number</b>	<b>Average molecular weight (g/gmol)</b>
Flopaam 3630S	GJ 1008	$20 \times 10^6$
Flopaam 3330S	V5054	$8 \times 10^6$
Flobeads AB005V	BB 2481	$0.5 \times 10^6$

### **3.2 COMPOSITIONS OF THE HPAM POLYMER TEST FLUIDS**

The test fluids in the present study were formulated by mixing three different grades of HPAM. The polymer test fluids used in the present study were classified into two groups, Group-A and Group-B. Further down, Group-B was classified into two sub-sets of test fluids, Set-I and Set-II.

The objective of Group-A test fluids was to prepare samples of almost similar shear viscosity characteristics while showing significantly different elastic properties. The aim of the Set-I test fluids in Group-B was also same as that of Group-A. However, the concentration of polymer blend in the test fluids of Group-A was higher than that of the test fluids in Set-I of Group B. The Set-II of Group B test fluids were prepared with the objective to have samples of similar elastic properties but significantly different shear viscosity characteristics. The schematic of this classification of test fluids along with their objectives is provided in **Figure 3-2**.

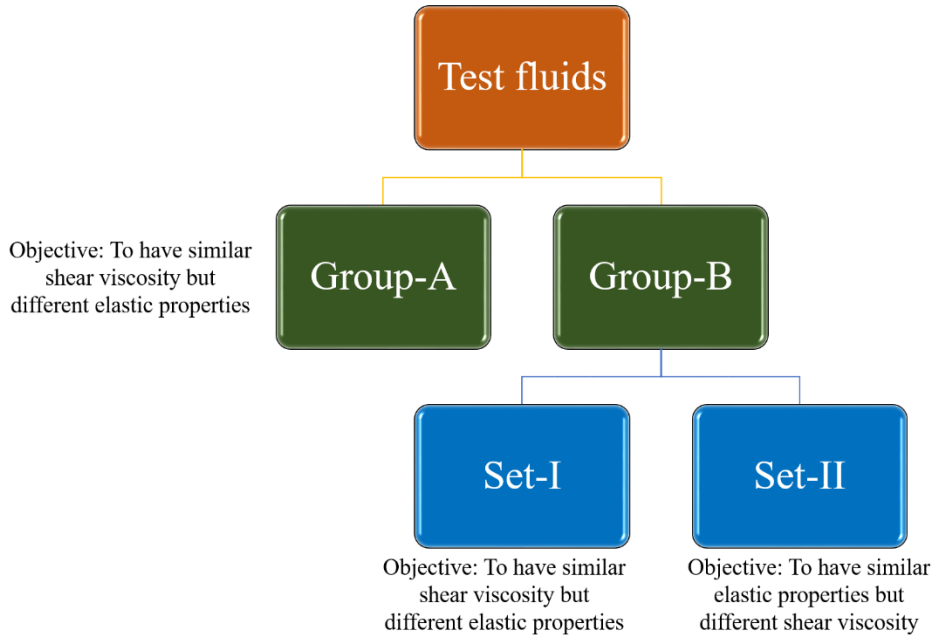


**Figure 3-2. Classification of the test fluids used in the present study**

### 3.2.1 Test fluids of Group-A

Group-A comprised of four test fluids and these were formulated in such a way that the average molecular weight of all test fluids was constant and the molecular weight distribution (MWD) was different. The average molecular weight of the polymer blend ( $M_{w,B}$ ) was calculated by using Equation 3-1, and molecular weight distribution (MWD) in the polymer blends was quantified in terms of polydispersity index (I) using Equation 3-2.

$$M_{w,B} = \prod_{i=1}^n M_{w,i}^{\omega_i} \quad \text{Equation 3-1}$$

$$I = \frac{M_w}{M_n} = \left( \sum_{i=1}^n \omega_i M_{w,i} \right) \times \left( \sum_{i=1}^n \frac{\omega_i}{M_{w,i}} \right) \quad \text{Equation 3-2}$$

The average molecular weight of the polymer blend ( $M_{w,B}$ ) in the test fluids of Group-A was maintained to be 8,000,000 g/gmol. In Group-A, the concentration of the polymer in the test

fluid A-1 was 0.09 wt% and in others (fluid A-2 to fluid A-4) was 0.1 wt%. The composition details of polymer blends of the Group-A test fluids are provided in **Table 3-3**.

**Table 3-3. Polymer blend composition details of Group-A test fluids**

Sample	Conc. of polymer blend (wt%)	Wt % of HPAM of Molecular weight (g/gmol)			Polydispersity Index (I)
		20 x 10 <sup>6</sup>	8 x 10 <sup>6</sup>	0.5 x 10 <sup>6</sup>	
Fluid A-1	0.09	0	100	1	1
Fluid A-2	0.1	35.64	52.58	11.8	3.6
Fluid A-3	0.1	42.13	43.95	13.9	4.26
Fluid A-4	0.1	53.58	28.72	17.7	5.5

### 3.2.2 Test fluids of Group-B

The Set-I of Group-B comprised of three test fluids (B-1, B-2, and B-3) and they were formulated in such a way that the average molecular weight of all test fluids was constant and the molecular weight distribution (MWD) was different. The average molecular weight of the polymer blend ( $M_{w,B}$ ) in the test fluids of Set-I of Group B was maintained to be 8,000,000 g/gmol. In Set-I of Group B, the concentration of the polymer in the test fluid B-1 was 0.045 wt% and in others (fluid B-2 & fluid B-3) was 0.05 wt%. The composition details of polymer blends of the Set-I of Group-B fluids are provided in **Table 3-4**

**Table 3-4. Polymer blend composition details of the test fluids in Set-I of Group-B**

Sample	Conc. of polymer blend (wt%)	Wt % of HPAM of Molecular weight (g/gmol)			Polydispersity Index (I)
		20 x 10 <sup>6</sup>	8 x 10 <sup>6</sup>	0.5 x 10 <sup>6</sup>	
Fluid B-1	0.045	0	100	1	1
Fluid B-2	0.05	35.64	52.58	11.8	3.6
Fluid B-3	0.05	42.13	43.95	13.9	4.26

The test fluids in Set-II of Group-B were formulated by maintaining constant average molecular weight and molecular weight distribution but different concentration of polymer in the test fluids. The HPAM polymer having molecular weight of 8,000,000 g/gmol (Flopaam 3330S) was used to prepare Set-II of Group B test fluids. The composition details of the Set-II of Group B test fluids are provided in **Table 3-5**.

**Table 3-5. Polymer blend composition details of the test fluids in Set-II of Group-B**

Sample	Conc. of polymer blend (wt%)	Wt % of HPAM of	Polydispersity
		Molecular weight (g/gmol)	Index
		$8 \times 10^6$	<b>(I)</b>
Fluid B-4	0.03	100	1
Fluid B-5	0.045	100	1
Fluid B-6	0.09	100	1

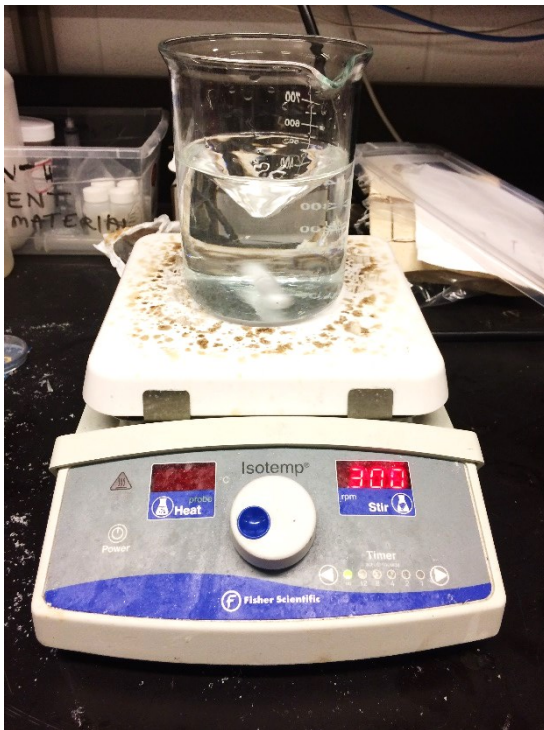
As it can be seen, the test fluid B-5 was same as the test fluid B-1 and also test fluid A-1 was same as test fluid B-6. However, they were named differently in the groups to avoid confusion and maintain better clarity.

### **3.3 MIXING PROCEDURE FOLLOWED TO PREPARE HPAM TEST FLUIDS**

The mixing procedure followed to prepare all the test fluids of Group-A and Group-B was similar to the one followed by Foshee et al.[3]. The steps followed to prepare the test fluids were: (i) De-ionized water of calculated amount was taken and kept for stirring at 300 rpm; (ii) Appropriate amounts (based on wt %) of HPAM polymers of three grades were added on to the well-developed vortex shoulder in the decreasing order of their molecular weights; (iii) After adding the polymers, the solution was stirred at 100 rpm for 2 h. The stirring speed was reduced from 300 to 100 rpm to avoid mechanical degradation of the polymers; (iv) Once the stirring was

completed, the solution was allowed to stand still overnight to remove air bubbles. Filtration was not required as all the test fluids of Group-A and Group-B were clear and transparent.

While scouting the combinations of HPAM polymers, test fluids were prepared in smaller amounts of 500g, and while preparing test fluids for settling velocity measurement experiments, test fluids were prepared in larger quantities of 10kg. Two instruments were used to prepare the test fluids depending upon the amount of the test fluid. A magnetic stirrer was used to prepare 500g of the test fluid, and the overhead mixer with a stirring blade was used to prepare 10kg of the test fluid. The speed of the overhead mixer was controlled by installing variable frequency drive (VFD). The magnetic stirrer and the overhead mixer with a stirring blade that were used for the study are shown in **Figure 3-3**.



(a)



(b)

**Figure 3-3. Equipment used: (a) Magnetic stirrer (b) Overhead mixer**

### **3.4 CHARACTERIZATION OF TEST FLUIDS**

#### **3.4.1 Density measurements**

The density of the test fluids was determined by measuring the weight of the test fluid using the weighing balance of intelligent weighing technology that could precisely measure up to 0.1mg and the volume of the test fluid using Pyrex Vista no. 70024 of 10 ml measuring jar that could accurately measure volume up to 0.1 ml. Later on, the density of the test fluid was calculated by dividing the weight of the test fluid by its volume. Average value of three density readings was taken for every test fluid.

#### **3.4.2 Rheometers used for rheological measurements**

All the test fluids in the present study were characterized depending upon their rheological properties. Therefore, performing accurate measurements of the rheological properties of the test fluids was an essential module of the experimental program. Two different rheometers i.e. Bohlin rheometer and AR G2 rheometer were used to perform rheological measurements in the study.

##### **3.4.2.1 Bohlin rheometer**

The rheological properties of the test fluids of Group-A were measured by using stress controlled mode of C-VOR rotational rheometer from Bohlin Instruments. 40mm & 4° cone and plate geometry was used and all the measurements are conducted at 25°C. The diameter of the fixed bottom plate was 60mm, and the gap between the cone and plate was 150 microns. **Figure 3-4** shows the image of the Bohlin rheometer. Due to lower viscosity levels, the test fluids of Group-B were not tested using Bohlin rheometer.



**Figure 3-4. Bohlin rheometer**

#### **3.4.2.2 AR G2 rheometer**

The rheological properties of the test fluids of Group-B (Set-I and Set-II) were measured by using stress controlled mode of AR G2 rheometer. Peltier steel 988689 concentric cylinder (cup and bob) geometry was used, diameters of cup and bob were 30 mm and 28 mm respectively and the bob length was 42 mm. All the rheological measurements were performed at 25°C. **Figure 3-5** shows the image of the AR G2 rheometer along with the concentric cylinder geometry used for the study.

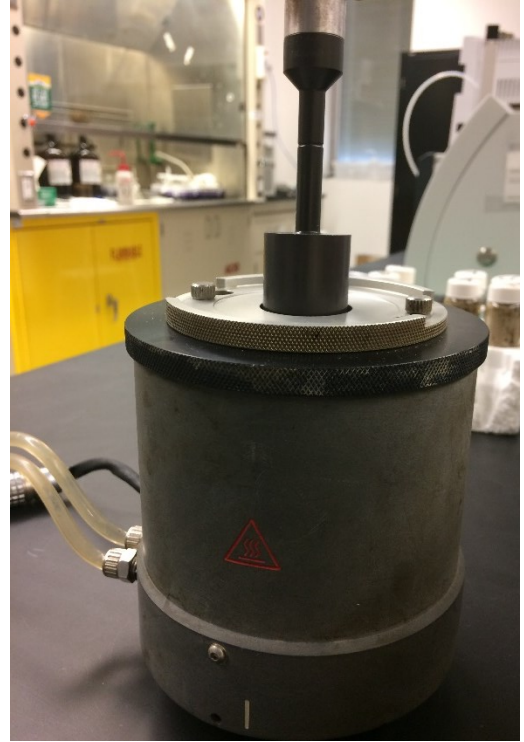
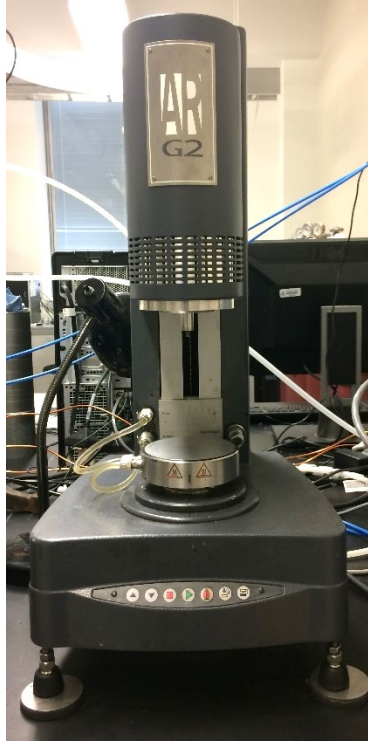


**Figure 3-5. AR G2 rheometer with concentric cylinder (cup and bob) geometry**

### **3.4.3 Rheological measurements performed**

In this study, the test fluids of HPAM polymers were characterized based upon their rheological properties. The rheological measurements such as shear viscosity and oscillatory frequency sweep measurements were performed on the rheometers shown in **Figure 3-4** and **Figure 3-5**. The details of those measurement conditions are explained below.

#### **3.4.3.1 Shear viscosity measurements**

In the shear viscosity measurements, the shear stress on the test fluid is measured for the applied shear rate, and the shear rate is measured if the shear stress is applied. The viscosity of the test fluid is then calculated from the shear stress and the shear rate relationship. In the present study, shear stress and viscosity of the test fluids were measured as a function of shear rates in the range of 1 to 200  $\text{s}^{-1}$ . The shear stress profile and the viscosity profile as a function of shear rate

were plotted using this data to represent and to compare the shear viscosity characteristics of the test fluids.

### 3.4.3.2 Oscillatory frequency sweep measurements

When a low stress or strain is applied to any viscoelastic material, the influence of elastic component of the material will be more dominant on its flow behavior. Therefore, proper rheological measurements such as oscillatory measurements are essential to characterize the viscoelastic properties of the test fluids.

In oscillatory frequency sweep measurements, a low value of stress is applied sinusoidally on the material at various ranges of angular frequencies. The elastic and viscous components of the material are determined by measuring the sinusoidal responses of strain in each cycle. The reason for applying the very low value of stress is to avoid breakage of material structure. For an ideal solid, the sinusoidal response of the strain will be completely in phase (phase angle,  $\delta$  will be  $0^\circ$ ) with the applied sinusoidal stress as the stress is directly proportional to strain for pure solids. Whereas, for an ideal liquid, the sinusoidal response of the strain will be completely out of phase (phase angle,  $\delta$  will be  $90^\circ$ ) with the applied sinusoidal stress as stress is directly proportional to strain rate for pure liquids.

The phase angle will always be between  $0^\circ$  and  $90^\circ$  for a viscoelastic material. In the oscillatory measurements, the instantaneous ratios of stress and strain applied to the material are represented by the Complex modulus ( $G^*$ ), which is the combination of both elastic modulus ( $G'$ ) and viscous ( $G''$ ) modulus. The elastic modulus represents the solid-like behavior, and the viscous component represents the liquid-like behavior of the material. The elastic modulus is also known as storage modulus as it denotes the energy stored in the material to recover and the viscous

modulus is also known as loss modulus as it signifies the energy dissipated in the flow. The relationship between  $G^*$ ,  $G'$ ,  $G''$  and  $\delta$  is shown in Equation 3-3 and Equation 3-4.

$$G' = G^* \cos \delta \quad \text{Equation 3-3}$$

$$G'' = G^* \sin \delta \quad \text{Equation 3-4}$$

In the present study, oscillatory frequency sweep measurements were performed to measure the elastic moduli and the viscous moduli of all the test fluids as a function of angular frequency in the range of  $10^{-3}$  to 5 rad/s at a constant stress of 0.006 Pa.

### **3.5 PARTICLE IMAGE SHADOWGRAPH (PIS) TECHNIQUE AND ITS EXPERIMENTAL SETUP**

The settling velocities of particles in the test fluids were measured using particle image shadowgraph technique. The following subsections will provide detailed description of the PIS technique, its experimental setup, experimental procedure to measure the settling velocities of particles and the process followed to calibrate the camera.

#### **3.5.1 PIS technique**

In the literature survey conducted by the researchers at Pacific Northwest National Laboratory (PNNL) about the available methods and technologies to investigate particle size and settling behavior, it was recognized that the most advantageous methodology is to employ settling columns equipped with image-capturing facility for recording and software to examine the recorded images [4-8]. Later on, various analytical approaches to find particle sizes and settling velocities were perceived and new measurement techniques were designed and constructed. The shadowgraph is one such technique that measures particle size and velocity by means of a non-intrusive optical image [9]. This method is independent of the material and shape of the particle being observed [10]. The shadowgraph technique has been proven to be more efficient and used extensively to measure settling velocities of interested objects in the past[6-8].

The shadowgraph technique is an optical technique that involves only a light source and a recording device to perform the measurements [11]. Since the light cannot pass through solid objects, it gets refracted around the object and the remaining un-deflected ones result in shadow formation [12]. Hence, the fundamental principle of this measurement technique is that whenever a light passes through the mediums of different refractive indices, shadows are formed [12]. In general, this technique is pertinent to use for the systems when the study involves transparent medium and large differences in refractive indices of media (such as air and water) [13]. The illumination source and the recording element are the two key elements in the shadowgraph setup. The illumination source is to maintain consistent background on the recording element, and the light from the source also gets refracted around the object in the study [13]. The recording element is an optical system in general used to capture the image of the object's shadow [13]. Since the parameters such as magnification, field of view, depth of field, focal length, light intensity and exposure time determine the quality of shadow images in terms of contrast, sharpness and brightness, the specifications of the illumination source and the recording element are critical [13]. However, this technique is independent of shape and material of the particles and efficient enough to measure the particle sizes as small as  $5\mu\text{m}$  [14].

### **3.5.2 PIS experimental setup and its components**

The Particle Image Shadowgraph (PIS) experimental setup and its components used to measure the settling velocities of particles are discussed in this section. The schematic of PIS experimental setup is shown in **Figure 3-6**. The type of illumination source and the camera specifications depend upon the particle size and its velocity in the medium. The components of the setup are:

- i. Illumination source – comprises of New wave research laser solo III, Lavigation illumination diffuser of higher efficiency and a diffuser

- ii. Recording device – comprises of Lavigation Image Intense Camera and 12x Navitar lens
- iii. Fluid particle column
- iv. Data Acquisition (DAQ) software – Lavigation Davis 8.3 software

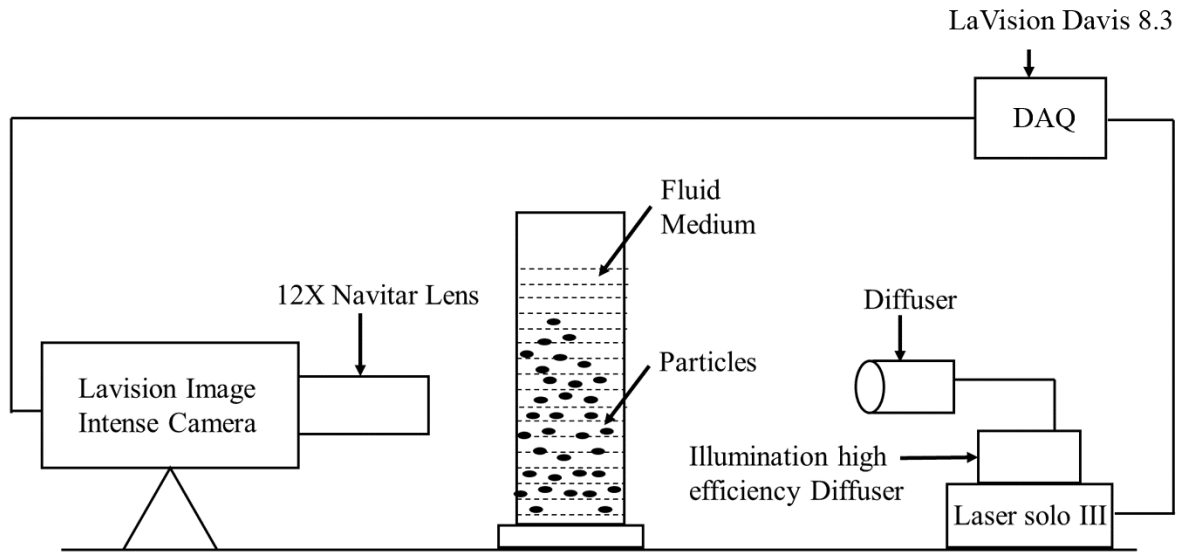


**Figure 3-6. Schematic diagram of particle image shadowgraph experimental setup**

A double pulsed Solo III Class 4 Laser was the illumination source which was attached to a Lavigation circular diffuser of high efficiency. As shown in **Figure 3-7**, it was a Nd:YAG laser from New Wave Research and its wavelength was 532 nm with a frequency of 15 Hz [9, 15]. This laser could produce two pulses of light in a modifiable time period [9, 15]. This pulsed laser was chosen because it was possible to capture the motions of more than 100 m/s by using short pulse laser [14].



**Figure 3-7. Nd:YAG laser from New Wave Research**

The double pulsed laser was connected to the diffuser which was used to diffuse the laser for better background illumination. A spot free backlighting with ultra-short light pulses of high intensity was delivered by the facility of wavelength conversion located inside this diffuser [9, 16]. Input and output apertures of this diffuser were 9 mm and 120 mm respectively. 100 mJ was the minimum recommended laser power for this diffuser and 20 ns as the duration of pulse [9, 16]. The diffuser and the illumination high-efficiency diffuser are shown in **Figure 3-8**.



(a)



(b)

**Figure 3-8. Picture of (a) diffuser and (b) illumination high efficiency diffuser**

Lavision image intense double framed camera and 12x Navitar lens were the essential parts of the image recording segment. The camera was a charge couple device (CCD) that works on the photoelectric principle that transforms photons into electric charge and becomes a digital copy of light patterns falling on this device [17]. This double framed high resolution camera had a CCD sensor of 1376×1040 pixels CCD sensor having 5 frames per sec framing rate and capacity to convey 12-bit digital images. This camera was selected to meet the requirement of capturing the particle image at high speed by tracking the particle movement in the fluid medium. The built-in electronic shutter in the camera was designed to capture images at two different exposure time within a short interval of the time duration (as short as 500 ns). The obtained two frames should be in coordinated with the pulsed light source because of their different exposures times [9]. The time durations between the two image frames were varied depending upon the particle velocity.



**Figure 3-9. LAvision image intense double framed camera with 12x Navitar lens**

The 12x Navitar lens was mounted on the camera, and this lens was suitable for a working distance of 32mm-341mm with a maximum magnification of 12x. The field of view was dependent upon the type of lens and distance between lens front and point of interest. The field of view with the current experimental setup was approximately 13 mm x10 mm. The double framed camera

having mounted with the 12x Navitar lens that was used in the present study is shown in **Figure 3-9**.

The fluid particle column was an acrylic-made transparent rectangular column of height 70 cm, and various test fluids of HPAM polymer solutions were used as fluid mediums in the experiments. Lavisision Davis 8.3 was used as a data acquisition software to obtain size and velocity of the particles in the images. Davis 8.3 followed two-step segmentation algorithm to perform size and velocity measurements. The first step of the algorithm was to detect the particles in the interested area whose dimensions were chosen based upon the field of view and the second step was to determine the particle size, shape and position by analyzing them in the interested area. Differences between the image intensity (object appears dark, and the background appears bright) were used to recognize the particles. Once the particles were recognized, the velocities were determined based on the particle displacement in x and y directions between the two consecutive images captured at a known time interval,  $\Delta t$ . The schematic of the particle velocity calculation is shown in **Figure 3-10**. Similar experimental setup was used in the past to measure particles settling velocity in the fluids [9, 18, 19].

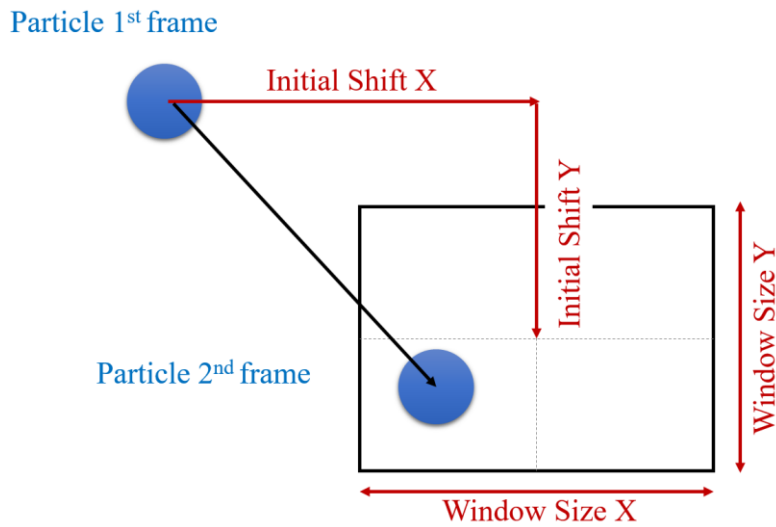


**Figure 3-10. Schematic of the particle velocity calculation [14]**

### 3.5.3 Camera calibration procedure

Accurate camera calibration and orientation procedures are most crucial steps to extract precise and reliable data from images [20]. Among the several methods to calibrate cameras, one of the most commonly practiced methods is physical calibration. In the physical calibration process, a pre-known distance value is assigned between two points, and the captured image is scaled accordingly. Conversion of the image's pixel into a real coordinates is very essential for accuracy. At the time of calibration and image acquisition, the position of camera should be fixed and undisturbed [21, 22].

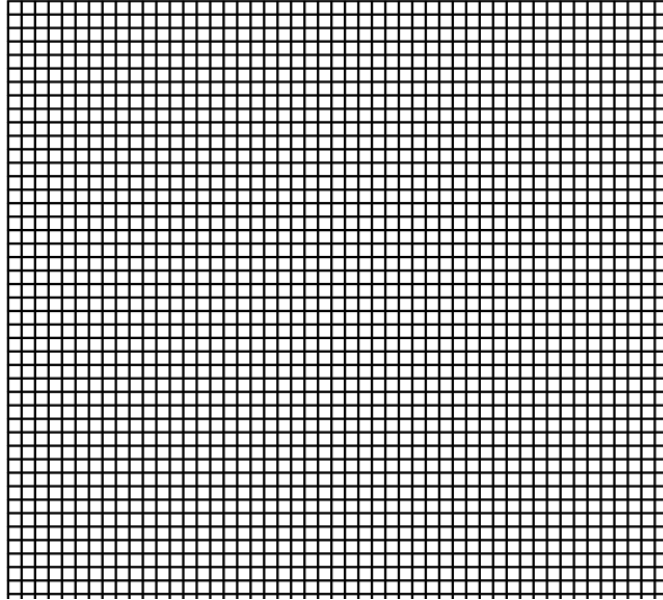


**Figure 3-11. Calibration sheet used to calibrate the camera**

The camera in the current experimental study was calibrated using a grid pattern mainly designed using MS Visio software. The grids were at distance of 1.5 mm from each other; they were printed in black color on a white background. The grid pattern used for the calibration of the camera is shown in **Figure 3-11**. Since this experiment was performed to capture the particles in a fluid media, the calibration was also performed in the same fluid media. The calibration sheet of the grid pattern shown in **Figure 3-11** was inserted in the fluid particle column having the test fluid. The camera lens was then adjusted to focus and capture the calibration sheet grid pattern. After capturing, the image of the calibration sheet was imported to Davis 8.3 software under ParticleMaster Shadow project. In scaling option of this software, as shown in **Figure 3-12**, two point marks on the image were selected in such a way that the distance between them must be large enough and also they had to be lying along the x-axis. The physical distance between the points selected was already known,  $d$  mm. From the pixel option in software, a number of pixels between

these two points was calculated to be  $n$  say. Then one pixel should be equal to  $d/n$  mm. By this way, the image was mapped from pixel space to physical space [14].

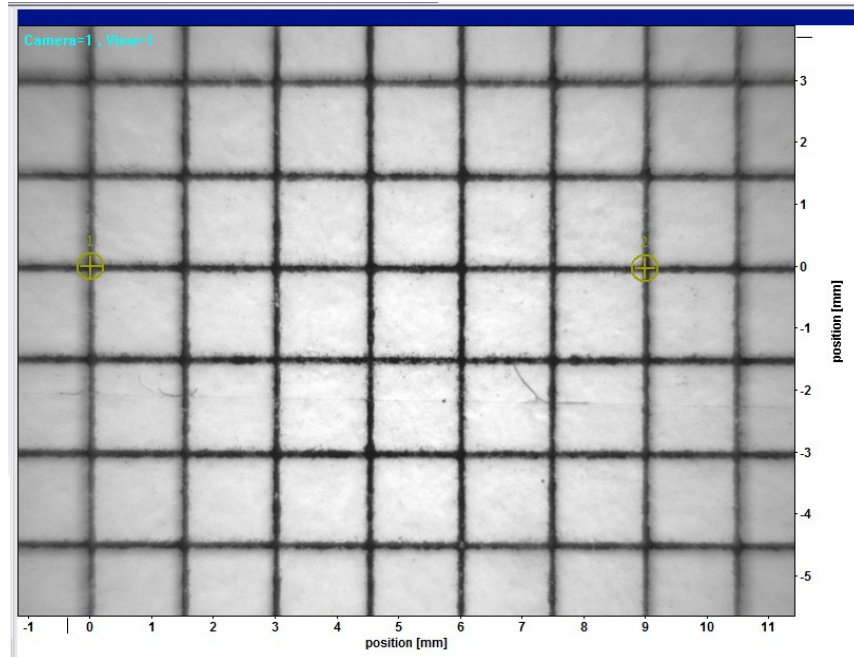


**Figure 3-12. Image scaling process in Davis 8.3 software**

### **3.6 PROCEDURE TO MEASURE PARTICLE SETTLING VELOCITY**

The fluid particle column was filled with the test fluid (in which the particle velocities are to be measured), and the test fluid was left undisturbed for at least 12h to remove air bubbles in the medium. Presence of any air bubbles in the fluid while capturing images would cause noise in the images. The double pulsed laser was placed on one side of the fluid particle column, and the double framed camera was placed on the opposite side. The calibration sheet was inserted in the fluid and the camera was connected to the computer in which Davis 8.3 software was installed. By adjusting the 12x Navitar lens that was attached to the camera, the grid pattern of the calibration sheet was focused in 13 mm x 10 mm of the field of view.

Davis 8.3 software was run by clicking on its icon on the computer, and new file was created under the project type of ParticleMaster Shadowgraph. The camera temperature was ensured to be below  $-11^{\circ}\text{C}$  before switching on the double pulsed laser. The mode of the laser system was first changed from internal to external by pressing down the buttons of the flash lamp, and SW and the knob for the load were turned to high on the processor. On the Davis 8.3 software interface, the laser power was adjusted so that first pulse (1A) was 20% and second pulse (1B) was 1%. The second pulse power had to be lower because its exposure would be higher compared to that of the first pulse. The timing between the image frames was chosen depending upon the particle sizes. For instance, higher timing was chosen for smaller particles and lower timing for larger particles. After completion of this physical setup, image system was scaled by capturing the image of the focused grid pattern of the calibration sheet. Two points were chosen on the captured image of the grid pattern and the distance between the two points was entered. Then the mapping from pixel space to the physical space was automatically done by the software. Once the scaling was done, the position of the calibration sheet was marked before removing it from the fluid particle column. The position was later used to drop the particles in the plane of focus.

Reference images were captured by choosing the recording mode as a reference image, and sufficient number of images (around 10-15) of fluid without particles were recorded. Now, these recorded reference images were processed by using batch processing option. The option "Average" was chosen under the parameter. A reference image was produced by averaging out all the recording images by reducing the noise in the background. Then, the recording mode was changed to experimental images and capturing the images were started. The spherical particles were then dropped in the fluid from the position that had been marked earlier. When the particles went through the plane of focus, they appeared as dark spots on Davis 8.3 because of the differences in

refractive indices. Images of a particle in focus were only recorded because they appeared sharp as shown in **Figure 3-13**.

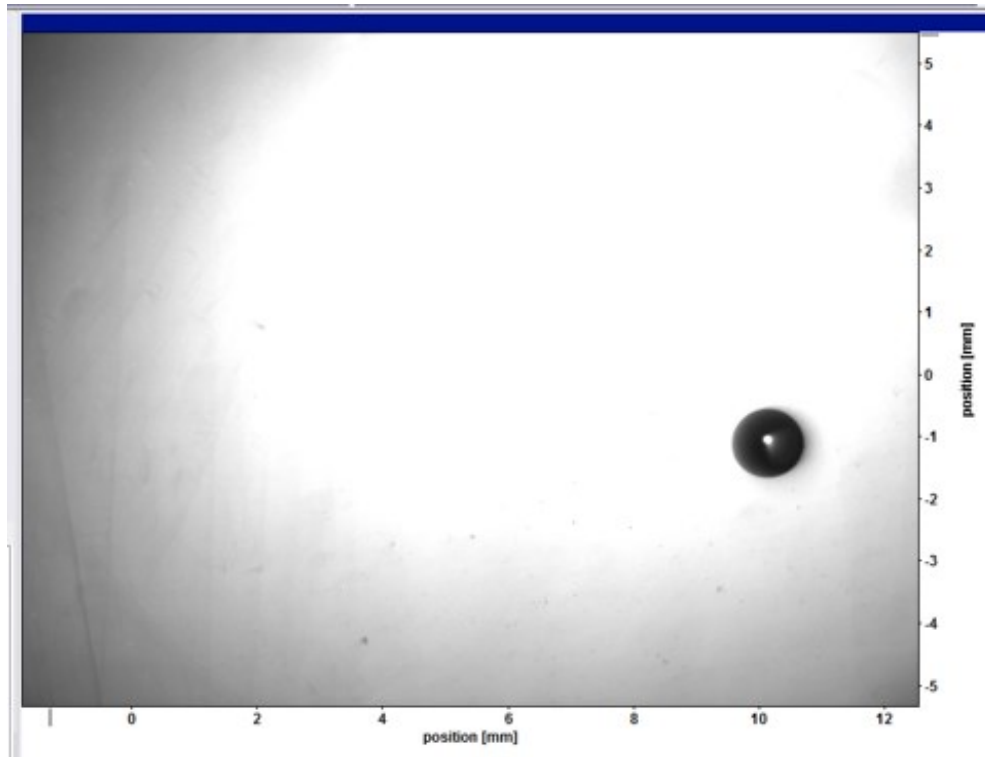


**Figure 3-13. Image of a particle in focus as appeared on the Davis 8.3 screen**

Later on, the experimental images were processed by using particle sizing option under Shadowgraph operation. The 1<sup>st</sup> and 2<sup>nd</sup> frames were assigned with number 0 and 1 in the multi-frame selection. No smoothing option was selected in the image preprocessing step, and the previously processed reference file was selected as the reference image against which the experimental images would now be compared. The values of low-level threshold, global threshold, high-level threshold and AOI expansion were entered as 40, 50, 60 and 50 respectively. These values were entered as the particle recognition was done depending upon the differences in the intensities. The outlier particles in the images could be further filtered out by using velocity parameters. The velocity of the particles in the images was determined by Davis 8.3 software from

the particle displacement and the time interval between the two frames as illustrated in **Figure 3-10**. By this way, the size and the velocity of particles in the experimental images could be obtained by processing them in Davis 8.3 software. The experimental image after processing in Davis 8.3 appeared like the one shown in **Figure 3-14**.

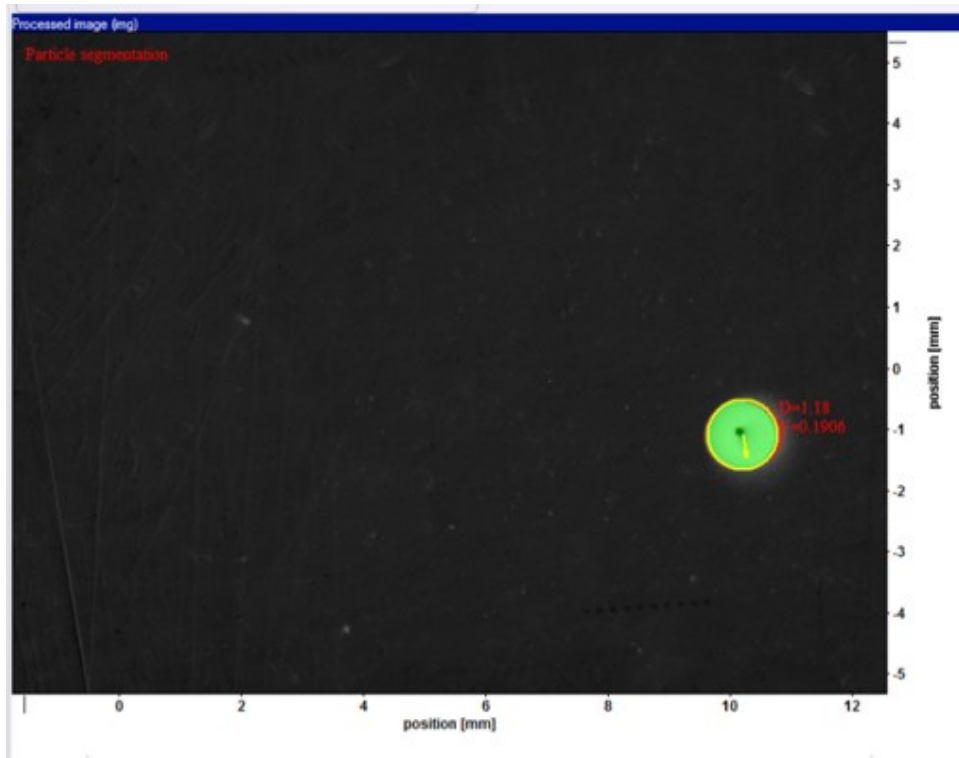


**Figure 3-14. Experimental image after processing in Davis 8.3 software**

The velocity measurements were performed at two different heights (20cm and 26cm) from the air-liquid interface to ensure that the particle had attained its terminal settling velocity. A sufficient number of measurements (at least 10-15) were taken to ensure the accuracy and the repeatability. Velocity values were reported along with the error bars. While performing settling velocity measurements experiments in test fluids of HPAM solutions, at any given time, only one particle was released at once in the test fluid and 20 min of waiting time was given before releasing

the second one such that the fluid structure would recover from any disturbance caused by settling of the earlier particle.

### 3.7 VERIFICATION OF PIS MEASUREMENTS

Particle Image Shadowgraph (PIS) measurements were verified by comparing the measured glass sphere diameters to that of given by the manufacturer of the glass beads. The glass spheres of each size were dropped in water, their diameters and settling velocities were measured by the procedure explained in Section 3.6. The size measurement results were given in **Table 3-6** and were also compared with the specifications data provided by the manufacturer.

**Table 3-6. Comparison of the manufacturer specified diameter versus the measured diameters of glass spheres**

Diameter specified by manufacturer (mm)	Diameter measured by PIS technique (mm)
$0.71 \pm 0.02$	$0.718 \pm 0.017$
$1.18 \pm 0.02$	$1.186 \pm 0.02$
$1.50 \pm 0.03$	$1.59 \pm 0.03$
$2.00 \pm 0.04$	$2.01 \pm 0.03$

Verification of the PIS measurements were also conducted by comparing the measured settling velocities of glass spheres in water to that of the values reported by Shahi [9] as shown in **Table 3-7**.

**Table 3-7. Comparison of the measured settling velocity values versus the values reported by Shahi [9]**

Sphere diameter (mm)	Settling Velocities (m/s)		Deviation %
	Measured	Reported by Shahi [9]	
0.71	0.11 ± 0.004	0.1141	3.6
1.18	0.19 ± 0.007	0.1845	3.0
1.50	0.23 ± 0.009	0.2347	2.0
2.00	0.27 ± 0.004	0.2740	1.5

In addition, drag coefficient ( $C_D$ ) values for four glass spheres were calculated by introducing the measured values of particle diameter,  $D_s$ , and settling velocity,  $V_s$ , into the Equation 3-5 [23].

$$C_D = \frac{4gD_s(\rho_s - \rho_f)}{3\rho_f V_s^2} \quad \text{Equation 3-5}$$

The universal drag coefficient versus the particle Reynolds number correlation for particles settling in Newtonian fluids is given by Equation 3-6 [24]. The particle Reynolds number ( $Re_p$ ) is defined by the Equation 3-7 [23], where  $D_p$  is the characteristic length of the particle,  $\rho_f$  is the density of the fluid and  $\mu_f$  is the viscosity of the fluid.

$$C_D = \frac{24}{Re_p} + \frac{2.6\left(\frac{Re_p}{5.0}\right)}{1 + \left(\frac{Re_p}{5.0}\right)^{1.52}} + \frac{0.411\left(\frac{Re_p}{26300}\right)^{-7.94}}{1 + \left(\frac{Re_p}{26300}\right)^{-8.00}} + \left(\frac{Re_p^{0.80}}{461,000}\right) \quad \text{Equation 3-6}$$

$$Re_p = \frac{D_p V_s \rho_f}{\mu_f} \quad \text{Equation 3-7}$$

Experimental values of  $C_D$  and the universal drag coefficients were plotted against particle Reynolds number ( $Re_p$ ) as shown in **Figure 3-15**.

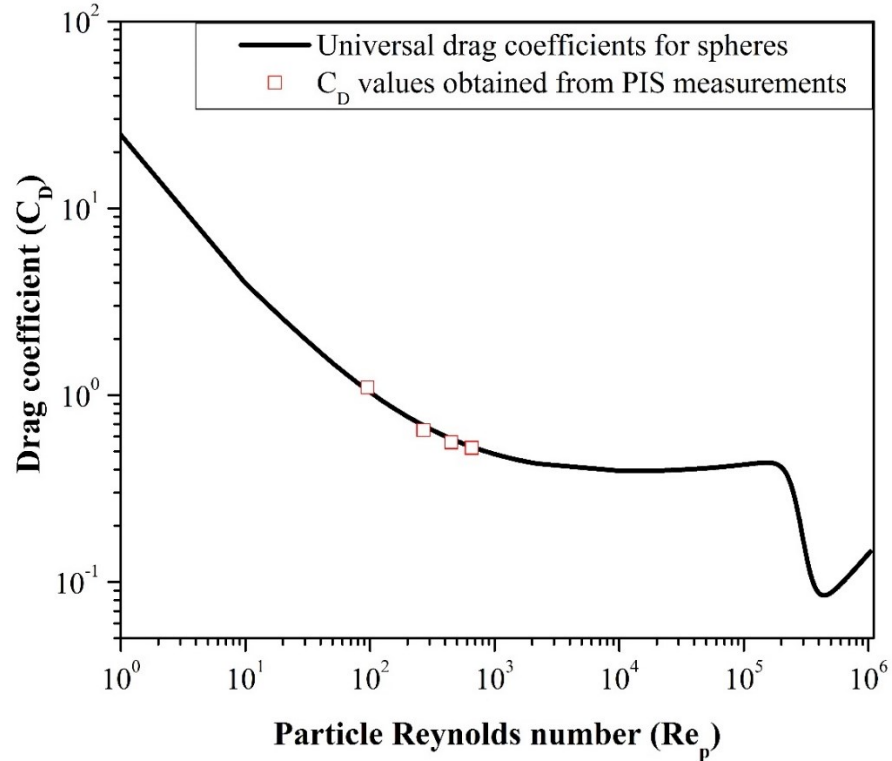


**Figure 3-15. Experimental values of  $C_D$  plotted on universal drag coefficient versus particle Reynolds number ( $Re_p$ ) curve**

The experimental drag coefficient values were within the 5% deviation from the theoretical values. This established the point that the PIS experimental setup and the procedure were efficient to measure the settling velocities of the experimental test fluids.

### **3.8 SOURCES OF ERRORS AND PRECAUTIONS TO BE FOLLOWED TO AVOID THE ERRORS**

There could be many sources of errors possible in any experimental program. Following are the most common sources of errors and their possible precautions when fluid preparation, PIS experimental setup, and procedure were concerned.

### **3.8.1 Fluid preparation and its rheology measurements**

The potential sources of errors during the fluid preparations and precautions to avoid them are:

- The addition of HPAM polymers to the water rapidly would result in agglomeration of polymers and improper dissolution. So polymer should be added gently on to the vortex shoulder.
- The addition of HPAM polymer of low molecular weight grade prior to high molecular weight grade ones would result in a rapid increase of fluid viscosity thereby increasing the time required to dissolve the polymer and also improper dissolution. Hence, the polymers should be added in the decreasing order of their molecular weights.
- Mixing the test fluids at very high speed would result in mechanical degradation the polymers and the fluids might lose their elastic properties. The mixing speed should always be maintained at 300 rpm until the polymers are added, then the speed should be reduced to 100 rpm and maintained at that speed until the polymer gets dissolved completely.
- Performing all the rheological measurements on the same sample placed on the rheometer geometry might sometimes lead to incorrect results. Because after performing viscosity measurements at high shear rates, the sample structure might have been changed or affected. So fresh sample should be used for every new measurement.
- All the rheological measurements should be performed at 25°C. Measurements carried out at higher temperature would be of no use as the settling velocity experiments were not performed at high temperatures.

### **3.8.2 PIS experimental setup and procedure**

The possible sources of errors during the fluid preparations and precautions to avoid them are:

- The presence of air bubbles in the fluid inside the container would lead to noise and disturbance in the captured images. Therefore, the fluid should be allowed to settle and left undisturbed in fluid particle column for at least 12h (overnight) before performing the experiment to avoid the presence of any air bubbles.
- Dropping the particles in the fluid out of the focal plane would result in blurred images. So, once the calibration of the camera was done, before removing calibration sheet, the plane should be marked so that the particles could be dropped at the same plane to be in focus. This will increase the sharpness of the captured images. A funnel was used in the present study to drop the particles effectively in the focal plane.
- Improper balancing level of the camera stand would lead to error in the images caused by the inclination of the camera view angle. The camera should be balanced by ensuring proper centering of the bubble in the balance. This would avoid any inclination in the camera view angle.
- Switching on the laser at high power facing the camera directly would result in damaging the camera sensor. So to avoid the over-saturation and the damage of the camera sensor, the laser power should be increased gradually from a low level. While increasing the laser power, the counts displayed on the captured image should never exceed 4000 at any given point of time. Also, the working resolution should be between 2K and 4K.
- Placing the diffuser at a far distance from the fluid particle column would result in scattering of laser light. So the distance should be optimized accordingly for better illumination of the light. In this study, the distance was around 8 to 10 cm.
- Camera temperature should always be below  $-11^{\circ}\text{C}$  to avoid any damage as the laser might increase the temperature of its sensor.

- During the camera calibration, there would be a high possibility for error in choosing two points exactly at 1.5mm distance apart. This would cause an error in image scaling and velocity calculation. So to reduce this possibility for error and also its error percentage, points should be chosen at a longer distance (around 10.5 or 12mm).
- Choosing the wrong reference images during the batch processing would result in completely wrong results. So appropriate reference images should be selected and also this reference images should be an average of 10-15 captured reference images.
- Capturing less number of experimental images would result in less accurate measurements. Hence, a sufficient number of experimental images (around 10-15) should be taken to ensure high accuracy and repeatability in the settling velocity measurements.

### 3.9 REFERENCES

- [1] Wilton, R.R. 2015. *Rheology and Flow Behaviour of Non-Newtonian, Polymeric Fluids in Capillary and Porous Media: Aspects Related to Polymer Flooding for Enhanced Recovery of Heavy Oil*. PhD thesis, University of Regina, Regina, Saskatchewan (Dec 2015).
- [2] Sorbie, K.S. 1991. *Polymer-Improved Oil Recovery*, Glasgow: Blackie and Son Ltd.
- [3] Foshee, W.C., Jennings, R.R. and West, T.J. 1976. Preparation and Testing of Partially Hydrolyzed Polyacrylamide Solutions. Presented at SPE Annual Fall Technical Conference and Exhibition, New Orleans, Louisiana, USA, 3-6 October. SPE-6202-MS. <https://doi.org/10.2118/6202-MS>.
- [4] Fountain, M.S., Blanchard, J., Erikson, R.L., Kurath, D.E., Howe, D.T., Adkins, H. and Jenks, J. 2012. Design of a Particle Shadowgraph Velocimetry and Size (PSVS) System to Determine Particle Size and Density Distributions in Hanford Nuclear Tank Wastes - 12280. Presented at Waste Management-Tucson, Phoenix, Arizona, USA.

- [5] Hubner, T., Will, S. and Leipertz, A. 2001. Sedimentation Image Analysis (SIA) for the Simultaneous Determination of Particle Mass Density and Particle Size. *Particle & Particle Systems Characterization* **18** (2): 70-78
- [6] Mantovanelli, A. and Ridd, P.V. 2006. Devices to Measure Settling Velocities of Cohesive Sediment Aggregates: A Review of the in Situ Technology. *Journal of Sea Research* **56** (3): 199-226. <http://dx.doi.org/10.1016/j.seares.2006.05.002>.
- [7] Nobbs, D., Tang, P. and Raper, J.A. 2002. The Design, Construction and Commissioning of a Low-Cost Optical Particle Size Analyser Specifically for Measurement of Settling Velocities and Size of Floccs (in English). *Measurement Science and Technology* **13**: 297-302.
- [8] Tang, P., Greenwood, J. and Raper, J.A. 2002. A Model to Describe the Settling Behavior of Fractal Aggregates. *Journal of Colloid and Interface Science* **247** (1): 210-219. <http://dx.doi.org/10.1006/jcis.2001.8028>.
- [9] Shahi, S. 2014. *An Experimental Investigation of Settling Velocity of Spherical and Industrial Sand Particles in Newtonian and Non Newtonian Fluids Using Particle Image Shadowgraph*. Master of Science Thesis, University of Alberta Edmonton, Canada (23rd June 2014).
- [10] Pimentel, R.G. 2006. *Measurement and Predictions of Droplet Size Distributions in Sprays*. PhD Thesis, University Laval, Quebec.
- [11] Merzkirch, W. Shadowgraph Technique, <http://www.thermopedia.com/content/1117/> (accessed on 28th June 2017).
- [12] Settles, G.S. 2001. Shadowgraph Techniques. In *Schlieren and Shadowgraph Techniques: Visualizing Phenomena in Transparent Media*, Chap. 6, 143-163. Berlin, Heidelberg: Springer Berlin Heidelberg.
- [13] Castrejón-García, R., Castrejón-Pita, J.R., Martin, G.D. and Hutchings, I.M. 2011. The Shadowgraph Imaging Technique and Its Modern Application to Fluid Jets and Drops. *Revista Mexicana de Física* **57** (3): 266-275.

- [14] LaVision. 2015. Davis 8.3, Product Manual.
- [15] LaVision. 2007. Product Manual for Double Pulsed Nd:Yag Laser.
- [16] LaVision. 2008. Product Manual for Diffuser.
- [17] Spectral Instruments, Inc. What Is a CCD?, [http://www.specinst.com/What\\_Is\\_A\\_CCD.html](http://www.specinst.com/What_Is_A_CCD.html) (accessed on 28th June 2017).
- [18] Shahi, S. and Kuru, E. 2015. An Experimental Investigation of Settling Velocity of Natural Sands in Water Using Particle Image Shadowgraph. *Powder Technology* **281**: 184-192. <http://dx.doi.org/10.1016/j.powtec.2015.04.065>.
- [19] Shahi, S. and Kuru, E. 2016. Experimental Investigation of the Settling Velocity of Spherical Particles in Power-Law Fluids Using Particle Image Shadowgraph Technique. *International Journal of Mineral Processing* **153**: 60-65. <http://dx.doi.org/10.1016/j.minpro.2016.06.002>.
- [20] Remondino, F. and Fraser, C. 2006. Digital Camera Calibration Methods: Considerations and Comparisons. *International Archives of Photogrammetry, Remote Sensing and Spatial Information Sciences* **36** (5): 266-272.
- [21] Adrian, R.J. 2005. Twenty Years of Particle Image Velocimetry. *Experiments in Fluids* **39** (2): 159-169. <http://dx.doi.org/10.1007/s00348-005-0991-7>.
- [22] Wieneke, B. 2005. Stereo-PIV Using Self-Calibration on Particle Images. *Experiments in Fluids* **39** (2): 267-280. <http://dx.doi.org/10.1007/s00348-005-0962-z>.
- [23] McCabe, W.L., Smith, J.C. and Harriott, P. 2004. *Unit Operations of Chemical Engineering*, New York: McGraw-Hill.
- [24] Morrison, F.A. 2013. Data Correlation for Drag Coefficient for Sphere. *Department of Chemical Engineering, Michigan Technological University, Houghton, MI*. [www.chem.mtu.edu/~fmorriso/DataCorrelationForSphereDrag2013.pdf](http://www.chem.mtu.edu/~fmorriso/DataCorrelationForSphereDrag2013.pdf).

## **CHAPTER 4: EXPERIMENTAL INVESTIGATION OF PARTICLE SETTLING VELOCITY IN VISCOELASTIC POLYMER FLUIDS USING PARTICLE IMAGE SHADOWGRAPH TECHNIQUE.<sup>1,2</sup>**

---

<sup>1</sup> The results and discussion part of Group-A test fluids is based on the paper that has been presented as “Effect of Elastic Properties of the Fluid on the Particle Settling Velocity” at ASME 36th International Conference on Ocean, Offshore and Arctic Engineering, OMAE, Trondheim, Norway on June 25-30, 2017.

<sup>2</sup> The results and discussion part of Group-B test fluids is based on the paper that has been submitted as “Settling Velocity of Particles in Viscoelastic Fluids: A Comparison of the Shear Viscosity vs Elasticity Effect” with paper number SPE-187255-MS for presentation at the 2017 SPE Annual Technical Conference and Exhibition to be held in San Antonio, Texas, 9-11 October 2017. This paper has also been submitted to SPE Journal for review and possible publication.

This chapter contains all the results of the rheological characterization of the HPAM test fluids (Group-A & Group-B) and the experimental measurements of settling velocity of spherical particles in the test fluids using Particle Image Shadowgraph (PIS) technique. In this chapter, results are categorized into two parts:

- Experimental results of Group-A test fluids &
- Experimental results of Group-B test fluids.

The test fluids of Group-A were used to investigate the effect of elasticity on settling velocity of particles in viscoelastic fluids. The test fluids of Group-B were used to perform a comparative study of the shear viscosity versus elasticity effect on settling velocity of particles in viscoelastic fluids. These test fluids were chosen to perform the respective experimental investigations because of their rheological characterization.

#### 4.1 EXPERIMENTAL RESULTS OF GROUP-A TEST FLUIDS

The Group-A comprised of four test fluids, Fluid A-1 to Fluid A-4, which were made up of HPAM polymer. The composition details of Group-A test fluids are provided in **Table 4-1**. The experimental results of these four test fluids are discussed in the following subsections.

**Table 4-1. Polymer blend composition details of Group-A test fluids**

Sample	Conc. of polymer blend (wt%)	Wt % of HPAM of Molecular weight (g/gmol)			Polydispersity Index (I)
		$20 \times 10^6$	$8 \times 10^6$	$0.5 \times 10^6$	
Fluid A-1	0.09	0	100	1	1
Fluid A-2	0.1	35.64	52.58	11.8	3.6
Fluid A-3	0.1	42.13	43.95	13.9	4.26
Fluid A-4	0.1	53.58	28.72	17.7	5.5

#### 4.1.1 Density measurements of Group-A test fluids

The densities of the test fluids are shown in **Table 4-2**. The densities of all the test fluids were seemed to be almost the same.

**Table 4-2. Densities of Group-A test fluids**

Test fluid	Density (kg/m <sup>3</sup> )
Fluid A-1	1005
Fluid A-2	1003
Fluid A-3	1002
Fluid A-4	1002

#### 4.1.2 Rheological characterization of Group-A test fluids

The rheological measurements were conducted to determine the viscous (shear viscosity) and the elastic properties (elastic modulus, relaxation time) of the test fluids. The test fluids were characterized based on their rheological properties.

The shear stress versus shear rate diagram of all the test fluids of Group-A is shown in **Figure 4-1**. The shear viscosity versus the shear rate data is shown in **Figure 4-2**. The rheological data confirmed that test fluids exhibited shear thinning characteristics (i.e. shear viscosity decreases with the increasing shear rate). Moreover, viscous characteristics of the fluids were almost the same as indicated by the similarities of the shear stress versus shear rate (**Figure 4-1**) and the shear viscosity versus the shear rate (**Figure 4-2**) profiles. There was a slight bump in the viscosity profile around the shear rates of 80-100 s<sup>-1</sup>. The exact reason for this was not clear, however, this bump caused no effect on the overall shear thinning behavior of the samples.

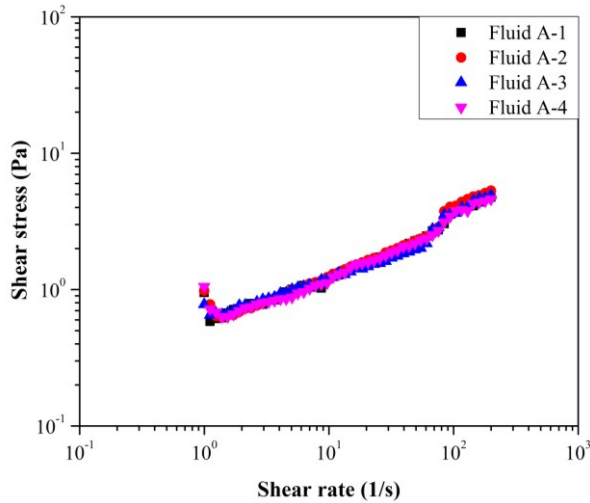


**Figure 4-1. Shear stress versus shear rate profiles of all the test fluids of Group-A**

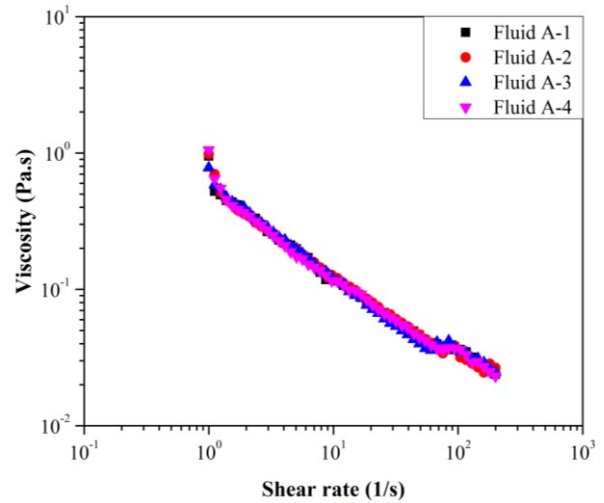


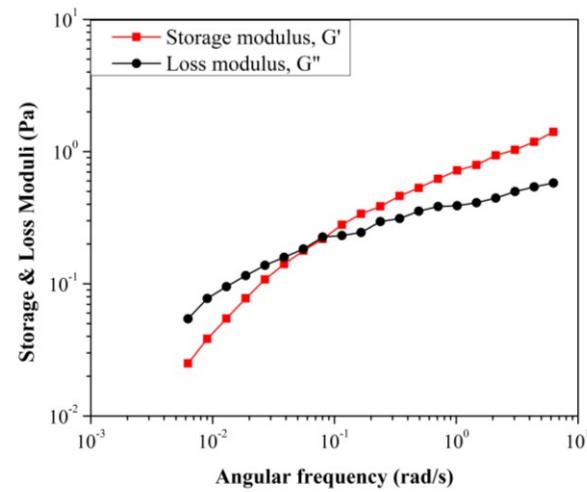
**Figure 4-2. Shear viscosity versus shear rate profiles of all the test fluids of Group-A**

The shear stress versus shear rate data were best fitted by the power law model. The values of the consistency index (K), the flow behavior index (n) along with the coefficient of determination ( $R^2$ ) are summarized in **Table 4-3**. The K & n values also confirmed that the test fluids had almost identical shear thinning characteristics.

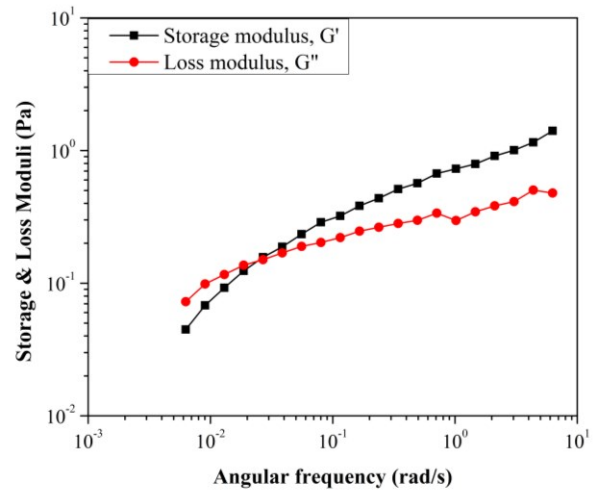
**Table 4-3. Power law parameters K & n for the test fluids of Group-A**

Test fluid	K (Pa.s <sup>n</sup> )	n	R <sup>2</sup>
Fluid A-1	0.53	0.38	0.96
Fluid A-2	0.54	0.38	0.96
Fluid A-3	0.54	0.37	0.95
Fluid A-4	0.53	0.37	0.96

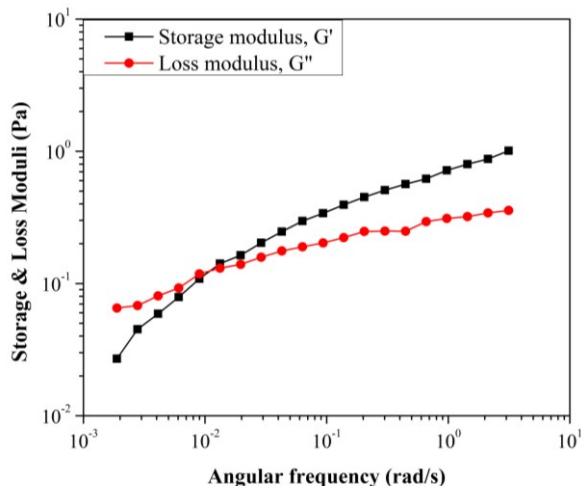
The viscoelastic properties exhibited by the test fluids were studied by performing frequency sweep oscillatory measurements. **Figure 4-3** shows the elastic modulus ( $G'$ ) and the viscous modulus ( $G''$ ) as a function of the angular frequency for all the test fluids of Group-A. Both the elastic and the viscous moduli increased as the frequency increased. However, the elastic modulus ( $G'$ ) increased more rapidly than the viscous modulus ( $G''$ ) and the solid-like behavior became dominant after certain frequency. Such a crossover point had a significance. The longest characteristic relaxation time of the polymer solution could be found by taking the inverse of this cross-over frequency [1, 2]. In general, the relaxation time defines the time taken by any deformed material to regain its original structure, and it is a direct measure of the elasticity [3]. So if one fluid has a higher relaxation time than another fluid, then it has the higher elasticity than the other fluid as well.



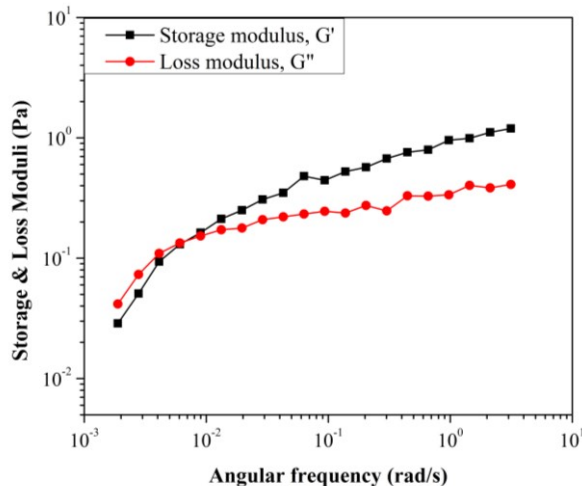
(a) Fluid A-1



(b) Fluid A-2



(c) Fluid A-3



(d) Fluid A-4

**Figure 4-3. Oscillatory frequency sweep data of all the test fluids of Group-A**

Experimentally measured relaxation times of all the four test fluids of Group-A together are given in **Table 4-4**. These experimentally measured relaxation time values were taken as the representative numbers to quantify the elastic properties of the fluids.

**Table 4-4. Longest relaxation times of the test fluids of Group-A**

Test fluid	Polydispersity	Longest relaxation time
	(I)	(s)
Fluid A-1	1	12
Fluid A-2	3.6	50
Fluid A-3	4.26	110
Fluid A-4	5.5	150

Results presented in **Table 4-4** indicated that the longest relaxation time values of test fluids increased along with the polydispersity index values. The longest relaxation time of the polymer blend appeared to be associated with the polymer of the highest molecular weight and its

weight percentage in the polymer blend. This was mainly because the relaxation time of the test fluid increased as the weight percentage of highest molecular weight polymer (i.e. 20,000,000 g/gmol) in the blend increased.

Based on the results of the viscosity and the frequency sweep measurements, we concluded that the four test fluids had the almost identical shear thinning viscosity behavior but significantly different elasticity characteristics.

#### 4.1.3 Settling velocity measurements of particles in Group-A test fluids

**Table 4-5** shows the experimentally measured settling velocity values of 2mm diameter spherical particles in the four test fluids of Group-A. It was found that the rate at which particles settled in the medium was decreasing from Fluid A-1 to A-4. Settling velocity of particles in Fluid A-1 being the highest and that in Fluid A-4 being the lowest. The ratio of the sphere diameter (2mm) to the distance between column walls (11cm) is very small (0.018), so the wall effects on the settling particles could be assumed to be negligible. Since the shear thinning (viscosity) behavior of the fluids was the same, the variation in the settling velocity values was solely due to the difference in the elastic properties of the fluids.

**Table 4-5. Settling velocities of 2mm diameter spherical particles in the test fluids of Group-A**

Test fluid	Longest relaxation time (s)	Settling velocity (m/s)	Standard deviation
Fluid A-1	12	0.011	5.90E-04
Fluid A-2	50	0.00732	1.99E-04
Fluid A-3	110	0.00345	1.69E-04
Fluid A-4	150	0.00296	2.66E-04

**Figure 4-4** shows the settling velocity of 2mm particles as a function of the longest relaxation times of the test fluids of Group-A. This relation implied that the settling velocity of the particles decreased significantly with the increasing longest relaxation time of the fluid. In other words, reduction of the settling velocity values could be attributed to the increased levels of the fluid elasticity. The possible reason for the settling velocity reduction could be due to the extensional effects in the wake of settling particle as mentioned by McKinley [4] in his comprehensive literature review. McKinley stated that the settling particle in the shear thinning viscoelastic liquid would result in the formation of the negative wakes around the particle, which causes drag at the higher levels of elasticity [4].

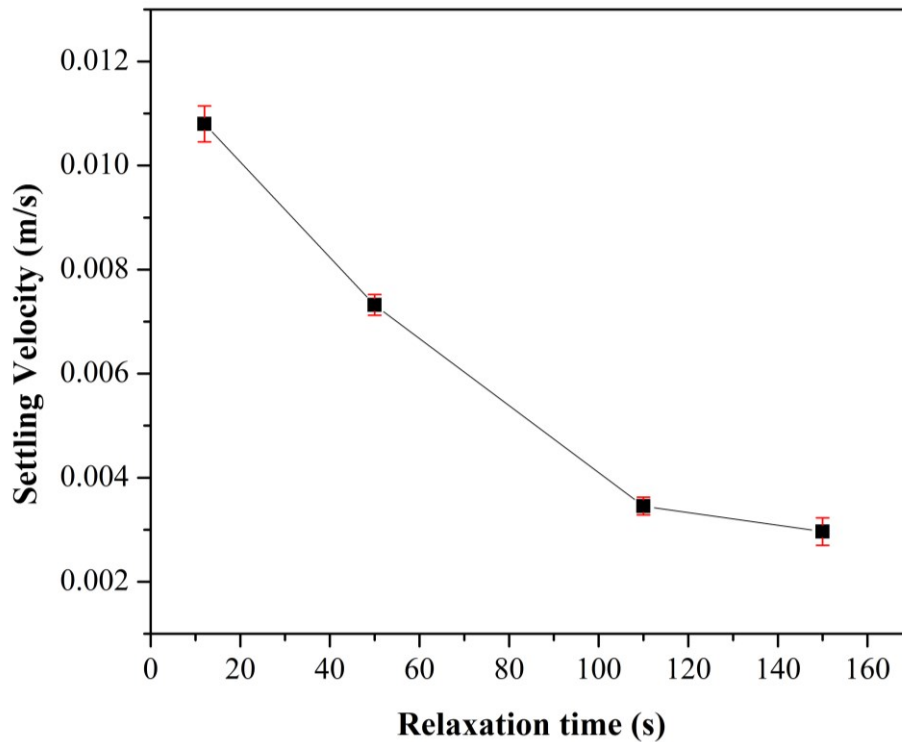


**Figure 4-4. Settling velocity of 2mm glass spheres versus the relaxation time of the test fluids of Group-A.**

In order to determine the impact of elasticity, the experimentally measured settling velocities were compared against the settling velocity values calculated by using the model developed by Shah et al. [5]. The model was developed for predicting settling velocity of spherical particles in visco-inelastic power law type fluids. The results of the comparisons are shown in **Figure 4-5**. The values of  $K$  and  $n$  were assumed to be  $0.53 \text{ Pa}\cdot\text{s}^n$  and  $0.38$ , respectively for determining the settling velocity in the visco-inelastic fluid. The details of the calculation procedure followed to determine the velocity of spherical particles in the visco-inelastic power law type fluid of  $K=0.53 \text{ Pa}\cdot\text{s}^n$  and  $n = 0.38$  using Shah et al. [5] model is provided in **Appendix 4.4.1**.

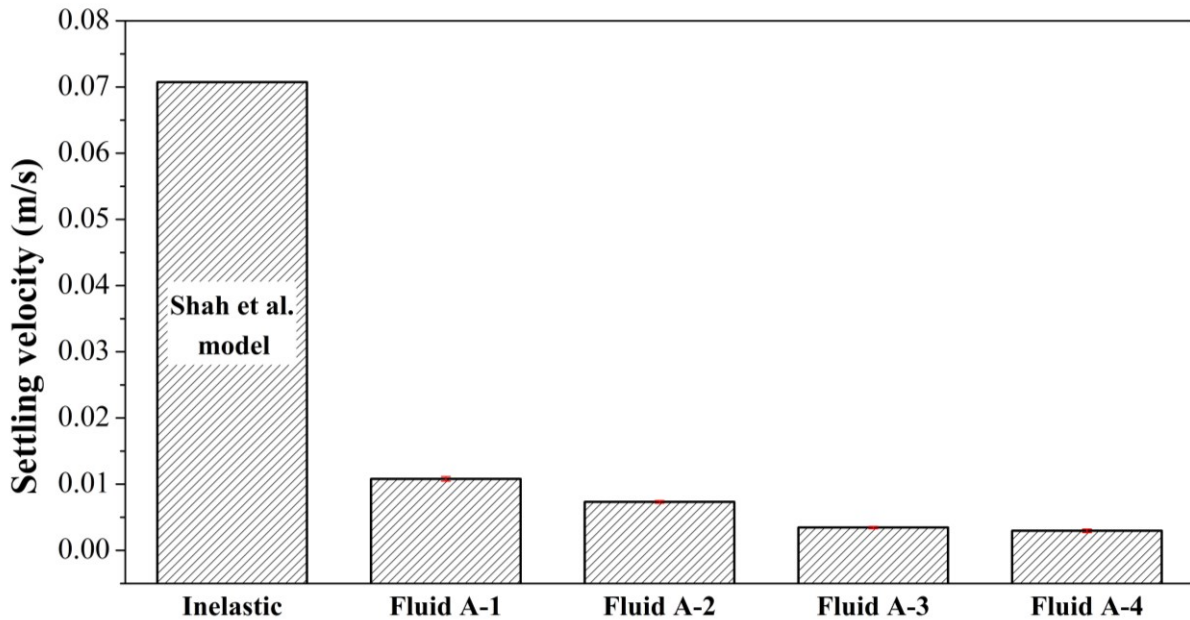


**Figure 4-5. Comparison of the measured settling velocity values of 2mm particles in all test fluids of Group-A to the velocity values calculated from Shah et al. [5] model.**

As shown in **Figure 4-5**, the predicted settling velocity of 2mm particle was significantly higher than the experimental values. In other words, if the effect of elasticity is neglected in the

calculation of the settling velocity of particles in viscoelastic fluids, the predicted values of settling velocities could be overestimated significantly.

To quantify the effect of elasticity on the settling velocity, the ratio of settling velocity in the inelastic fluid to that in the elastic fluid versus the relaxation time are plotted in **Figure 4-6**. The results showed that as the relaxation times varied from 12 sec to 150 sec (i.e. increasing elasticity), the predicted settling velocity values were about 6.5 to 24 times higher than the measured ones.

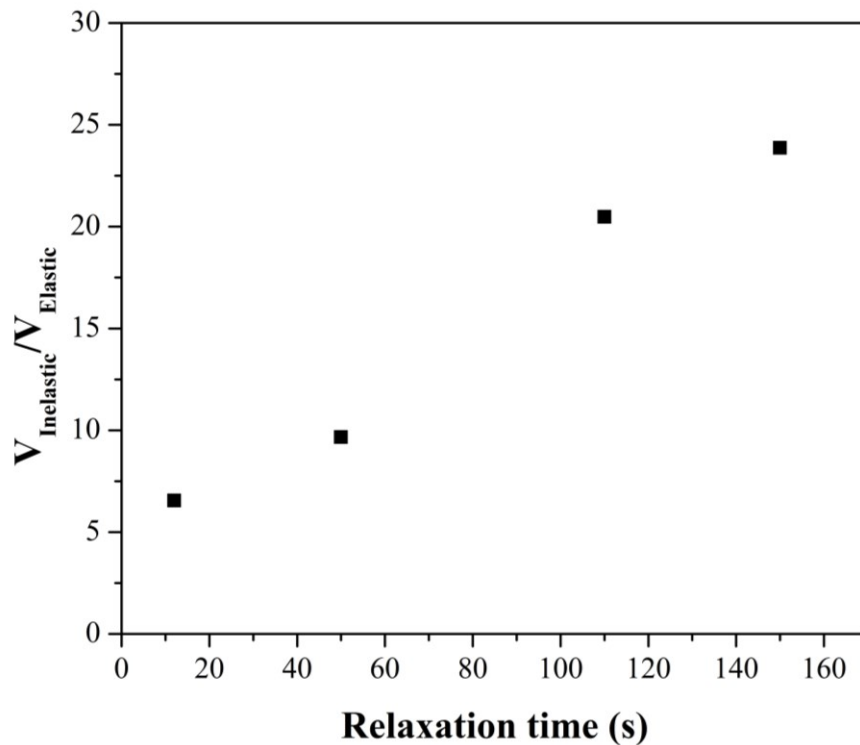


**Figure 4-6. Ratio of the settling velocity of 2mm particles in the inelastic fluid to that of the ones in the elastic fluid as a function of the relaxation time of the fluid.**

The results presented here confirmed that the settling velocity of the particles is strongly influenced by the elastic properties of the fluids. Moreover, the longest relaxation time of the fluid can be used to quantify such effect. Further experimentation was done at lower viscosities with

Set-I of Group-B test fluids to confirm the validity of these observations. Also by performing experiments in Group-B (Set-I & Set-II) fluids, the effect of elasticity was further compared with the effect of shear viscosity on the settling velocity of particles to determine the more dominant factor between the two to reduce the settling velocity of the particles.

## 4.2 EXPERIMENTAL RESULTS OF GROUP-B TEST FLUIDS

The Group-B comprised of two sets of test fluids: Set-I and Set-II. Set-I contained test fluid B-1, fluid B-2 and fluid B-3 whereas Set-II contained test fluid B-4, fluid B-5 and fluid B-6. The composition details of Set-I test fluids and Set-II test fluids are provided in **Table 4-6** and **Table 4-7** respectively. The experimental results of these six test fluids are discussed in the following subsections.

**Table 4-6. Polymer blend composition details of the test fluids in Set-I of Group-B**

Sample	Conc. of polymer blend (wt%)	Wt % of HPAM of Molecular weight (g/gmol)			Polydispersity Index (I)
		20 x 10 <sup>6</sup>	8 x 10 <sup>6</sup>	0.5 x 10 <sup>6</sup>	
Fluid B-1	0.045	0	100	1	1
Fluid B-2	0.05	35.64	52.58	11.8	3.6
Fluid B-3	0.05	42.13	43.95	13.9	4.26

**Table 4-7. Polymer blend composition details of the test fluids in Set-II of Group-B**

Sample	Conc. of polymer blend (wt%)	Wt % of HPAM of Molecular weight (g/gmol)	Polydispersity Index (I)
		8 x 10 <sup>6</sup>	
Fluid B-4	0.03	100	1
Fluid B-5	0.045	100	1
Fluid B-6	0.09	100	1

#### 4.2.1 Density measurements of Group-B test fluids

The densities of all the test fluids are provided in **Table 4-8**. All the fluids seemed to have practically same densities.

**Table 4-8. Densities of Group-B (Set-I and Set-II) test fluids**

Test fluid	Density (kg/m <sup>3</sup> )
Fluid B-1	998
Fluid B-2	997
Fluid B-3	997
Fluid B-4	998
Fluid B-5	998
Fluid B-6	1005

#### 4.2.2 Rheological characterization of Group-B test fluids

##### 4.2.2.1 Rheological characterization of Set-I test fluids

All the Set-I test fluids of Group-B were rheologically characterized based upon their viscous and elastic properties. **Figure 4-7** and **Figure 4-8** provide the shear stress versus shear rate and the shear viscosity versus shear rate profiles for all the Set-I test fluids, respectively. Within the studied range of shear rate (from 1 to 200 s<sup>-1</sup>), all the test fluids were found to exhibit the shear thinning behavior as their shear viscosities were decreasing with increasing shear rate. The data shown in **Figure 4-7** and **Figure 4-8** confirmed that the test fluids 1, 2 and 3 had similar viscous characteristics.

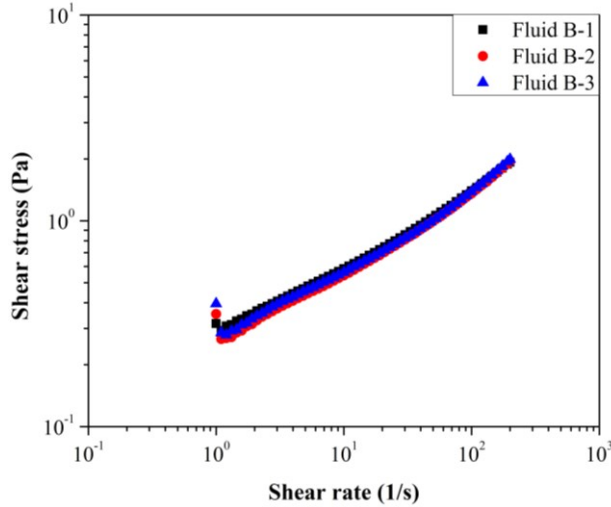


**Figure 4-7. Shear stress versus shear rate profiles of Set-I test fluids of Group-B**

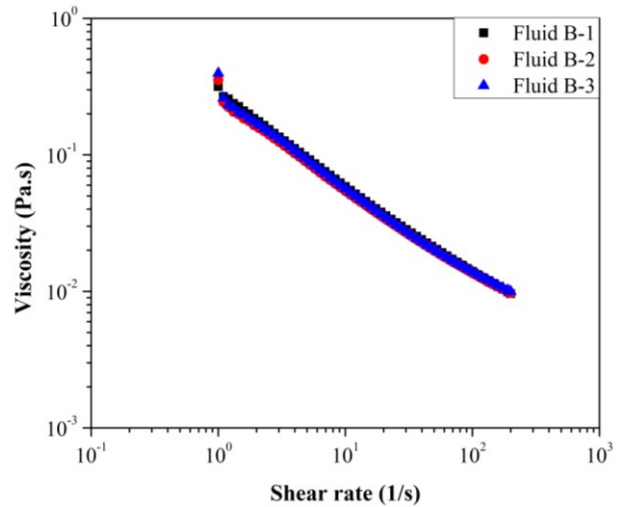


**Figure 4-8. Shear viscosity versus shear rate profiles of Set-I test fluids of Group-B**

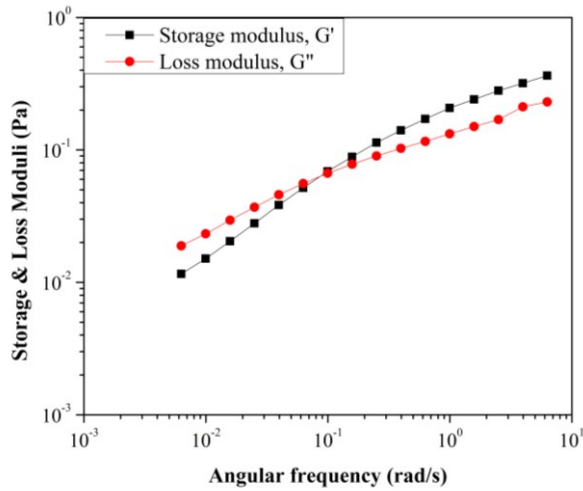
To further verify the similarity, power law model was fitted to shear stress vs shear rate data of all the test fluids. The values of consistency index (K) and the flow behavior index (n) are provided in **Table 4-9**. The values of K and n also substantiate the fact that the Set-I fluids had almost identical viscous characteristics.

**Table 4-9. Power law parameters K & n for Set-I test fluids of Group-B**

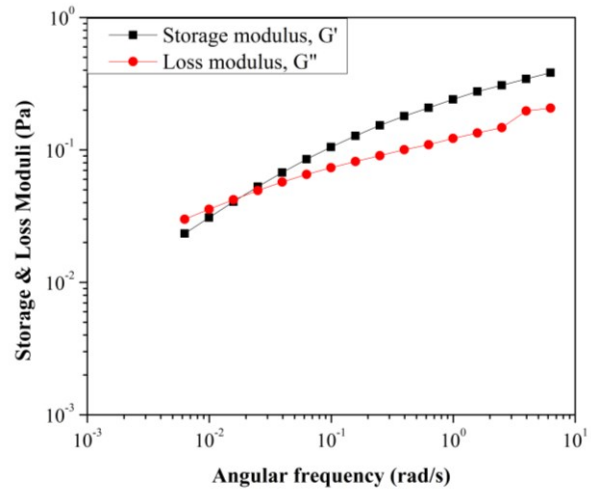
Test fluid	K (Pa.s <sup>n</sup> )	n	R <sup>2</sup>
Fluid B-1	0.27	0.35	0.99
Fluid B-2	0.25	0.36	0.98
Fluid B-3	0.26	0.35	0.98

Oscillatory frequency sweep measurements were performed to study the viscoelastic properties of the Set-I test fluids. The storage modulus ( $G'$ ) and the loss modulus ( $G''$ ) profiles as a function of angular frequency for the Set-I test fluids (Fluid B-1, Fluid B-2 and Fluid B-3) are

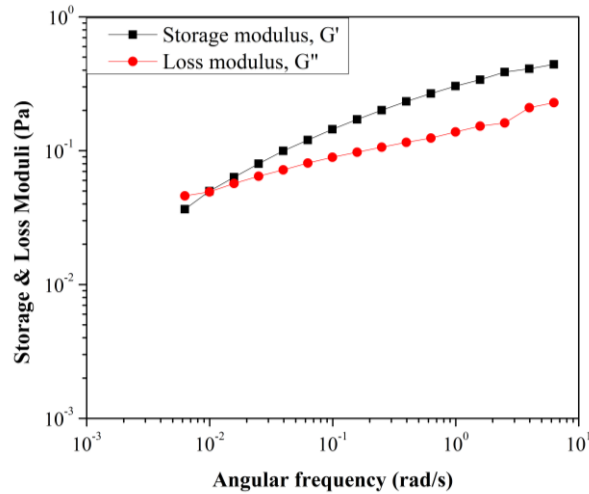
shown in **Figure 4-9**. The storage modulus ( $G'$ ) represents the solid-like behavior of the test fluid whereas the liquid-like behavior is represented by the loss modulus ( $G''$ ).



**(a) Fluid B-1**



**(b) Fluid B-2**



**(c) Fluid B-3**

**Figure 4-9. Oscillatory frequency sweep data for Set-I test fluids of Group-B**

As presented in **Figure 4-9**, initially storage moduli of the test fluids were lower than their loss moduli. For all the three test fluids, both the storage and the loss moduli were increasing as

the angular frequency increases. Nevertheless, increase in the storage modulus was more prompt compared to the increase in the loss modulus. The frequency at which the storage modulus crosses over the loss modulus is called cross-over frequency. The inverse of the cross-over frequencies provides the longest characteristic relaxation times of the test fluids [1, 2]. The elasticity of a fluid can be quantified by its relaxation time as it is the time needed for any deformed material to regain its original structure [3]. Therefore, in this study, elastic properties of the test fluids were measured in terms of their relaxation times. Higher the relaxation time, higher is the elastic property of the test fluid in comparison to other test fluids.

**Table 4-10. Longest relaxation times of the Set-I test fluids of Group-B**

Test fluid	Polydispersity (I)	Longest relaxation time (s)
Fluid B-1	1	12
Fluid B-2	3.6	50
Fluid B-3	4.26	110

**Table 4-10** presents the longest relaxation times of Set-I test fluids, and as expected, polydispersity seemed to be controlling the elastic properties of these polymer solutions. It was found that Fluid B-3 (having higher polydispersity) had the highest relaxation time among the three test fluids. Hence, the test fluid B-3 was more elastic followed by the test fluid B-2 and then the test fluid B-1. Based on the above rheological characterization, it was concluded that all the test fluids in Set-I had almost identical shear thinning viscous properties (on average  $K=0.26 \text{ Pa}\cdot\text{s}^n$  &  $n=0.35$ ) but significantly different elasticity properties.

#### 4.2.2.2 Rheological characterization of Set-II test fluids

Figure 4-10 and Figure 4-11 provide the shear stress versus shear rate and the shear viscosity versus shear rate profiles for all the Set-II test fluids. Within the studied range of shear rates (from 1 to 200  $\text{s}^{-1}$ ), all the test fluids were found to exhibit shear thinning behavior as their shear viscosities were decreasing with the increasing shear rate. However, among the three, fluid B-6 seemed to have the highest shear viscosity, fluid B-4 to have the lowest shear viscosity and the fluid B-5 shear viscosity was in between the other two.

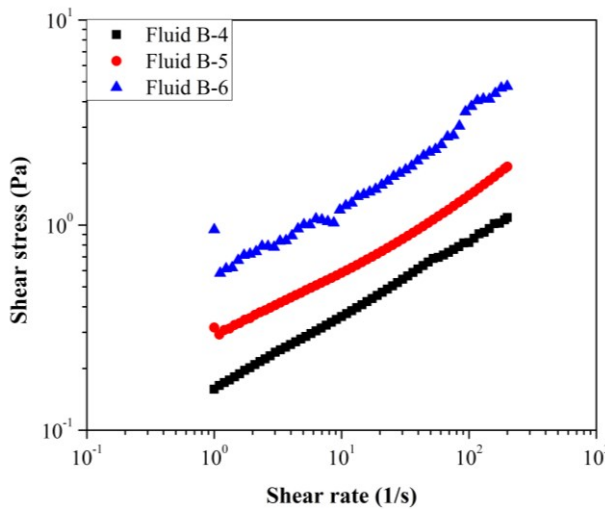


Figure 4-10. Shear stress versus shear rate profiles of Set-II test fluids of Group-B

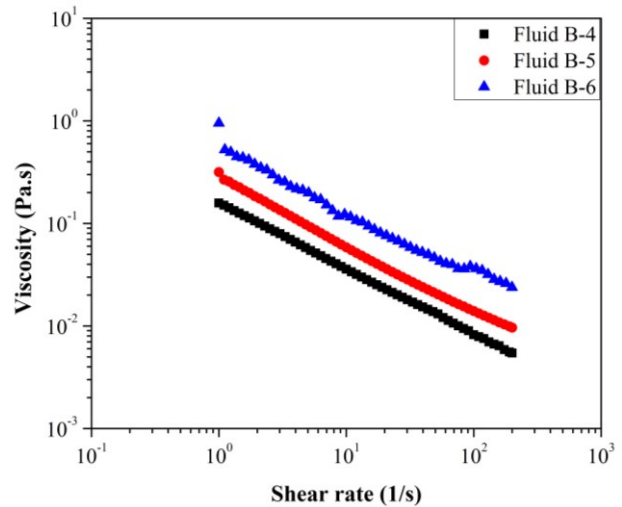


Figure 4-11. Shear viscosity versus shear rate profiles of Set-II test fluids of Group-B

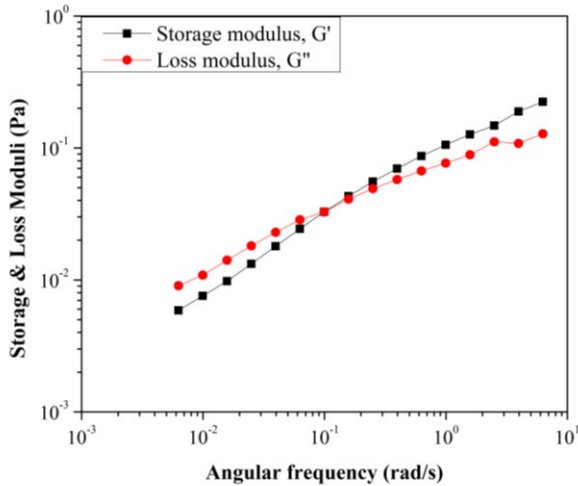
The consistency index ( $K$ ) and the flow behavior index ( $n$ ) values of the test fluids were obtained by curve fitting the power law model to the shear stress versus shear rate data. The data provided in Table 4-11 shows that the all three test fluids had shear thinning characteristics. The flow behavior index values were almost the same for the Set-II test fluids. The consistency index of fluid B-6 was, however, greater than that of the fluid B-5 followed by the fluid B-4. The fluid

B-6 was found to be nearly 2 times more viscous than the fluid B-5 and was also nearly 3.5 times more viscous than the fluid B-4.

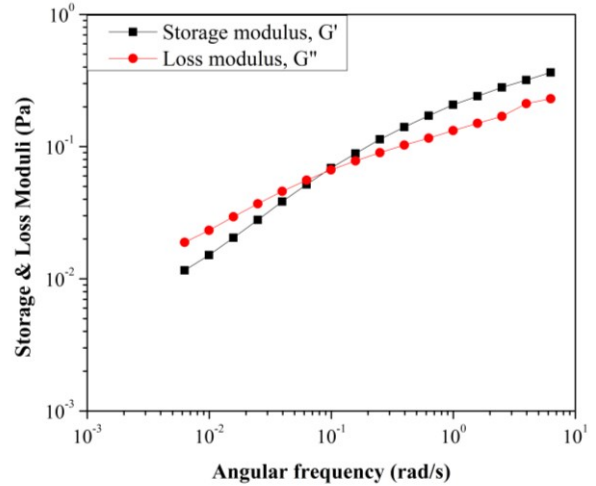
**Table 4-11. Power law parameters of K & n of the Set-II test fluids**

Test fluid	K (Pa.s <sup>n</sup> )	n	R <sup>2</sup>
Fluid B-4	0.16	0.38	0.99
Fluid B-5	0.27	0.35	0.99
Fluid B-6	0.53	0.38	0.96

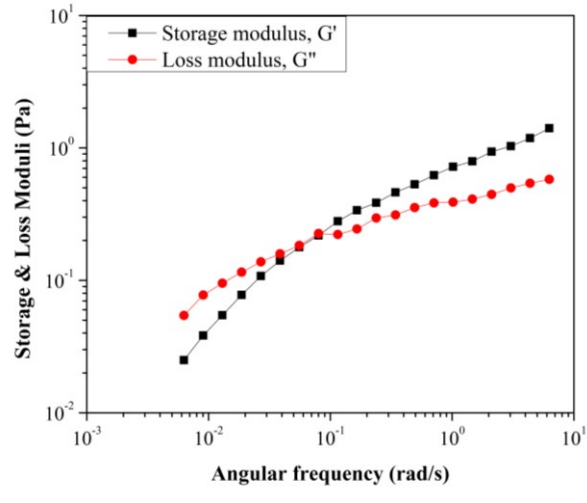
Oscillatory frequency sweep measurements were performed to study the viscoelastic properties of the Set-II test fluids. The storage modulus ( $G'$ ) and the loss modulus ( $G''$ ) profiles as a function of the angular frequency for the Set-II test fluids (Fluid B-4, Fluid B-5 and Fluid B-6) are shown in **Figure 4-12**. For all the three test fluids of Set-II, both the storage and the loss moduli increased as the angular frequency increased.



**(a) Fluid B-4**



**(b) Fluid B-5**



(c) Fluid B-6

**Figure 4-12. Oscillatory frequency sweep data of Set-II test fluids of Group-B**

The longest relaxation times of the test fluids were determined by taking the inverse of the cross-over frequency. As shown in **Table 4-12**, Set-II test fluids had the same longest relaxation times of 12 sec. Therefore, fluids B-4, B-5 and B-6 were similar in terms of elasticity.

**Table 4-12. Longest relaxation times of Set-II test fluids of Group-B**

Test fluid	Polydispersity	Longest relaxation time
	(I)	(s)
Fluid B-4	1	12
Fluid B-5	1	12
Fluid B-6	1	12

From the results given in **Table 4-11** and **Table 4-12**, it could be concluded that fluid B-4, B-5 and B-6 of Set-II had similar elasticity but very different shear viscosity.

### 4.2.3 Settling velocity measurements of particles in Group-B test fluids

The Set-I test fluids of Group-B were used to investigate the effect of elasticity on particle settling velocities by performing settling velocity measurements of 2mm spherical particles in these test fluids. The Set-II test fluids of Group-B were used to investigate the effect of shear viscosity on particle settling velocities by performing the settling velocity measurements of 2mm spherical particles in these test fluids. The comparison between the effect of elasticity and shear viscosity on settling velocity was investigated by measuring settling velocities of particles of various diameters in Set-I and Set-II test fluids.

#### 4.2.3.1 Effect of Elasticity on Particles Settling Velocities

Settling velocities of spherical particles of 2mm diameter in Set-I test fluids having a similar shear viscosity ( $K=0.26 \text{ Pa}\cdot\text{s}^n$  &  $n=0.35$ ) and different elasticity were measured by using the PIS technique. The settling velocity experimental results along with standard deviations are summarized in **Table 4-13**. The results indicated that the settling velocity value of 2mm spheres in the fluid B-1 was higher than that of the values in the fluid B-2, followed by the fluid B-3.

**Table 4-13. Settling velocities of spherical particles of diameter 2 mm in Set-I test fluids of  $K=0.26 \text{ Pa}\cdot\text{s}^n$  &  $n=0.35$**

Test fluid	Relaxation time ( $\lambda$ ) (s)	Settling velocity (m/s)	Standard deviation
Fluid B-1	12	0.0307	$3.60 \times 10^{-4}$
Fluid B-2	50	0.0144	$3.40 \times 10^{-4}$
Fluid B-3	110	0.0084	$4.50 \times 10^{-4}$

The hinderance effect due to container walls was negligible as the ratio of sphere diameter to the test column width is very low (less than 0.02). Since the shear thinning viscosity behavior

of all the fluids was almost identical, the variation in the settling velocity values was predominantly caused by the differences in their elastic properties. Therefore, the settling velocity values of 2mm spheres are plotted against the fluid relaxation times in **Figure 4-13** to show the effect of elasticity. The model proposed by Shah et al. [5] for predicting settling velocity of spheres in visco-inelastic power law type fluids was used to determine the settling velocity of 2mm spheres in the fluid having  $K=0.26$  and  $n=0.35$  without any elasticity and this value is plotted in **Figure 4-13** as the settling velocity at zero relaxation time. The details of the settling velocity calculations using Shah et al. [5] model are given in **Appendix 4.4.2**.

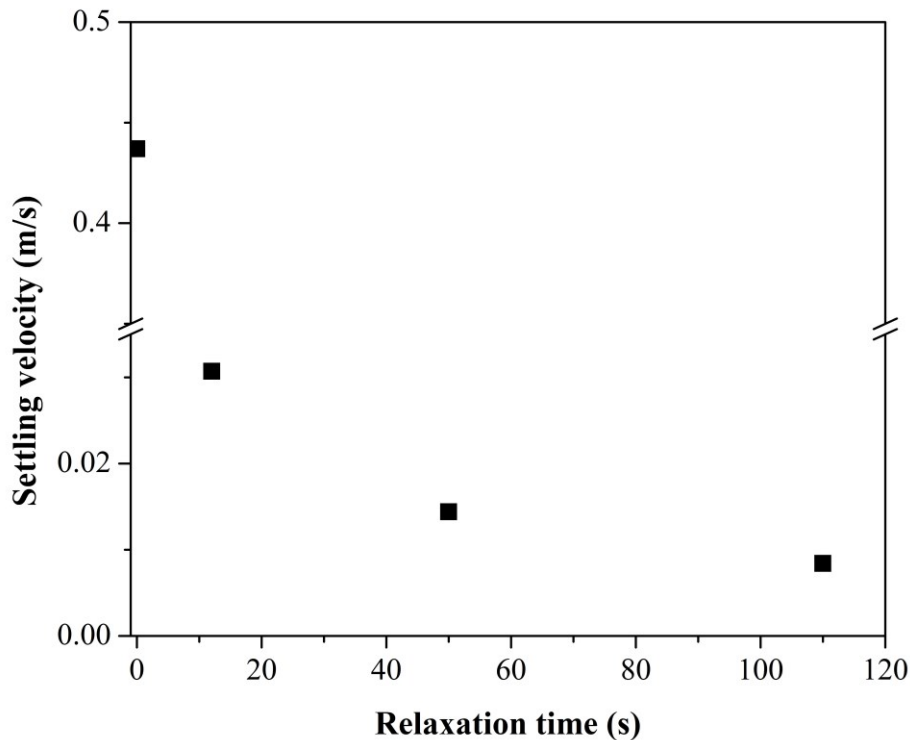


**Figure 4-13. Settling velocity of glass spheres of 2mm diameter versus relaxation time of the Set-I test fluids having similar viscosity but different elasticity.**

**Figure 4-13** demonstrates that the particle settling velocity is a strong function of the fluid's relaxation time. The settling velocity of the sphere decreased significantly as the relaxation

time (and, hence, the elasticity) of the fluid increased. As the relaxation time increased from 12 s to 50 s, the settling velocity decreased by about 2 times. The reduction in settling velocity was 3 times when the relaxation time was increased from 12 s to 110 s. These results of the effect of relaxation time (and hence, the elasticity) on settling velocity of particles were in agreement with Gomaa et al.[6], who observed an increase in the fluids ability to suspend proppant particles when the crossover point of  $G'$  and  $G''$  in the frequency sweep of the fluid was decreased.

We have calculated the ratio of the settling velocity of a 2mm sphere in visco-inelastic shear thinning fluid (Shah et al. [5] model;  $K=0.26$  and  $n=0.35$ ,  $\lambda=0$ ) to the measured values of the settling velocities in fluids with different elasticities ( $\lambda=12$  s,  $\lambda=50$  s, and  $\lambda=110$  s). As shown in **Figure 4-14**, when the relaxation time of the fluid was 12 s, the settling velocity decreased by about 14 times as compared to the visco-inelastic fluid having the almost identical shear viscosity. Similarly, when we used the fluids with the relaxation times of 50 s and 110 s, the measured settling velocities were about 29 times and 50 times lower than that of the case with visco-inelastic fluid having the similar shear viscosity, respectively. These results clearly indicate that settling velocity values can be significantly over predicted if they are calculated by using models not considering the elasticity effect (e.g. Shah et al. [5]).

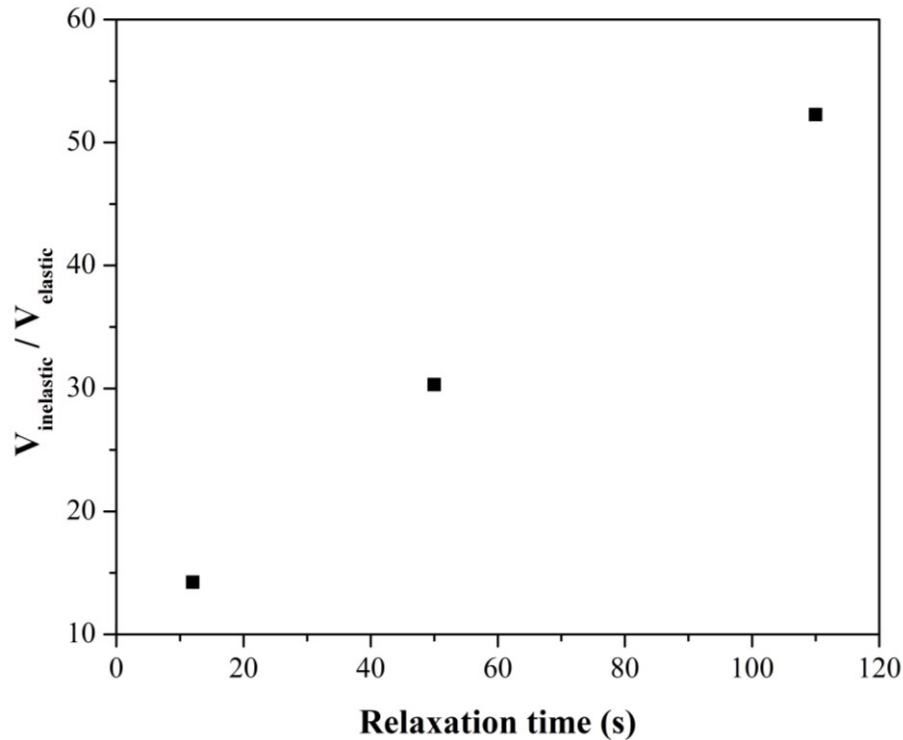


**Figure 4-14. Over-estimation of settling velocities if the effect of elasticity is not considered.**

The reason for this drastic reduction in the particle settling velocity can possibly be attributed to the formation of negative wake observed in the elastic fluids that opposes the motion of the particle [4]. Movement of fluid past the settling particle in the opposite direction to that of the particle movement is termed as “Negative Wake” [7]. This negative wake is perceived to happen only in shear thinning viscoelastic fluids [8]. These results substantiate the fact that the settling velocity of the particle can be reduced significantly by enhancing the elasticity of the fluid and, therefore, this vital elasticity effect on the particle settling velocity should be taken into consideration in order to develop more realistic models of particle settling velocity in viscoelastic fluids.

#### 4.2.3.2 Effect of Shear Viscosity on the Particle Settling Velocity

The effect of the shear viscosity of the fluid on the settling velocity of particles was studied by evaluating the settling velocities of 2mm spheres in Set-II fluids having relaxation time 12 s. The apparent shear viscosity of the fluids was approximated by using the Equation 4-1 [9].

$$\mu_a = K \dot{\gamma} \quad \text{Equation 4-1}$$

In Equation 4-1, the maximum value of shear rate,  $\dot{\gamma}_s$ , induced by the settling particle in polymer fluids was calculated by using Equation 4-2 [10]. The measured values of settling velocity values were used to evaluate the shear rates (Equation 4-2), which were then used to determine the apparent shear viscosity. The settling velocity results along with apparent shear viscosities and other rheological properties (K, n) of the fluids are shown in **Table 4-14**.

$$\dot{\gamma}_s = \frac{v_s}{D_p} \quad \text{Equation 4-2}$$

Note that measured settling velocity values consider the effects of the shear viscosity as well as the elasticity. Therefore, shear rates estimated using Equation 4-2 are actually lower than what would have been observed in fluids with the same shear viscosity but no elasticity. As a result, the apparent viscosity values calculated using Equation 4-1 (and reported in **Table 4-14**) are actually on the high side.

**Table 4-14. Settling velocities of spherical particles of 2 mm diameter in Set-II test fluids along with apparent shear viscosities and other rheological properties (K, n).**

Test fluid	Consistency index, K (Pa.s <sup>n</sup> )	Flow behavior index, n	Apparent shear viscosity, Pa.s	Settling velocity (m/s)	Standard deviation
Fluid B-4	0.16	0.38	0.0167	0.039	1.70x10 <sup>-3</sup>
Fluid B-5	0.27	0.35	0.0281	0.0307	3.60x10 <sup>-4</sup>
Fluid B-6	0.53	0.38	0.1198	0.011	5.90x10 <sup>-4</sup>

The settling velocity of the particles was the highest in the test fluid which had the lowest apparent shear viscosity (Test fluid B-4) and was the lowest in the test fluid which had the highest apparent shear viscosity (Test fluid B-6). As the elasticities of all the test fluids in Set-II were the same, the disparity in the settling velocity results was attributed to the variation in shear viscosity characteristics of the fluids. **Figure 4-15** shows the correlation between the particle settling velocity and the apparent shear viscosity of the fluids.

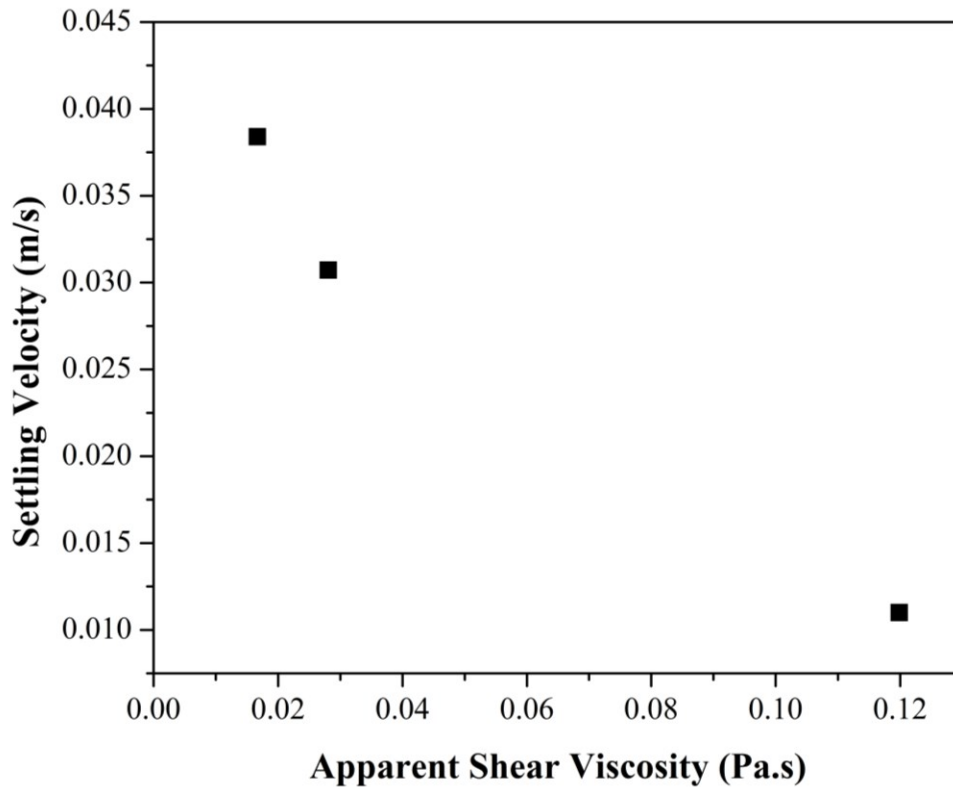


**Figure 4-15. Settling velocity of glass spheres of 2mm diameter versus apparent shear viscosity of the Set-II test fluids of Group-B.**

The particle settling velocity also correlated well with the consistency index,  $K$ . As the consistency index,  $K$ , of the fluid increased, the particle settling velocity reduced noticeably. Since the flow behavior indices,  $n$ , of the fluids were almost the same, we could say that there was a strong correlation between the drop in the settling velocity and the increase in the consistency index. When  $K$  changed from 0.16 to 0.53 Pa.s <sup>$n$</sup> , the settling velocity decreased by nearly 3.5 times.

The correlation between the particle settling velocity and the consistency index,  $K$ , of the fluids is shown in **Figure 4-16**.

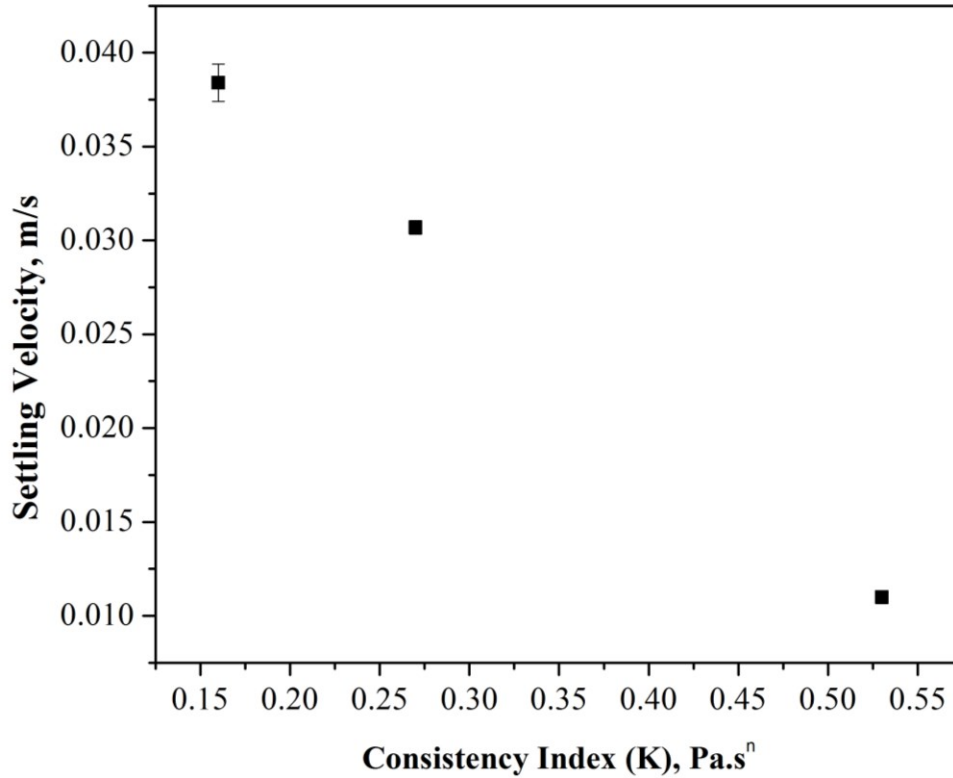


**Figure 4-16. Settling velocity of glass spheres of 2mm diameter in the Set-II test fluids of Group-B having similar elasticity ( $\lambda = 12$  s) and different consistency index ( $K$ ).**

#### 4.2.3.3 Effect of Particle Size on Settling Velocities

In general, the size of the particle has a pivotal role in regulating the particle settling velocity in any type of fluid. To assess the effect of particle size on the settling velocity of particles in shear thinning viscoelastic fluids, spheres of varying diameters (1.18 mm – 3.0 mm) were dropped in Set-I and Set-II test fluids and the corresponding settling velocities were measured. The settling velocities of spherical particles of various diameters in Set-I test fluids having similar shear thinning behavior ( $K=0.26$  Pa.s<sup>n</sup> &  $n=0.35$ ) and significantly different elastic properties are given

in **Table 4-15** and that of in Set-II test fluids having the same elastic property ( $\lambda = 12$  s) and different shear viscosities are given in **Table 4-16**.

**Table 4-15. Settling velocities of spherical particles of various diameters in Set-I test fluids with different elasticity and similar shear viscosity ( $K= 0.26 \text{ Pa}\cdot\text{s}^n$  and  $n=0.35$ )**

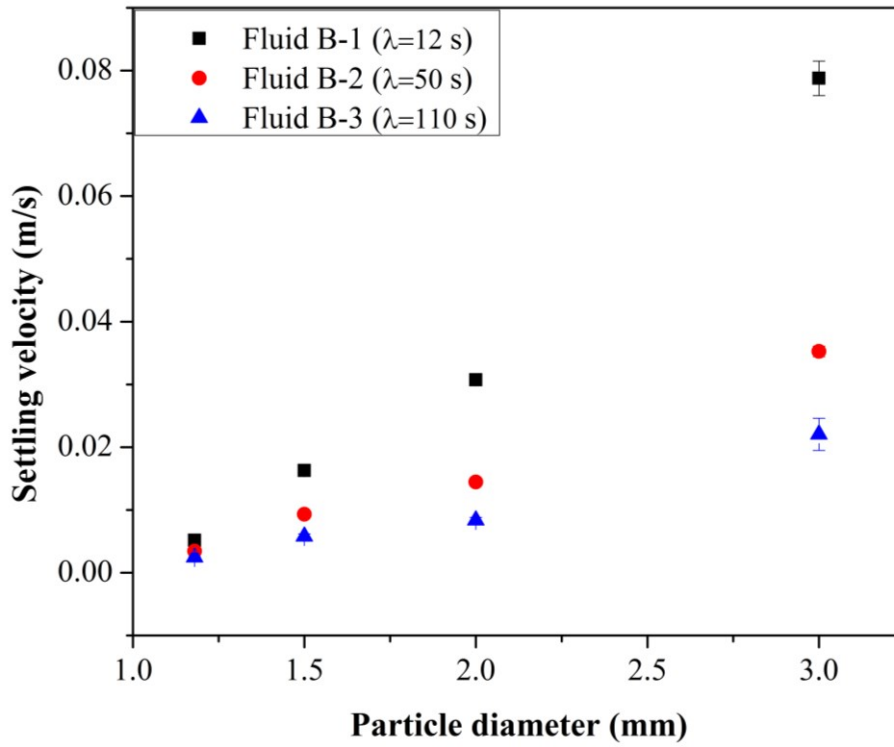
Test fluid	Relaxation time (s)	Diameter of spherical particles (mm)	Settling velocity (m/s)	Standard deviation
Fluid B-1	12	1.18	0.0052	$4.52 \times 10^{-4}$
		1.5	0.0163	$4.43 \times 10^{-4}$
		2.0	0.0307	$3.60 \times 10^{-4}$
		3.0	0.0788	$2.74 \times 10^{-3}$
Fluid B-2	50	1.18	0.0034	$9.42 \times 10^{-5}$
		1.5	0.0093	$5.58 \times 10^{-4}$
		2.0	0.0144	$3.40 \times 10^{-4}$
		3.0	0.0353	$8.45 \times 10^{-4}$
Fluid B-3	110	1.18	0.0025	$1.11 \times 10^{-4}$
		1.5	0.0058	$4.03 \times 10^{-4}$
		2.0	0.0084	$4.50 \times 10^{-4}$
		3.0	0.0220	$2.57 \times 10^{-3}$

**Table 4-16. Settling velocities of spherical particles of various diameters in Set-II test fluids with different shear viscosities and similar elasticity ( $\lambda = 12$  s)**

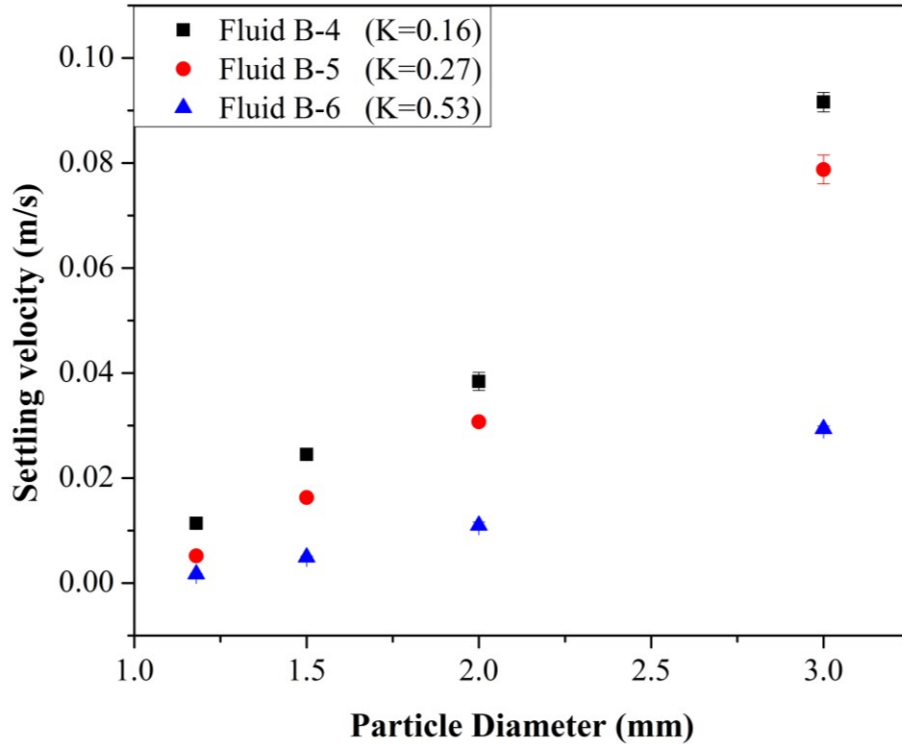
Test fluid	Consistency Index, K (Pa.s <sup>n</sup> )	Diameter of spherical particles (mm)	Settling velocity (m/s)	Standard deviation
Fluid B-4	0.16	1.18	0.0114	5.65x10 <sup>-4</sup>
		1.5	0.0245	4.50x10 <sup>-4</sup>
		2.0	0.039	1.70x10 <sup>-3</sup>
		3.0	0.0916	1.86x10 <sup>-3</sup>
Fluid B-5	0.27	1.18	0.0052	4.52x10 <sup>-4</sup>
		1.5	0.0163	4.43x10 <sup>-4</sup>
		2.0	0.0307	3.60x10 <sup>-4</sup>
		3.0	0.0788	2.74x10 <sup>-3</sup>
Fluid B-6	0.53	1.18	0.0017	1.08x10 <sup>-4</sup>
		1.5	0.0049	2.15x10 <sup>-4</sup>
		2.0	0.0110	5.90x10 <sup>-4</sup>
		3.0	0.0294	5.29x10 <sup>-4</sup>

In **Figure 4-17**, settling velocity values are also plotted against the particle diameter for comparison purpose. In Set-I fluids, the settling velocities of all particles in fluid 1 ( $\lambda=12$  s) were highest, followed by fluid 2 ( $\lambda=50$  s) and then fluid 3 ( $\lambda=110$  s). In Set-II fluids, the settling velocities of all particles in fluid 4 ( $K=0.16$  Pa.s<sup>n</sup>) were highest, followed by fluid 5 ( $K=0.26$  Pa.s<sup>n</sup>) and then fluid 6 ( $K=0.53$  Pa.s<sup>n</sup>). This reasserts the observation that when the fluid shear viscosity is constant, particle settling velocity will be lower in the fluids having higher elasticity (Fluid B-3) and when the fluid elasticity is constant, particle settling velocity will be lower in the fluids having the higher shear viscosity (Fluid B-6). Moreover, the settling velocity values were overall in an increasing trend with respect to the increase in particle diameter for all the test fluids in Set-I and Set-II. It was, however, noticeable that the magnitude of the change in settling velocity values was not the same for all the test fluids. The magnitude of the increase in settling velocity values

(with increasing particle size) seemed to occur at a lower rate when the relaxation time of the fluid was increased as shown in **Figure 4-17(a)** than that of the case when the fluid consistency index (as well as the fluid shear viscosity) was increased as shown in **Figure 4-17(b)**.



(a)



(b)

**Figure 4-17. Settling velocity versus diameter of glass spheres in (a) Set-I test fluids having a similar shear viscosity ( $K= 0.26 \text{ Pa}\cdot\text{s}^n$  and  $n=0.35$ ) but different elasticity and (b) Set-II test fluids having similar elasticity ( $\lambda = 12 \text{ s}$ ) but different shear viscosity.**

To identify the change in the magnitude of the settling velocities due to particle size increase, we have defined an “increase factor” as the ratios of settling velocities of 1.5mm, 2mm and 3mm particles to that of 1.18mm particles. The increase factors for different particle size and fluid combinations were calculated and tabulated in **Table 4-17**.

**Table 4-17. Increase factor of settling velocities of glass spheres in Set-I and Set- II test fluids**

Ratio of velocities of spheres of diameter	Set-I fluids			Set-II fluids		
	Fluid B-1 ( $\lambda=12 \text{ s}$ )	Fluid B-2 ( $\lambda=50 \text{ s}$ )	Fluid B-3 ( $\lambda=110 \text{ s}$ )	Fluid B-4 (K=0.16)	Fluid B-5 (K=0.26)	Fluid B-6 (K=0.53)
1.5 mm to 1.18 mm	3.2	2.7	2.3	2.2	3.2	2.9
2 mm to 1.18 mm	5.9	4.2	3.4	3.4	5.9	6.4
3 mm to 1.18 mm	15.2	10.3	8.9	8.0	15.2	17.2

For the Set-I fluids, the increase factor in particle settling velocity (due to increasing particle size) was found to be decreasing from fluid 1 to fluid 3 as the relaxation times (and hence the elasticity) of the fluids increased from 12sec to 110sec. That is larger particles settle down at a slower rate as the elasticity of the fluid increases. In other words, as the particle size increases, the increase in particle settling velocity occurs at a relatively lower rate as the fluid elasticity increases. From the practical point of field operations, these results imply that increasing the fluid elasticity may be a good solution for controlling particle settling velocity of large size drilled cuttings.

For the Set-II fluids, the magnitude of the increase in the settling velocity of the particles (due to increasing particle size) was observed at a higher rate as the shear viscosity of the fluid increased. In other words, the effect of particle size increase on the particle settling velocity becomes more dominant at the high shear viscosity values. From the practical point of field operations, these results imply that increasing the shear viscosity may not be the most effective solution for controlling particle settling velocity of large size drilled cuttings.

Based on these experimental results, it can be concluded that increasing the fluid elasticity (rather than the fluid shear viscosity) would be more effective way of controlling the particle settling velocity when dealing with large size drilled cuttings. However, consequential effects of increasing fluid elasticity on the other operational parameters are still uncertain and yet to be investigated. One area of interest, for example, would be to determine how the increasing fluid elasticity would influence the frictional pressure losses while drilling deep vertical wells, and/or long horizontal and extended reach wells.

### 4.3 CONCLUSIONS

The key conclusions from the experimental results of Group-A test fluids are summarized below:

- The results of the rheological measurements demonstrated that test fluids of Group-A had almost identical shear thinning viscosity behavior but different elasticity that was quantified in terms of the longest relaxation times as 12, 50, 110 and 150 sec.
- The results of settling velocity measurements of 2mm spherical particles in these test fluids of Group-A presented here confirmed that the settling velocity of the particles was strongly influenced by the elastic properties of the fluids. Moreover, the longest relaxation time of the fluid can be used to quantify such effect.
- When the longest relaxation time of the fluids was varied from 12 to 150 sec, the settling velocity of the particles in these fluids decreased from 0.0108 m/s to 0.00296 m/s, respectively.
- Finally, within the range of the tests conducted in this study, if the influence of elasticity was not taken into consideration, the settling velocities would have been overpredicted by anywhere from 6.5 to 24 times.

The key conclusions from the experimental results of Group-B (Set-I & Set-II) test fluids are summarized below:

- Results of rheological measurements indicated that Set-I of Group-B test fluids had almost identical shear viscosity, but significantly different elasticity properties and Set-II of Group-B test fluids had similar elasticity but different shear viscosities.
- Settling velocities of glass spheres in these two sets of test fluids were measured using Particle Image Shadowgraph (PIS) technique, and the experimental results showed that:

- In fluids of almost identical shear viscosity, the settling velocity of spherical particles decreased significantly with the increasing fluid elasticity.
- In fluids of constant elasticity, the settling velocity of spherical particles also decreased significantly when the fluid shear viscosity was increased.
- The settling velocity of spherical particles increased significantly in both sets of the test fluids as the particle diameter increased from 1.18mm to 3mm. However, the magnitude of the increase in settling velocity with the increasing particle diameter was considerably less with the fluids having higher elasticity and similar shear viscosity characteristics.
- The experimentally measured settling velocities in the fluids of almost identical shear viscosity but different elasticity were compared with the settling velocity values calculated from Shah et al. [5] model developed for predicting the settling velocity of spherical particles in visco-inelastic power law type fluids. Results showed that the settling velocity values could be overpredicted by a range of 14 to 50 times if the effect of the fluid elasticity was not considered.

To sum it up, the fluid shear viscosity and the elasticity both seem to have a significant effect on the particle settling velocity. However, from the field operational point of view, fluids with high shear viscosity values may not always be practical to use as the high shear viscosity values increase the parasitic pressure losses. In such cases, increasing the fluid elasticity may help to reduce the particle settling velocity even when using fluids with low shear viscosity values, especially when large size drill cuttings need to be transported. Though practical problems associated with the increasing elasticity of fluids are yet to be investigated, leveraging the effect of elasticity to reduce settling velocity of particles appears to be beneficial.

## 4.4 APPENDIX

### 4.4.1 Settling velocity in Group-A fluids as per Shah et al. model

The settling velocity of the spherical particle in a power law inelastic fluid ( $K=0.53 \text{ Pa}\cdot\text{s}^n$  &  $n=0.38$ ) was determined using the model developed by Shah et al.[5] as follows:

$$K = 0.53 \text{ Pa}\cdot\text{s}^n, n = 0.38, \rho_f = 1005 \text{ kg/m}^3, \rho_s = 2510 \text{ kg/m}^3 \text{ \& } d_p = 0.002 \text{ m}$$

$$\begin{aligned} \text{Step-1:} \quad A &= 6.9148n^2 - 24.838n + 22.642 = 14.202 \\ B &= -0.5067n^2 + 1.3234n - 0.1744 = 0.2554 \end{aligned}$$

$$\text{Step-2:} \quad (C_D^{2-n} \text{Re}^2)^{\frac{1}{2}} = \left( \frac{13.08^{2-n} d_p^{n+2} \rho_f^n (\rho_p - \rho_f)^{2-n}}{2^{2(n-1)} K^2} \right)^{\frac{1}{2}} = 19.9185$$

$$\text{Step-3:} \quad \text{Re} = \left( \frac{(C_D^{2-n} \text{Re}^2)^{\frac{1}{2}}}{A} \right)^{\frac{1}{B}} = 3.76$$

$$\text{Step-4:} \quad V_t = \left( \frac{2^{n-1} K \text{Re}}{d_p^n \rho_f} \right)^{\frac{1}{2-n}} = 0.07 \frac{\text{m}}{\text{s}}$$

### 4.4.2 Settling velocity in Set-I of Group-B test fluids as per Shah et al. model

The settling velocity of the spherical particle in a power law inelastic fluid ( $K=0.26 \text{ Pa}\cdot\text{s}^n$  &  $n=0.35$ ) was determined using the model developed by Shah et al.[5] as follows:

$$K = 0.26 \text{ Pa}\cdot\text{s}^n, n = 0.35, \rho_f = 998 \text{ kg/m}^3, \rho_s = 2510 \text{ kg/m}^3 \text{ \& } d_p = 0.002 \text{ m}$$

$$\begin{aligned} \text{Step-1:} \quad A &= 6.9148n^2 - 24.838n + 22.642 = 14.7957 \\ B &= -0.5067n^2 + 1.3234n - 0.1744 = 0.2267 \end{aligned}$$

Step-2: 
$$\left(C_D^{2-n} \text{Re}^2\right)^{\frac{1}{2}} = \left(\frac{13.08^{2-n} d_p^{n+2} \rho_f^n (\rho_p - \rho_f)^{2-n}}{2^{2(n-1)} K^2}\right)^{\frac{1}{2}} = 47.7074$$

Step-3: 
$$\text{Re} = \left(\frac{\left(C_D^{2-n} \text{Re}^2\right)^{\frac{1}{2}}}{A}\right)^{\frac{1}{B}} = 175$$

Step-4: 
$$V_s = \left(\frac{2^{n-1} K \text{Re}}{d_p^n \rho_f}\right)^{\frac{1}{2-n}} = 0.4374 \frac{m}{s}$$

#### 4.5 REFERENCES

- [1] Larson, R.G. 1998. *The Structure and Rheology of Complex Fluids*, New York: Oxford University Press.
- [2] Sunthar, P. 2010. Polymer Rheology. In *Rheology of Complex Fluids*, 171-191. Springer New York.
- [3] Choi, S.K. 2008. *pH Sensitive Polymers for Novel Conformance Control and Polymer Flooding Applications*. PhD Thesis, University of Texas, , Austin.
- [4] McKinley, G.H. 2002. Steady and Transient Motion of Spherical Particles in Viscoelastic Liquids. In *Transport Processes in Bubbles, Drops & Particles*, 2nd edition,ed. Chhabra, R. and De Kee, D., Chap. 14. New York: Talylor & Francis.
- [5] Shah, S.N., El Fadili, Y. and Chhabra, R.P. 2007. New Model for Single Spherical Particle Settling Velocity in Power Law (Visco-Inelastic) Fluids. *International Journal of Multiphase Flow* **33** (1): 51-66. <http://dx.doi.org/10.1016/j.ijmultiphaseflow.2006.06.006>.
- [6] Gomaa, A.M., Gupta, D.V.S.V. and Carman, P.S. 2015. Proppant Transport? Viscosity Is Not All It's Cracked up to Be. Presented at SPE Hydraulic Fracturing Technology

- Conference, 3-5 February., The Woodlands, Texas, USA., 2015/2/3/. SPE-173323-MS.  
<http://dx.doi.org/10.2118/173323-MS>.
- [7] Hassager, O. 1979. Negative Wake Behind Bubbles in Non-Newtonian Liquids. *Nature* **279** (5712): 402-403. <http://dx.doi.org/10.1038/279402a0>.
- [8] Maalouf, A. and Sigli, D. 1984. Effects of Body Shape and Viscoelasticity on the Slow Flow around an Obstacle. *Rheologica Acta* **23** (5): 497-507. <http://dx.doi.org/10.1007/bf01329282>.
- [9] Lali, A.M., Khare, A.S., Joshi, J.B. and Nigam, K.D.P. 1989. Behaviour of Solid Particles in Viscous Non-Newtonian Solutions: Settling Velocity, Wall Effects and Bed Expansion in Solid-Liquid Fluidized Beds. *Powder Technology* **57** (1): 39-50. [http://dx.doi.org/10.1016/0032-5910\(89\)80102-0](http://dx.doi.org/10.1016/0032-5910(89)80102-0).
- [10] Chhabra, R.P. 2007. *Bubbles, Drops, and Particles in Non-Newtonian Fluids, Second Edition*: CRC Press, Taylor & Francis Group.

**CHAPTER 5: EXPERIMENTAL INVESTIGATION OF FLOW  
FIELD PAST A SPHERICAL PARTICLE SETTLING IN  
VISCOELASTIC FLUIDS USING PARTICLE IMAGE  
VELOCIMETRY TECHNIQUE**

In chapter-4, the results of the settling velocity measurements demonstrated the reduction of settling velocity of the spherical particles with the increase of elasticity of the fluid. However, our understanding of why the change in fluid elasticity influences the particle settling velocity was very limited at this point. For that reason, in Chapter-5, an experimental study was performed to investigate the fluid flow field behind the settling particle by using particle image velocity (PIV) technique to understand the changes caused by the elasticity of the fluid. The chapter-5, therefore, comprises of: (1) the composition details of the HPAM test fluids and their mixing procedure. (2) The description of PIV technique, its experimental setup, and the procedure to investigate the flow field past the settling particle in the test fluids using PIV technique. (3) The results and discussions of the rheological measurements of test fluids; and the experimental investigation of flow fields behind the settling particle in the viscoelastic fluids.

## 5.1 MATERIALS AND METHODS

### 5.1.1 Test fluids and their rheological measurements

Two test fluids, Fluid A-1 and Fluid A-4, were prepared using partially hydrolyzed polyacrylamide (HPAM) polymer of three different grades of molecular weight. The test fluids were formulated in such a way that the average molecular weight of all test fluids was constant and the molecular weight distribution (MWD) was different. The average molecular weight of the polymer blend ( $M_{w,B}$ ) was calculated by using Equation 5-1, and its molecular weight distribution (MWD) was quantified in terms of polydispersity index (I) using Equation 5-2.

$$M_{w,B} = \prod_{i=1}^n M_{w,i}^{\omega_i} \quad \text{Equation 5-1}$$

$$I = \frac{M_w}{M_n} = \left( \sum_{i=1}^n \omega_i M_{w,i} \right) \times \left( \sum_{i=1}^n \frac{\omega_i}{M_{w,i}} \right) \quad \text{Equation 5-2}$$

The average molecular weight of the polymer blend ( $M_{w,B}$ ) in the test fluids was maintained to be 8,000,000 g/gmol. The objective behind the test fluids preparation was to have identical shear thinning viscosity behavior and significantly different elastic properties. The preparation procedure of test fluids, Fluid A-1 and Fluid A-4, was already discussed in Chapter 3, Section 3.3. The composition details of test fluid A-1 and fluid A-4 are shown in **Table 5-1**.

**Table 5-1. Polymer blend composition details of the test fluids**

Sample	Conc. of polymer blend (wt%)	Wt % of HPAM of Molecular weight (g/gmol)			Polydispersity Index (I)
		20 x 10 <sup>6</sup>	8 x 10 <sup>6</sup>	0.5 x 10 <sup>6</sup>	
Fluid A-1	0.09	0	100	1	1
Fluid A-4	0.1	53.58	28.72	17.7	5.5

The method followed to perform the rheological measurements such as shear viscosity and oscillatory frequency sweep on the test fluids were discussed in Chapter 3, Section 3.4.3.

### 5.1.2 Particle Image Velocimetry (PIV) Technique

Particle image velocimetry (PIV) is an optical technique widely employed to visualize the fluid flow in various the applications. This technique measures the instantaneous velocities of fluid flow [1]. Buoyant tracer-particles(i.e., small sized seeding particles) closely moving along with the flow of fluid are added to the flow so that velocity of the fluid particles could be recorded using PIV techniques [1]. The movement of these tracer particles in the flow is visualized by illuminating them using a light source, and their movement is captured by using a recording element. The light from the illumination source gets scattered by the tracer particles, and the intensity of the scattered light should be sufficient enough so that the tracer particles can be detected in the captured images. Therefore, the concentration of the tracer particles is crucial to acquire adequate spatial details of the fluid flow [2]. The magnitude of the fluid flow velocity and its direction are then determined

by calculating the tracer particles velocity within the flow from the captured images [1]. Two images of the tracer particles are captured at a known interval of time ( $dt$ ). The velocity of the tracer particles is calculated by obtaining the displacement of tracer particles ( $ds$ ) between the two captured images using various statistical evaluation techniques [1]. The PIV technique is a non-intrusive optical technique for velocity measurements of fluid as the flow is not being disturbed by introducing any probes or devices in it [1]. The fluid medium has to be transparent for the best results of velocity measurement.

### 5.1.3 PIV Experimental Setup

The experimental setup consisted of a New Wave Research Solo III laser, a diffuser, a Lavisson Image Intense CCD camera, Nikon 50mm AF Nikkor lens of 1.4 mm aperture, fluid particle column, Lavisson Davis 8.3 software. **Figure 5-1** illustrates the schematic diagram of the PIV setup used for the current experimental study to visualize the fluid flow field.

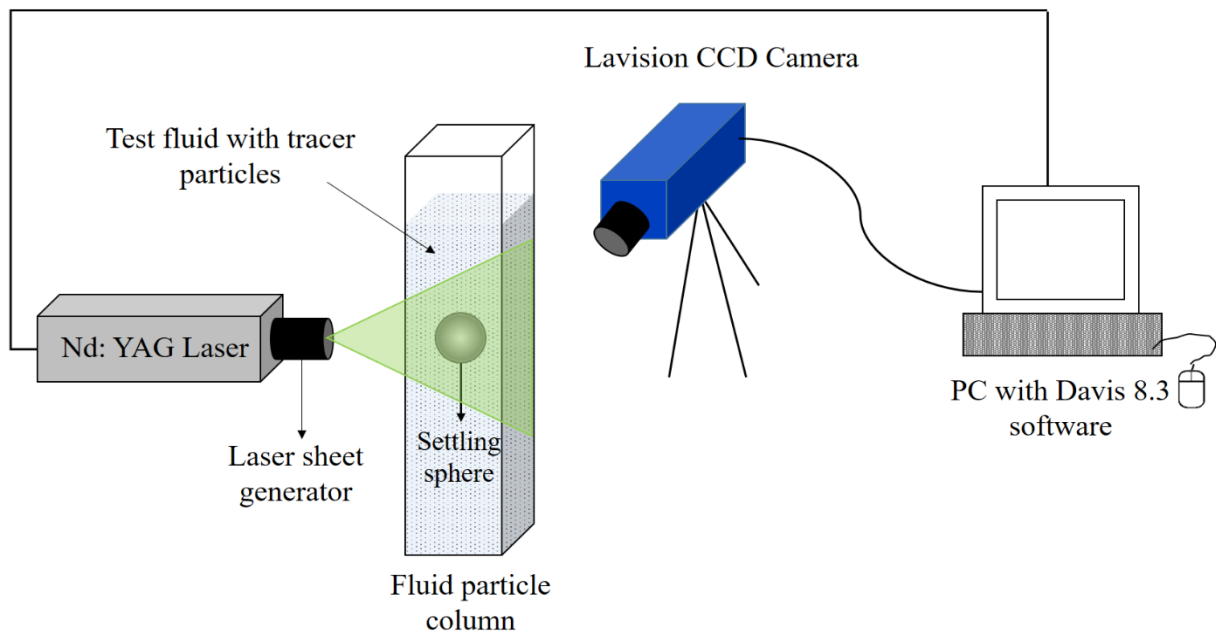


**Figure 5-1.** The schematic diagram of the PIV experimental setup used to visualize the fluid flow field past the settling spherical particle

The New Wave Research Solo III laser was a 50 mJ double pulsed Nd:YAG class 4 laser that produces a green laser beam of wavelength 532 nm at a frequency of 15Hz. This laser was used as an illuminating source in the study. The special diffuser was attached to the laser so that a thick laser sheet was generated and the thickness of the generated laser sheet was maintained at 3.0 mm. The laser setup was placed at 35 cm height and 15 cm away from the fluid particle column.

Lavision Image Intense CCD camera was a double frame high-resolution camera with a CCD (charge couple device) sensor of 1376x1040 pixels and with a framing rate of 5 frames per second. The CCD sensor delivered the digital copy of the light patterns by converting the photons into electric charge. The camera was able to capture images at two different exposure times with the time interval of as short as 500 ns. The time interval between the images was adjusted according to the velocity of the fluid flow. The typical time interval between the images should be sufficient enough to let the tracer particles move by 5 to 8 pixels from the first frame to the second frame [3, 4]. A 50 mm Nikon AF Nikkor lens of 1.4 mm aperture was used to capture broader flow fields, and this lens was connected to the camera with a 12 mm long extension tube.

The fluid particle column was a transparent cubical container made up of acrylic. The dimensions of the fluid particle column were 11 cm x 11 cm x 70 cm. The tracer particles used in the study were glass hallow spheres having a mean diameter of 10  $\mu\text{m}$  and density of  $1.1 \pm 0.05$  g/cc. These glass hallow spheres were obtained from Lavision and were typically used for water based fluid solutions.

Data acquisition and image processing were done using commercial software, Lavision Davis 8.3. The camera and the laser were connected to a computer having Davis 8.3 software running on it from which both the camera and the laser were synchronized. Once all the image processing was done on the PIV mode of the Davis 8.3 software, the output data was then

transferred as a text file to Microsoft excel for further analysis. In the post-processing, for the first image, an interrogation window of size 256x256 pixels was selected as a beginning step, and this interrogation window was compared with the second image to correlate the possible similarities [5]. The process of identification of local resemblances of the brightness intensities in the two images was done by employing Direct Cross-Correlation Method (DCM) [5, 6]. The region in the second image that cross-correlates very well with the interrogation window of the first image provides the highest peak in the correlation plane as shown in **Figure 5-2** [7].

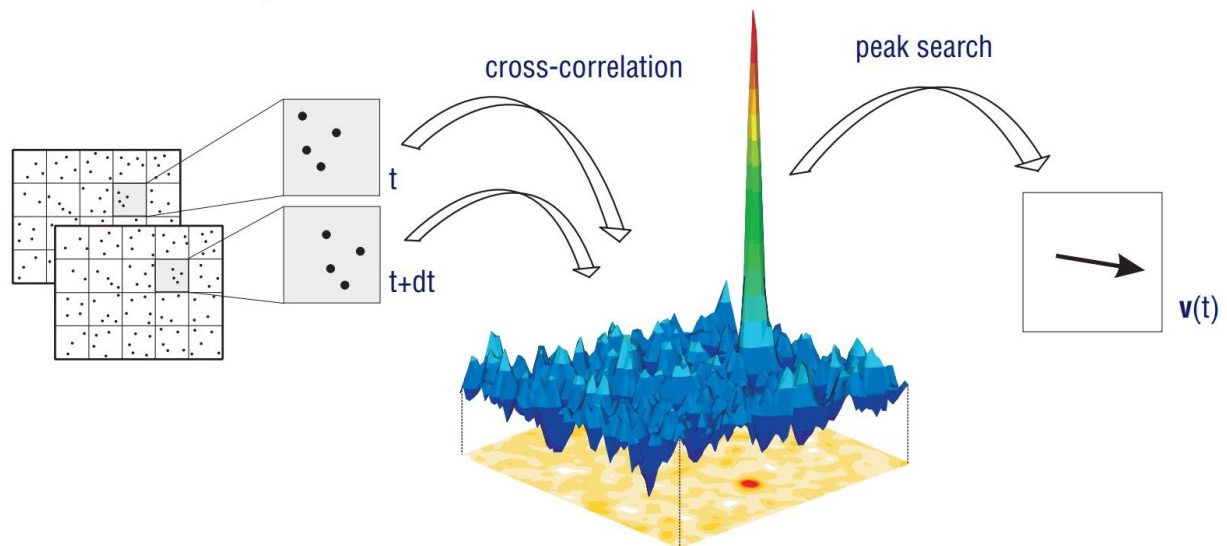


**Figure 5-2. The PIV post processing schematic to determine instantaneous velocity [7]**

The mean displacement of the tracer particles,  $ds$  ( $dx$  and  $dy$ ) in the respective interrogation window is obtained from the location of the highest peak in the correlation plane. Since the time interval between the two images is known, the instantaneous velocity in  $x$  and  $y$  direction can be determined using Equation 5-3.

$$U = \frac{dx}{dt}$$
$$V = \frac{dy}{dt}$$

Equation 5-3

#### 5.1.4 Experimental procedure to investigate the fluid flow field by PIV technique

Once the test fluid was prepared, tracer particles (glass hallow spheres) were added at an optimized concentration of 20ppm to the test fluid and mixed for 20 min. The test fluid with entrained tracer particles was then transferred into the fluid particle column and left undisturbed for overnight to remove all the air bubbles from the test fluid. The double pulsed laser along with the diffuser and the double framed camera were placed on two adjacent sides of the fluid particle column so that they were orthogonal to each other. The laser and the camera were connected to the computer on which Davis 8.3 software was running. A calibration sheet with a grid pattern was inserted into the fluid particle column. The grids were at distance of 1.5 mm from each other; they were printed in black color on a white background as shown in **Figure 5-3**.

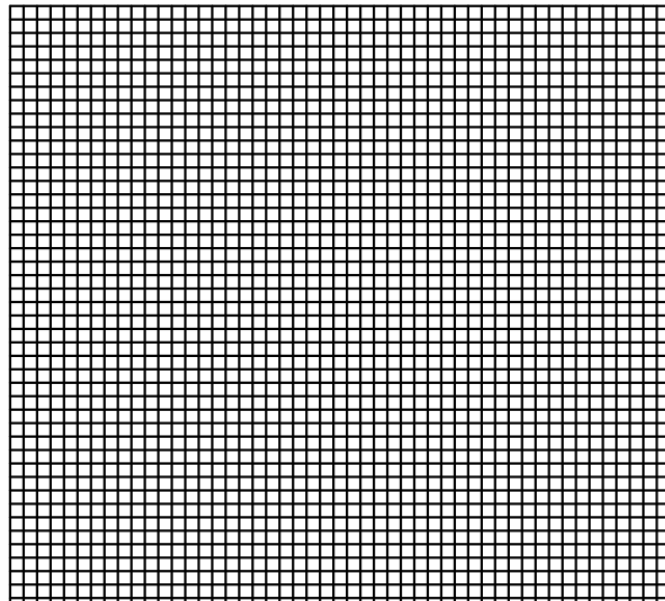


**Figure 5-3. Calibration sheet used to calibrate the camera**

Now, 50 mm Nikon lens was mounted onto the camera and adjusted so that the grid pattern of calibration sheet was in focus. The imaging system was then scaled by choosing two points on the captured image of the grid pattern and defining the distance between the two points. The position of the calibration sheet was marked before removing it so that it would be convenient to drop the spherical particles in the focal plane later on.

After ensuring the camera temperature was below  $-11^{\circ}\text{C}$ , the laser was switched on. The energy of laser source was adjusted to maximum, the powers of laser 1A (first pulse) and laser 1B (second pulse) were adjusted to 30% and 20% respectively. The power of the second pulse was kept lower than that of the first pulse because the exposure time of the second frame would be more than that of the first frame. The diffuser that was attached to the laser was adjusted so that the thickness of the laser sheet was about 3.0 mm. Once the laser was incident on the fluid, the picture of the fluid was then checked to make sure that the image was not saturated (counts should be less than 4000).

The PIV experimental images were now captured by dropping the 2mm spherical particles from the earlier marked position. The time gap of 20 min was maintained before dropping the second spherical particle so that the fluid would recover from the disturbance created by the first settling spherical particle. Several experimental images were captured to ensure repeatability and reproducibility in data. The captured PIV image of the settling particle in the illuminated test fluid with entrained tracer particles would be similar to the one shown in **Figure 5-4**. The bright spots on the black background in the **Figure 5-4** were the tracer particles in the test fluid.

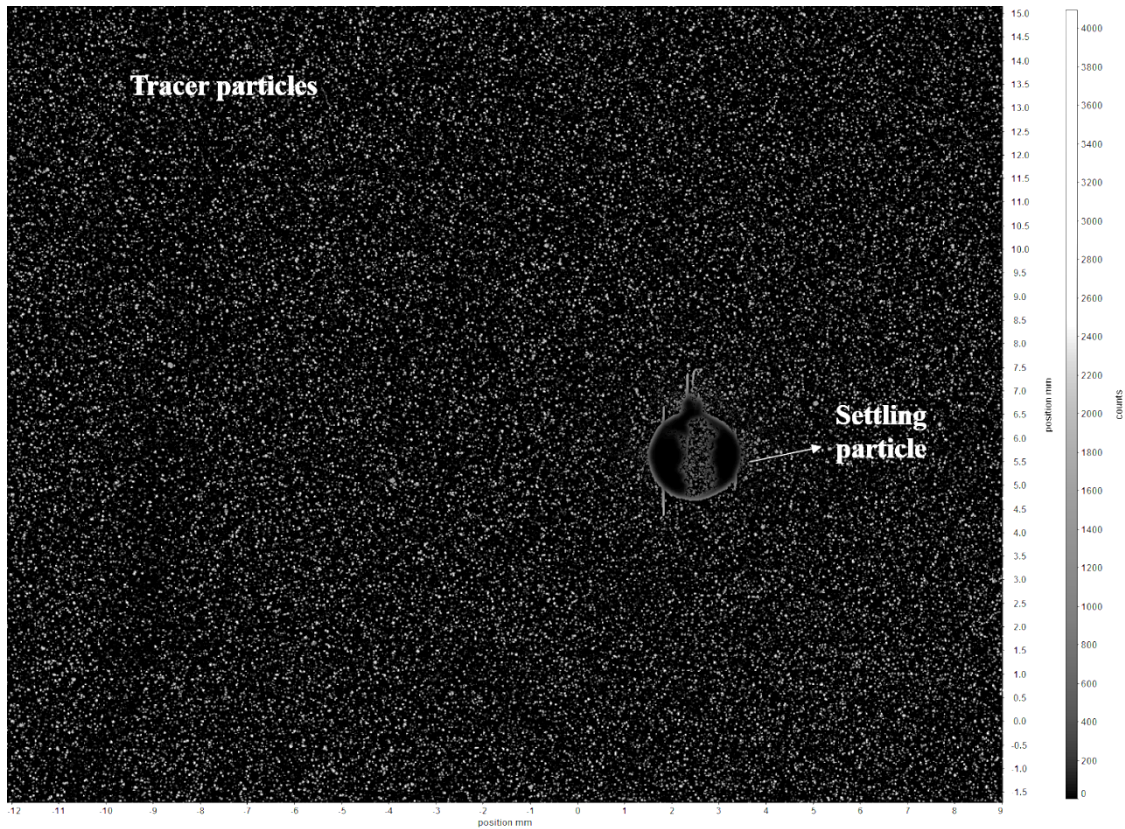


**Figure 5-4. The captured PIV image of a settling particle in the test fluid containing tracer particles**

The experimental images were then post-processed to determine the instantaneous velocity field of the fluid flow. The first interrogation window size was chosen as 256x256 pixels, and the DCM algorithm was applied to detect the highest cross correlation peak region. Later, the second interrogation window size was reduced to 96x96 pixel. The overlapping percentage for the multi-pass DCM was chosen as 75%. Non-linear post-processing filter was then applied to the computed vector field to remove outlier vectors. The setting for the post-processing filter was the “universal outlier detection”.

### 5.1.5 PIS experimental setup and experimental procedure

The settling velocity values of the spherical particles in test fluid A-1 and fluid A-4 were measured by particle image shadowgraph (PIS) technique. The details of the PIS experimental setup and the experimental procedure followed to measure the settling velocity of the particles were discussed in Chapter 3, Section 3.5 and Section 3.6 respectively.

## 5.2 RESULTS AND DISCUSSIONS

### 5.2.1 Test fluids characterizations

**Figure 5-5** and **Figure 5-6** provide the shear stress versus shear rate and the shear viscosity versus the shear rate profiles of the test fluids A-1 & A-4. From the rheological data, it was confirmed that both test fluids exhibited shear thinning characteristics (i.e. decrease of shear viscosity with the increasing shear rate). Furthermore, the viscous characteristics of the fluids were almost the same as indicated by the similarities of the shear stress versus shear rate (**Figure 5-5**) and the shear viscosity versus the shear rate (**Figure 5-6**) profiles.

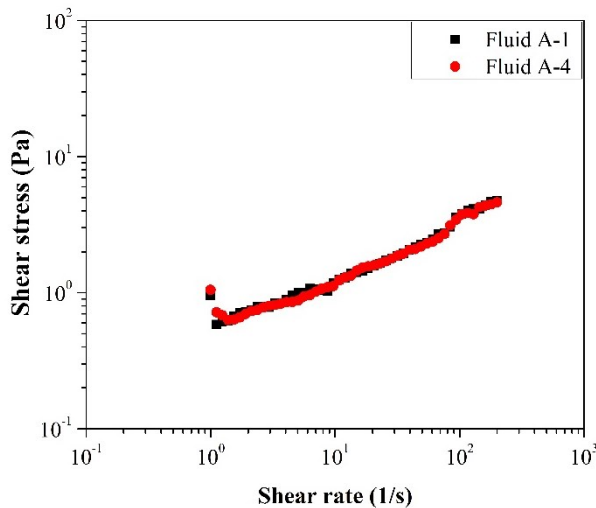


**Figure 5-5. Shear stress versus shear rate profiles of test fluids A-1 and A-4**

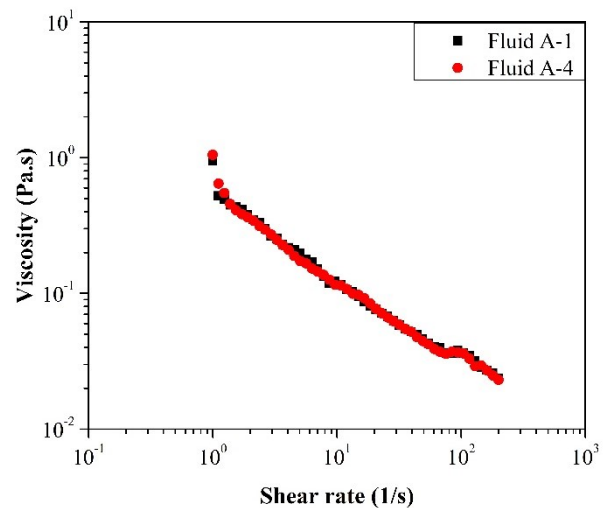


**Figure 5-6. Shear viscosity versus shear rate profiles of test fluids A-1 and A-4**

The values of the consistency index (K), the flow behavior index (n) of the test fluids were obtained by fitting power law model to the shear stress versus shear rate data and same are summarized along with the coefficient of determination ( $R^2$ ) in **Table 5-2**. The K & n values also confirmed that the test fluids had almost identical shear thinning characteristics.

**Table 5-2. Power law parameters K & n for the test fluids A-1 & A-4**

Test fluid	K (Pa.s <sup>n</sup> )	n	R <sup>2</sup>
Fluid A-1	0.53	0.38	0.96
Fluid A-4	0.53	0.37	0.96

**Figure 5-7** and **Figure 5-8** provide the oscillatory frequency sweep data of test fluids A-1 and A-4, respectively. The frequency sweep data provided the dependence of storage modulus ( $G'$ , represents the solid-like behavior) and loss modulus ( $G''$ , represents the liquid-like behavior) of the fluid on the angular frequency. The longest relaxation time of the fluid was determined by taking the inverse of the crossover frequency at which storage modulus ( $G'$ ) and loss modulus ( $G''$ ) became equal. The relaxation time is the time required to regain the original structure after deformation and can be used as a measure of the elasticity [8]. The fluid with the higher relaxation time will be the fluid with higher elasticity.

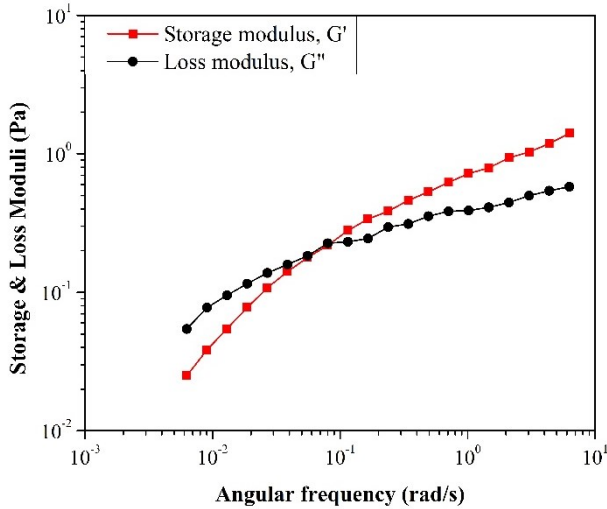


**Figure 5-7. Oscillatory frequency sweep data of fluid A-1**

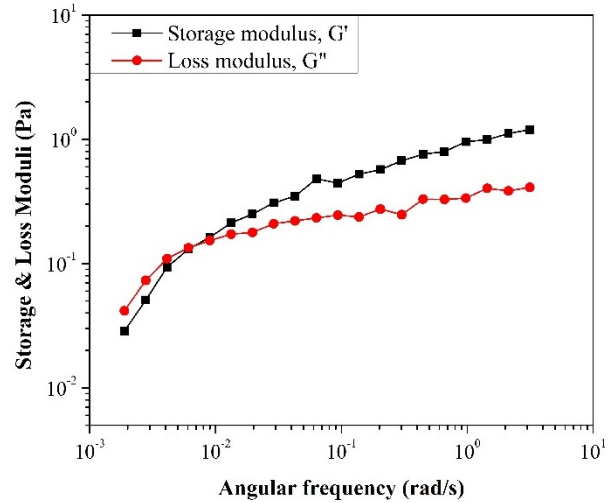


**Figure 5-8. Oscillatory frequency sweep data of fluid A-4**

Experimentally measured relaxation times of the test fluids A-1 and A-4 are given in **Table 5-3**. These experimentally measured relaxation time values were taken as the representative numbers to quantify the elastic properties of the test fluids.

**Table 5-3. Longest relaxation times of the test fluids A-1 & A-4**

Test fluid	Polydispersity (I)	Longest relaxation time (s)
Fluid A-1	1	12
Fluid A-4	5.5	150

From the results of the viscosity and the frequency sweep measurements, it was concluded that test fluids A-1 and A-4 had almost identical shear thinning viscosity behavior but significantly different elasticity characteristics.

### 5.2.2 PIV results

**Figure 5-9** and **Figure 5-10** represent the PIV images of the velocity fields around and past the settling spherical particle in the test fluid A-1 and test fluid A-4 respectively. It can be noticed from **Figure 5-9** and **Figure 5-10** that the fluid surrounding the settling particle (i.e. at the immediate vicinity of the particle) was moving downwards. This downward movement of the fluid was caused by the particle settling down in the fluid around it.

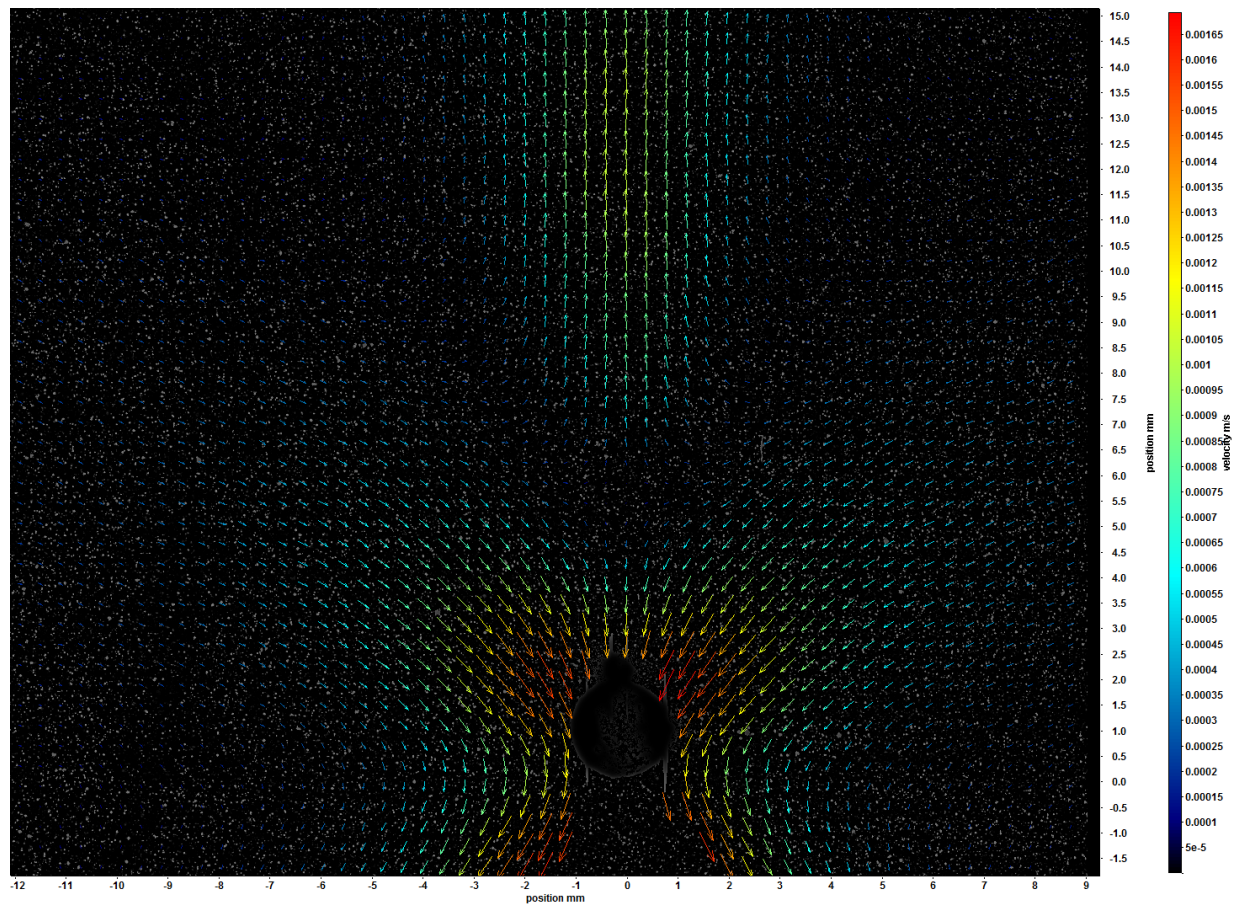


**Figure 5-9. Velocity field around and past the settling particle in the test fluid A-1**

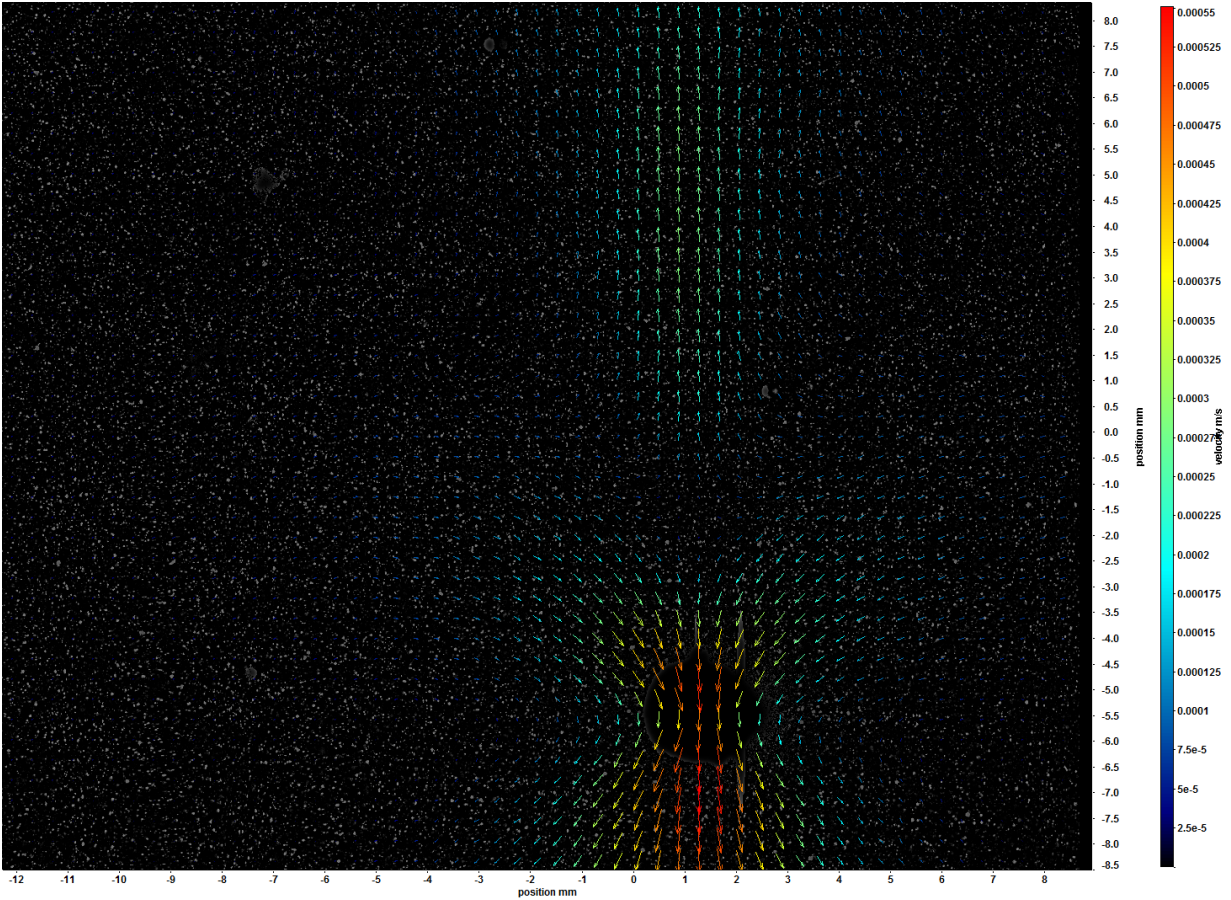


**Figure 5-10. Velocity field around and past the settling particle in the test fluid A-4**

However, past the settling particle, the downward movement of fluid in y-direction was gradually reduced in both fluids and at a certain point the velocity of the fluid in both cases became zero. Beyond this point, the recirculation regions were observed in both fluid A-1 and fluid A-4. The recirculation region was the region in which the fluids started moving in the opposite direction to the particle movement as seen in **Figure 5-9** and **Figure 5-10**. In the past, this type of recirculation region in the sphere wake was observed by Sigli and Coutenceau [9] during their flow visualization studies conducted in shear thinning fluids such as polyethylene oxide. The point at which the velocity of the fluid became zero was the stagnation point of the settling particle wake [10].

The recirculation region where the fluid moves in the opposite direction of particle movement was referred as the “negative wake” by Hassager [11] as he had similar observations when the bubbles were rising in polyacrylamide and glycerol viscoelastic solutions. This phenomenon of the negative wake was observed only in the viscoelastic fluids. In a viscous Newtonian fluid, however, the movement of the fluid behind the settling particle was downward [12]. Maalouf & Sigli [13] and Zheng et al. [14] deduced that the negative wake generation was due to shear thinning and viscoelastic properties of the fluid. Harlen [15] reported that there were two opposite forces acting on the particle settling in a viscoelastic fluid. The force due to relaxation of shear stresses created near the settling particle causes the fluid to move in the opposite direction of the particle movement and the force due to extensional stresses created behind the settling particle causes the fluid to move in the same direction of the particle movement [15]. The recent work by Frank et al. [16, 17] also showed that the generation of the negative wake was due to the viscoelasticity of the fluid.

The fluid velocity values along y-direction from the surface of the settling spherical particle in the test fluid A-1 and the test fluid A-4 were quantified. As the velocity of the fluid was directly dependent upon the settling velocity of the spherical particle, the fluid velocity values were normalized using the settling velocity of the spherical particle in the respective fluids to evaluate the normalized velocity profiles of fluid A-1 and fluid A-4. The settling velocity values of the spherical particles in test fluid A-1 and test fluid A-4 that were measured using particle image shadowgraph technique (PIS) technique are provided in **Table 5-4**.

**Table 5-4. Settling velocities of 2mm diameter spherical particles in the test fluids**

Test fluid	Longest relaxation time (s)	Settling velocity (m/s)	Standard deviation
Fluid A-1	12	0.011	5.90E-04
Fluid A-4	150	0.00296	2.66E-04

The normalized velocity profiles of fluid A-1 and fluid A-4 along the streamline past the settling particle are shown in **Figure 5-11**. The positive values of the velocity profiles represent the fluid movement in the direction same as that of the settling spherical particle (i.e. downwards direction), and the negative values of the velocity profiles represent the fluid movement in the opposite direction as that of the settling spherical particle (i.e. upwards direction).

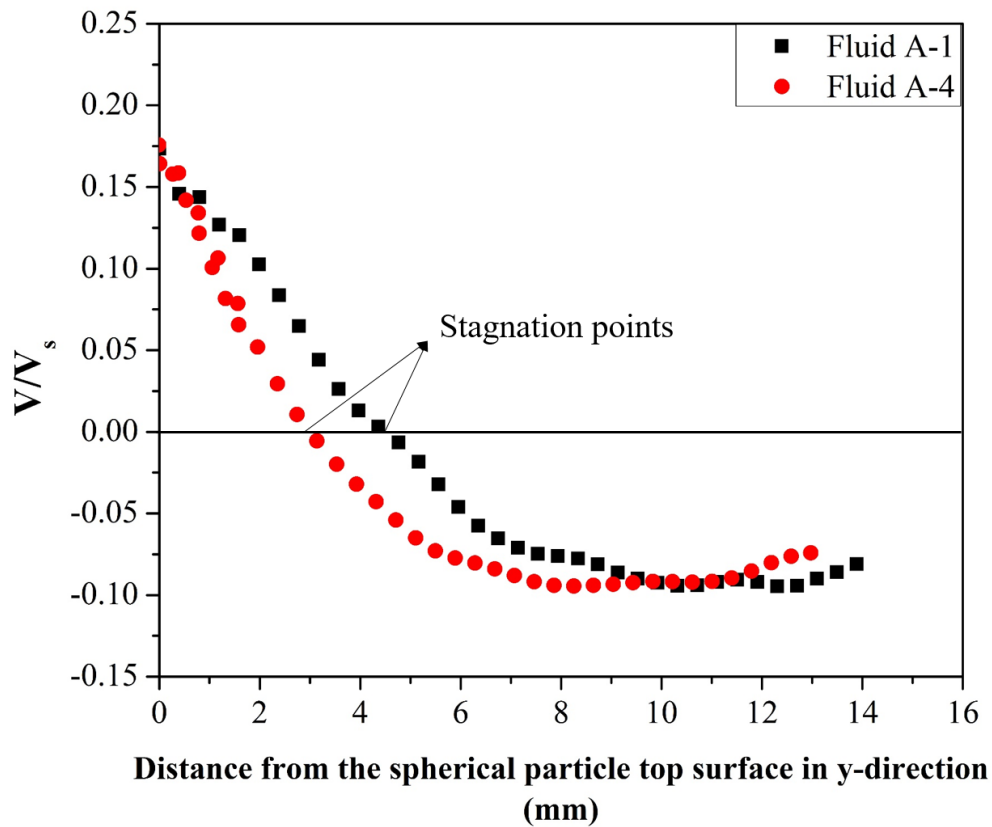


**Figure 5-11. Velocity profiles of the fluid A-1 and fluid A-4 along the streamline past the settling particle.**

It can be noticed from **Figure 5-11** that though the initial velocity of the fluid at  $y=0$  was almost same for both fluid A-1 and fluid A-4, afterwards, the magnitude of fluid velocity around the settling particle was lower in the fluid A-4 than that of fluid A-1. The velocity of the fluid in the downward direction gradually decreased for both cases and eventually became zero. However, the velocity in the downward direction reached zero value first for the test fluid A-4. The point at which velocity became minimum ( $V/V_s = 0$ ) was the stagnation point above that the fluid movement changed to reverse direction. The stagnation points in the wakes of fluid A-1 and fluid A-4 were nearly 4.56 mm and 2.94 mm away from the particle surface respectively. So the stagnation point in the wake of fluid A-4 was closer to the settling particle than the stagnation point in the wake of fluid A-1. Since both the fluids have almost identical shear thinning viscous behavior, the differences in the fluid velocity field near and past the settling spherical particle were attributed to the difference in the elastic properties of the fluids. That means, stagnation point in the wake approached closer to the settling particle with the increase of fluid elasticity. This observation was in agreement with those reported by Sigli and Coutanceau [9] and Mendoza-Fuentes et al. [10] where they noticed that the increase of Weissenberg number ( a measure of elasticity) resulted in shifting of the stagnation point nearer to the settling sphere in the shear thinning viscoelastic fluids.

In **Figure 5-11**, beyond the stagnation points, the velocity values became negative as the direction of the fluid movement got reversed. Above the stagnation point, the magnitude of the fluid velocity along the streamline was higher in fluid A-4 than that of fluid A-1. In other words, the fluid moved at a faster rate in the reverse direction in the recirculation region of fluid A-4 (i.e. higher elastic fluid) compared to that of fluid A-1 (i.e. lower elastic fluid). The movement of the fluid in the reverse direction could possibly affect the settling velocity of the spherical particle.

Since the stagnation point in the wake of the higher elastic fluid (fluid A-4) was closer to the surface of the settling particle, the effect of the negative wake of the higher elastic fluid could possibly be more prominent on the settling velocity of the particle as compared to one of the lower elasticity fluid. As a result, the settling velocity of the particle in the higher elastic fluid (0.00296 m/s) was lower than that of the one in the lower elasticity fluid (0.011 m/s). Nevertheless, the further experimental investigation is recommended with fluids having a wide range of shear thinning viscous and elastic properties to confirm validity of these observations regarding the role of negative wake in the reduction of settling velocity due to elasticity.

### **5.3 CONCLUSIONS**

The key conclusions from the experimental investigation of the fluid field past the settling spherical particle in viscoelastic test fluids A-1 and A-4 using particle image velocimetry (PIV) are summarized below:

- The results of the rheological measurements demonstrated that test fluids A-1 & A-4 had almost identical shear thinning viscosity behavior but different elasticity that was quantified in terms of the longest relaxation times as 12 and 150 sec, respectively.
- The results of PIV measurements demonstrated that negative wake was present in both test fluids. However, the stagnation point (the point at which fluid velocity becomes zero and above that the fluid starts moving in the opposite direction to the particle movement) was closer to the particle settling in the higher elasticity fluid than that in the lower elasticity fluid.
- The velocity of the fluid in the recirculation region was higher for the higher elasticity fluid than that of the lower elasticity fluid. Therefore, the presence of negative wake having fast

moving fluid in reverse direction nearer to the settling particle could possibly affect the settling velocity of the particle.

## 5.4 REFERENCES

- [1] Raffel, M., Willert, C.E., Wereley, S.T. and Kompenhans, J. 2007. *Particle Image Velocimetry: A Practical Guide*, 2nd edition, Berlin Heidelberg: Springer.
- [2] Melling, A. 1997. Tracer Particles and Seeding for Particle Image Velocimetry. *Measurement Science and Technology* **8** (12): 1406.
- [3] Bizhani, M. 2013. *Solids Transport with Turbulent Flow of Non-Newtonian Fluid in the Horizontal Annuli*. Masters Thesis, University of Alberta, Edmonton, Canada (25th Sep 2013).
- [4] LaVision. 2006. Image Intense, Product Catalogue.
- [5] Bizhani, M., Corredor, F.E.R. and Kuru, E. 2015. An Experimental Study of Turbulent Non-Newtonian Fluid Flow in Concentric Annuli Using Particle Image Velocimetry Technique. *Flow, Turbulence and Combustion* **94** (3): 527-554. <http://dx.doi.org/10.1007/s10494-014-9589-6>.
- [6] Nezu, I. and Sanjou, M. 2011. PIV and PTV Measurements in Hydro-Sciences with Focus on Turbulent Open-Channel Flows. *Journal of hydro-environment research* **5** (4): 215-230.
- [7] LaVision. 2016. Flow Master, Advanced PIV/PTV Systems for Quantitative Flow Field Analysis Product Manual
- [8] Choi, S.K. 2008. *pH Sensitive Polymers for Novel Conformance Control and Polymer Flooding Applications*. PhD Thesis, University of Texas, , Austin.
- [9] Sigli, D. and Coutanceau, M. 1977. Effect of Finite Boundaries on the Slow Laminar Isothermal Flow of a Viscoelastic Fluid around a Spherical Obstacle. *Journal of Non-Newtonian Fluid Mechanics* **2** (1): 1-21. [http://dx.doi.org/10.1016/0377-0257\(77\)80029-3](http://dx.doi.org/10.1016/0377-0257(77)80029-3).

- [10] Mendoza-Fuentes, A.J., Montiel, R., Zenit, R. and Manero, O. 2009. On the Flow of Associative Polymers Past a Sphere: Evaluation of Negative Wake Criteria. *Physics of fluids* **21** (3). <http://dx.doi.org/10.1063/1.3090180>.
- [11] Hassager, O. 1979. Negative Wake Behind Bubbles in Non-Newtonian Liquids. *Nature* **279** (5712): 402-403. <http://dx.doi.org/10.1038/279402a0>.
- [12] Arigo, M.T. and McKinley, G.H. 1998. An Experimental Investigation of Negative Wakes Behind Spheres Settling in a Shear-Thinning Viscoelastic Fluid. *Rheologica Acta* **37** (4): 307-327. <http://dx.doi.org/10.1007/s003970050118>.
- [13] Maalouf, A. and Sigli, D. 1984. Effects of Body Shape and Viscoelasticity on the Slow Flow around an Obstacle. *Rheologica Acta* **23** (5): 497-507. <http://dx.doi.org/10.1007/bf01329282>.
- [14] Zheng, R., Phan-Thien, N. and Tanner, R.I. 1991. The Flow Past a Sphere in a Cylindrical Tube: Effects of Inertia, Shear-Thinning and Elasticity. *Rheologica Acta* **30** (6): 499-510. <http://dx.doi.org/10.1007/bf00444368>.
- [15] Harlen, O.G. 2002. The Negative Wake Behind a Sphere Sedimenting through a Viscoelastic Fluid. *Journal of Non-Newtonian Fluid Mechanics* **108** (1): 411-430. [http://dx.doi.org/10.1016/S0377-0257\(02\)00139-8](http://dx.doi.org/10.1016/S0377-0257(02)00139-8).
- [16] Frank, X. and Li, H.Z. 2006. Negative Wake Behind a Sphere Rising in Viscoelastic Fluids: A Lattice Boltzmann Investigation. *Physical Review E* **74** (5): 056307.
- [17] Frank, X., Dietrich, N. and Li, H.Z. 2014. A Damping Phenomenon in Viscoelastic Fluids. *EPL (Europhysics Letters)* **105** (5).

**CHAPTER 6: ANALYSES OF THE DIMENSIONLESS  
PARAMETERS AFFECTING PARTICLE SETTLING  
VELOCITY IN VISCOELASTIC FLUIDS**

The purpose of the chapter-6 is to analyze and discuss the dimensionless parameters that affect the particle settling velocity in viscoelastic fluids. In this regard, this chapter provides the details of the dimensionless parameters such as Weissenberg numbers, Reynolds numbers, drag coefficients, drag corrector factors, etc. that are determined from the experimentally measured values of particle settling velocities in viscoelastic fluids. It also discusses the functional relationship between those parameters.

## **6.1 ANALYSES OF PARAMETERS AFFECTING THE SHEAR RATES INDUCED BY THE SETTLING PARTICLE**

The maximum shear rates induced by the particles settling in the fluid were determined by using Equation 6-1 [1].

$$\text{Shear rate} = \frac{2V_s}{D_p} \qquad \text{Equation 6-1}$$

**Table 6-1** provides the compiled data of experimentally measured settling velocity of particles and their calculated shear rates along with the fluid properties. The shear rate profiles with respect to each factor were plotted to investigate the effect of the relaxation time, the consistency index, and the particle diameter on the shear rates induced by the particle upon the fluid.

**Table 6-1. Compiled data of experimentally measured settling velocity and calculated shear rates along with fluid properties**

Density ( $\rho_f$ ), kg/m <sup>3</sup>	Consistency Index (K), Pa.s <sup>n</sup>	Flow Behavior Index (n)	Relaxation time ( $\lambda$ ), s	Diameter ( $D_p$ ), m	Average settling velocity ( $V_s$ ), m/s	Shear rate ( $\dot{\gamma}$ ), s <sup>-1</sup>
1005	0.53	0.38	12	0.00200	0.0108	10.80
1005	0.53	0.38	12	0.00118	0.0017	2.88
1005	0.53	0.38	12	0.00150	0.0049	6.53
1005	0.53	0.38	12	0.00300	0.0294	19.60
1003	0.53	0.38	50	0.00200	0.0073	7.32
1002	0.53	0.38	110	0.00200	0.0035	3.45
1002	0.53	0.38	150	0.00200	0.0030	2.96
998	0.26	0.35	12	0.00118	0.0052	8.76
998	0.26	0.35	12	0.00150	0.0163	21.72
998	0.26	0.35	12	0.00200	0.0307	30.72
998	0.26	0.35	12	0.00300	0.0788	52.51
998	0.26	0.35	50	0.00118	0.0034	5.82
998	0.26	0.35	50	0.00150	0.0093	12.43
998	0.26	0.35	50	0.00200	0.0144	14.43
998	0.26	0.35	50	0.00300	0.0353	23.50
998	0.26	0.35	110	0.00118	0.0025	4.18
998	0.26	0.35	110	0.00150	0.0058	7.72
998	0.26	0.35	110	0.00200	0.0084	8.37
998	0.26	0.35	110	0.00300	0.0220	14.69
998	0.16	0.38	12	0.00118	0.0114	19.32
998	0.16	0.38	12	0.00150	0.0245	32.67
998	0.16	0.38	12	0.00200	0.0390	39.00
998	0.16	0.38	12	0.00300	0.0916	61.07

**Figure 6-1** provides the shear rate profiles versus the relaxation time when spherical particles of 2mm diameter were settling in 2 fluids having  $K=0.53 \text{ Pa}\cdot\text{s}^n$  &  $n=0.38$  and  $K=0.26 \text{ Pa}\cdot\text{s}^n$  &  $n=0.35$  respectively. It is noticeable from **Figure 6-1** that the shear rate induced by the 2mm spherical particle on the fluids were decreasing with the increase of fluid relaxation time from 12s to 150s. Besides, the shear rate profile for the fluid having  $K=0.26 \text{ Pa}\cdot\text{s}^n$  &  $n=0.38$  was higher than that of the fluid having fluid consistency index of  $0.53 \text{ Pa}\cdot\text{s}^n$  &  $n=0.35$ . Higher shear rates were induced by the particle while settling in the fluids of lower consistency index (thereby lower apparent viscosity). This confirmed that the shear rates induced by the particle were affected by the relaxation time and the consistency index of the fluid.

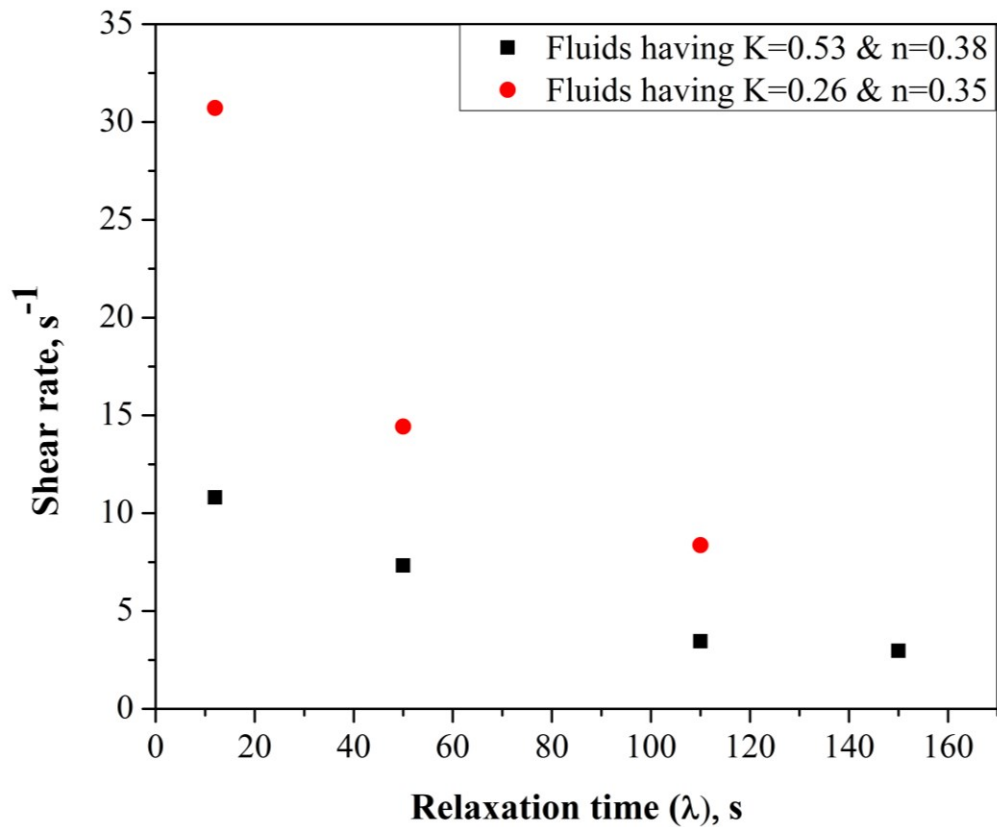


**Figure 6-1. Shear rate profiles versus the relaxation time in fluids having  $K=0.53 \text{ Pa}\cdot\text{s}^n$  &  $n=0.38$  and  $K=0.26 \text{ Pa}\cdot\text{s}^n$  &  $n=0.35$**

**Figure 6-2** provides the shear rate profiles versus the apparent viscosity of the fluids having relaxation time of 12 sec. **Figure 6-2** demonstrated that the shear rates induced by the particle were decreasing with the increase of apparent viscosity.

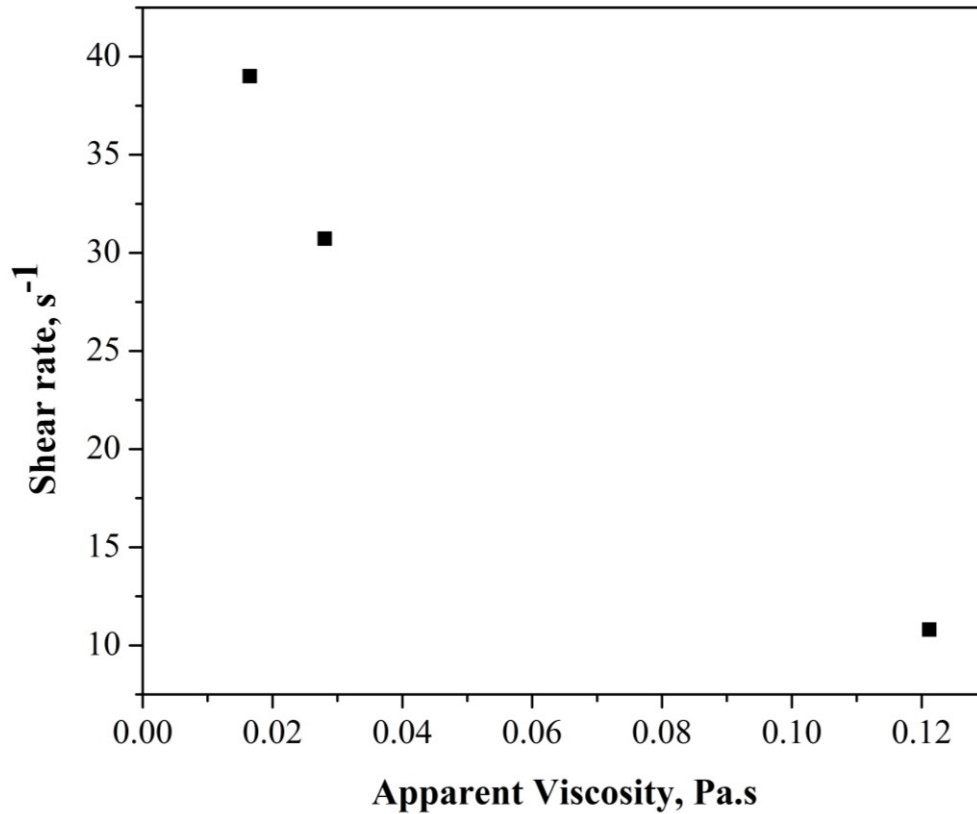


**Figure 6-2. Shear rate profiles versus the apparent viscosity of fluids having  $\lambda=12$  s**

**Figure 6-3** provides the shear rate profiles versus the diameter of the spherical particles when settling in the fluids having relaxation time 12s, 50s and 110s respectively. **Figure 6-3** demonstrated that the shear rates induced by the particles in the fluid were increasing with the increase of particle diameter for all the fluid cases. The magnitude of the increase in the shear rates with particle diameter was, however, less for the fluid having the relaxation time of 110s followed by the fluid of 50s and then the fluid of 12s. Since the shear rate is directly related to the settling velocity of the particles, the data from **Figure 6-1**, **Figure 6-2** and **Figure 6-3**, therefore,

established the fact that the particle settling velocity and thereby the shear rate induced by the settling particle on the fluid was affected by the factors such as the fluid's relaxation time, the fluid's consistency index, thereby apparent viscosity and the particle diameter.

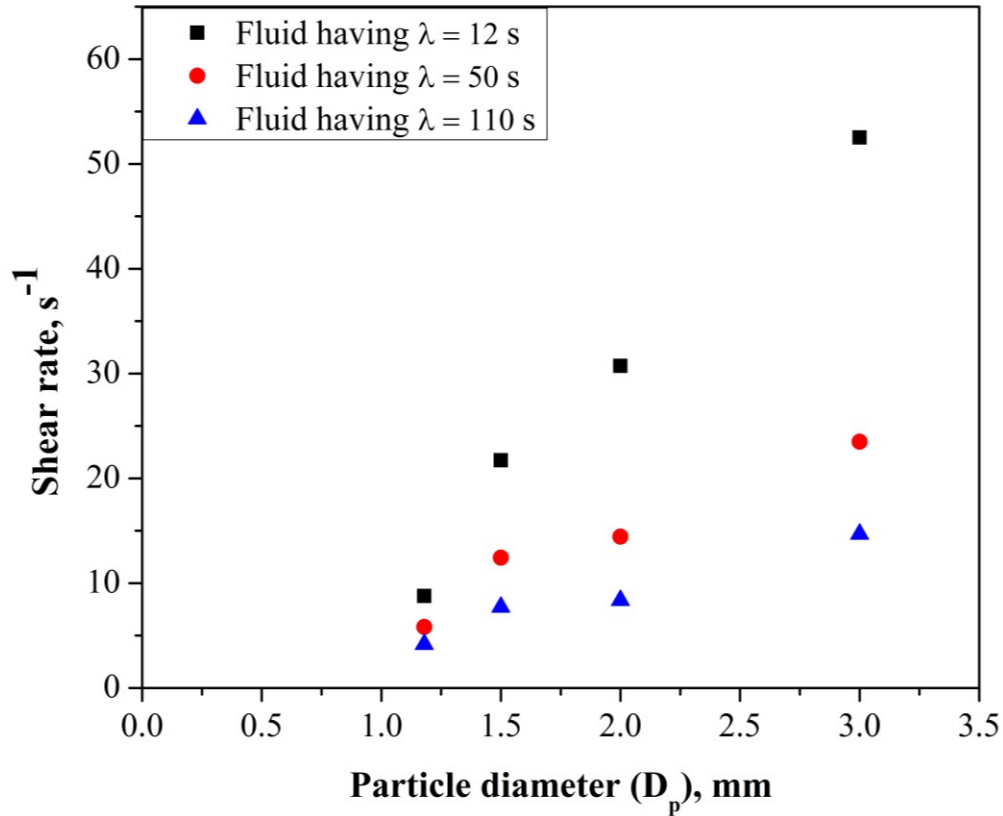


**Figure 6-3. Shear rate profiles versus the particle diameters in fluids having  $K=0.26$  Pa.s<sup>n</sup>,  $n=0.35$  and relaxation time 12, 50 and 110 s**

## **6.2 ANALYSES OF DIMENSIONLESS PARAMETERS AFFECTING THE PARTICLE SETTLING VELOCITY**

As the settling behavior of the particle in the non-Newtonian viscoelastic fluid seemed to be dependent on fluid's relaxation time (a measure of elasticity), fluid's apparent viscosity and particle diameter, the profiles of settling velocity values were observed by combining all the governing factors into one. To do this, the ratio of Weissenberg number to Reynolds number was determined and plotted against its respective experimentally measured settling velocity values as

shown in **Figure 6-4**. The Weissenberg number is defined as the ratio of the elastic forces to viscous forces and is given by Equation 6-2 [1, 2]. The Reynolds number is defined as the ratio of inertial forces to viscous forces and is given by Equation 6-3 [3].

$$Wi = \frac{\text{Elastic forces}}{\text{Viscous forces}} = \lambda \cdot \dot{\gamma} \quad \text{Equation 6-2}$$

$$Re = \frac{\text{Inertial forces}}{\text{Viscous forces}} = \frac{\rho_f V_s D_p}{\mu_a} = \frac{\rho_f V_s D_p}{K';} \quad \text{Equation 6-3}$$

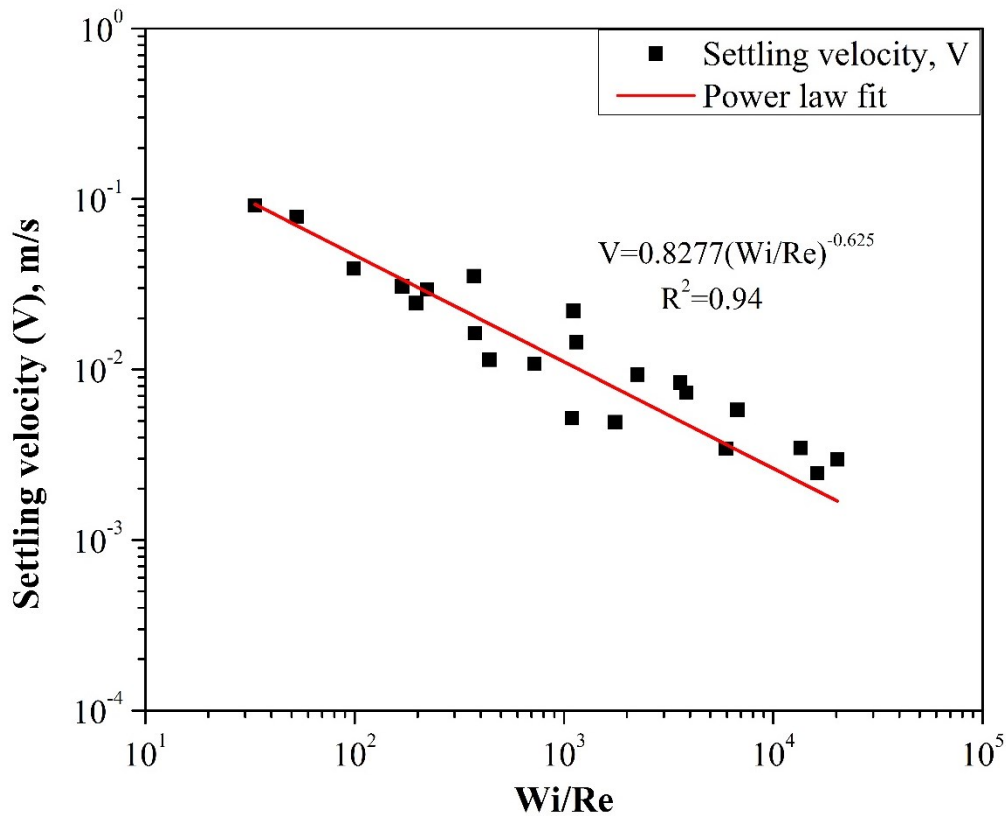


**Figure 6-4. Experimental settling velocity values versus Wi/Re**

As shown in **Figure 6-4**, with the increase in the ratio of Weissenberg number to Reynolds number, the settling velocity of the particles decreased and the settling velocity and Wi/Re ratio

seemed to have power law functional relationship. The Wi/Re ratio collectively accounted the influence of all the parameters affecting the settling velocity. To illustrate, when the relaxation time of the fluid increased, the Weissenberg number would be increased thereby increasing the Wi/Re ratio and as the Wi/Re ratio increased, the settling velocity of the particles noticed to decrease as shown in **Figure 6-4**. Similarly, when the apparent viscosity of the fluid decreased or when the particle diameter increased, the Reynolds number would be increased thereby decreasing the Wi/Re ratio, and as Wi/Re decreased, the settling velocity of the particles noticed to increase in **Figure 6-4**. Therefore, when dealing with fluids of lower shear viscosity or with particles of higher diameter (i.e. high Reynolds numbers), the settling velocity of the particles could be reduced by enhancing the elastic properties of the fluid.

### **6.3 ANALYSES OF DIMENSIONLESS PARAMETERS AFFECTING DRAG COEFFICIENT AND DRAG CORRECTION FACTOR**

When a particle is settling in a fluid, the particle experiences a fluid drag to oppose its motion. The drag or resistance on a settling particle in a fluid is quantified by a dimensionless parameter called drag coefficient. The drag coefficient of a spherical particle settling in a fluid is given by the Equation 6-4.

$$C_D = \frac{4gD_s(\rho_s - \rho_f)}{3\rho_f V_s^2} \quad \text{Equation 6-4}$$

The experimental values of the drag coefficient of the spherical particles were determined from the respective settling velocity values of the settling particle, the relevant properties of the HPAM test fluids and the spherical particles. The calculated experimental values of drag coefficients were then plotted against Wi/Re ratio as shown in **Figure 6-5**. The drag coefficient values were found to be increasing with the increase of Wi/Re ratio. More precisely, drag enhancement was observed with the increase of fluid elasticity, and drag reduction was observed

with the decrease of fluid viscosity or with the increment of particle diameter. The power law functional relationship between drag coefficient and  $Wi/Re$  ratio seemed to be a good fit as shown in **Figure 6-5**.

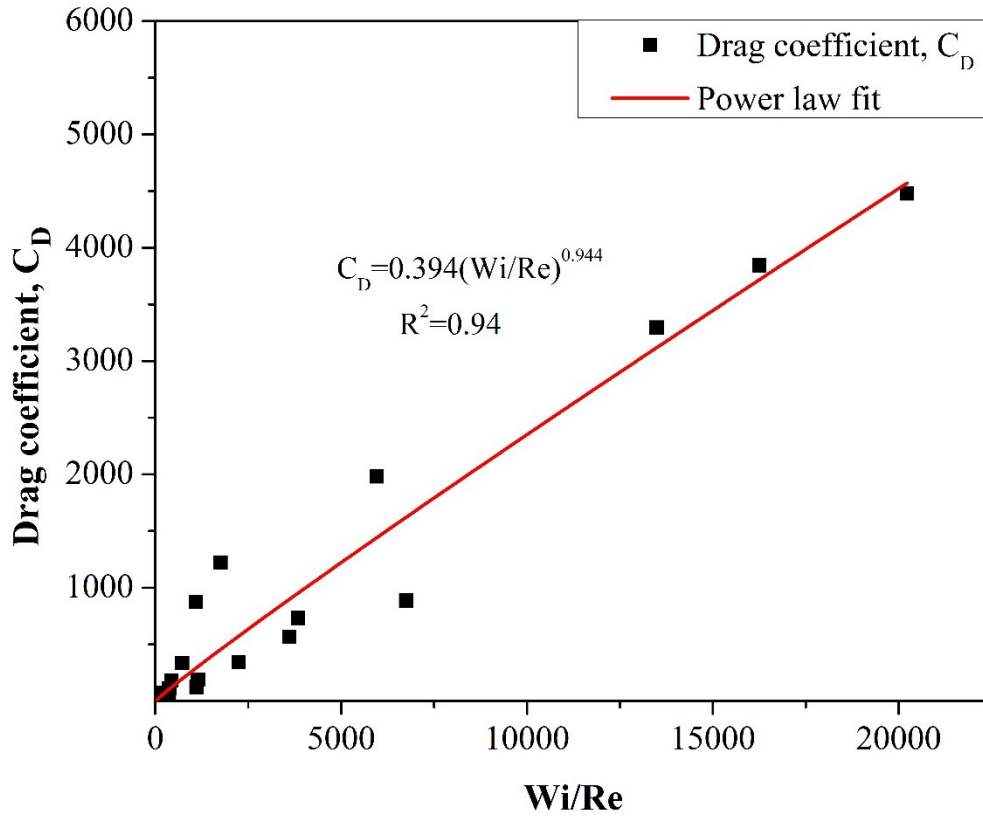


**Figure 6-5. Drag coefficient profile versus  $Wi/Re$  ratio**

For a Newtonian fluid, the drag coefficient of the settling spherical particle in a creeping flow regime is given by the Stokes law [3]. However, this Stokes solution is not appropriate to determine the drag on the spherical particle settling in the non-Newtonian viscoelastic fluid as the effects of the viscoelasticity, confined container walls, etc. are not taken into consideration [4]. Therefore, drag correction factor ( $K$ ) has been employed in several studies to determine the deviation of the drag coefficient value in a non-Newtonian viscoelastic fluid from its Newtonian

value [4-9]. In case of the particle settling in Newtonian fluid, the value of the drag correction factor is 1.

$$K = f\left(Wi, Re, \frac{a}{R}\right) \quad \text{Equation 6-5}$$

In case of a particle settling in non-Newtonian viscoelastic fluid, the drag correction factor (K) is a function of the Weissenberg number, Reynolds number, and the ratio of the particle radius to that of the container as shown in Equation 6-5 [6]. The drag deviation due to the effect of confined container walls is given by Equation 6-6 [9].

$$\text{Drag deviation due to walls} = \frac{1}{1 - f\left(\frac{a}{R}\right)} \quad \text{Equation 6-6}$$

where  $a$  is the spherical particle radius,  $R$  is the container radius and  $f\left(\frac{a}{R}\right)$  is given by Faxen's series [9] in Equation 6-7.

$$f\left(\frac{a}{R}\right) = 2.1044\left(\frac{a}{R}\right) - 2.0877\left(\frac{a}{R}\right)^3 + 0.84913\left(\frac{a}{R}\right)^5 + 1.3720\left(\frac{a}{R}\right)^6 - 3.87\left(\frac{a}{R}\right)^8 + 4.19\left(\frac{a}{R}\right)^{10} \quad \text{Equation 6-7}$$

The spherical particles of diameters 1.18mm, 1.5mm, 2.0 mm and 3.0 mm were used in the present study, and the width of the container was 11cm. Hence, by using Equation 6-6, the maximum and minimum deviations in drag due to the wall effects were determined to be 1.06 and 1.02. The wall effects in the present study were, therefore, considered to be negligible.

For the creeping flow regime, the drag correction factor that accounts the deviation due to fluid viscoelasticity is given by Equation 6-8 [6].

$$K = \frac{(\rho_s - \rho_f)gD_s^2}{18\mu_a V_s} \quad \text{Equation 6-8}$$

So, the drag correction factors for the respective values of experimentally measured settling velocities in creeping flow regime of shear thinning viscoelastic HPAM solutions were determined using Equation 6-8, and the drag correction factor values versus the Weissenberg number values are plotted as shown in **Figure 6-6**. As it can be seen in **Figure 6-6**, the drag correction factor increased as the Weissenberg number increased in the studied range. In other words, the deviation of the drag value from its Newtonian value noticed to be augmenting with the increase of the fluid elasticity. These observations were in agreement with Fabris et al. [6], Solomon and Muller [10], Jones et al. [11] and Arigo et al. [12] who also observed enhanced drag correction factors with the increase of Weissenberg number in their studies of viscoelastic fluids. The drag correction factors reported in the past studies were in the range of 2 to 8 at high Weissenberg numbers [6, 10, 11, 13]. The highest drag correction factor observed in the present study was around 6.02 as shown in **Figure 6-6**. The drag enhancement could be attributed to the presence of negative wake in the flow field past the settling sphere.

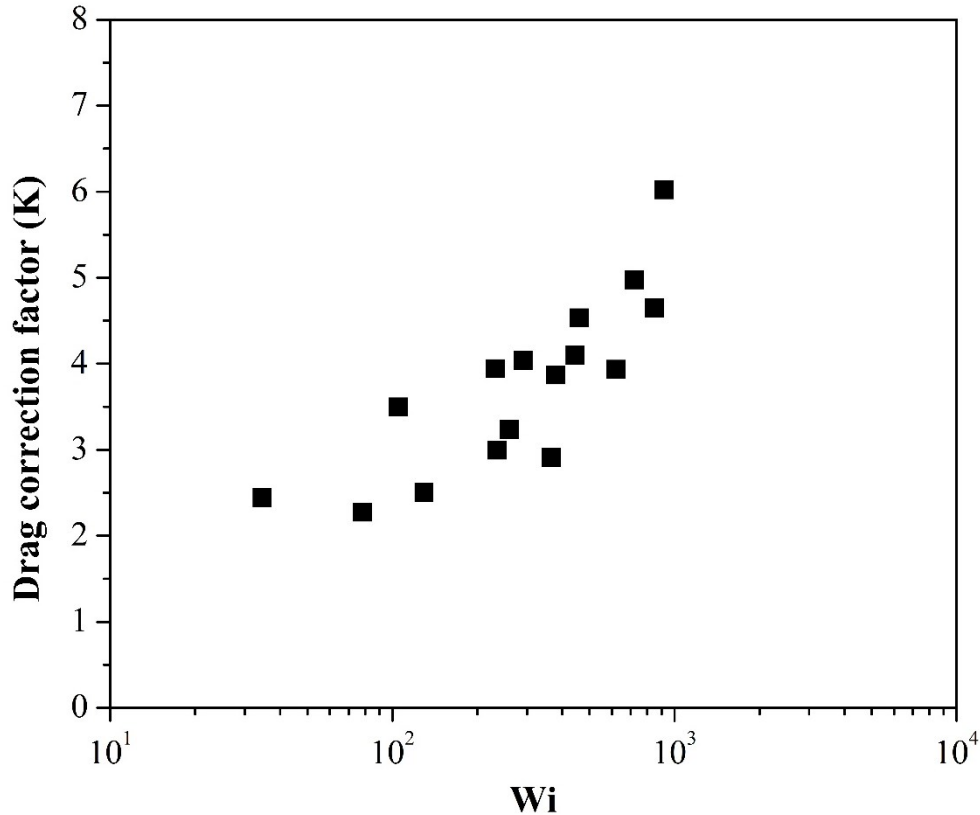


**Figure 6-6. Drag correction factor profile versus Weissenberg number**

Based on the above-mentioned results, the increase of elasticity of the HPAM test fluids seemed to cause the settling velocity reduction and the drag enhancement on the settling particle within the studied flow ranges. However, further experimentation at low levels of Weissenberg number needs to be performed to confirm the validity of these observations at broader ranges.

#### 6.4 REFERENCES

- [1] Chhabra, R.P. 2007. *Bubbles, Drops, and Particles in Non-Newtonian Fluids, Second Edition*: CRC Press, Taylor & Francis Group.
- [2] Barnes, H.A., Hutton, J.F. and Walters, K. 1989. *An Introduction to Rheology*, Amsterdam: Elsevier.

- [3] McCabe, W.L., Smith, J.C. and Harriott, P. 2004. *Unit Operations of Chemical Engineering*, New York: McGraw-Hill.
- [4] Mohammadigoushki, H. and Muller, S.J. 2016. Sedimentation of a Sphere in Wormlike Micellar Fluids. *Journal of Rheology* **60** (4): 587-601. <http://dx.doi.org/10.1122/1.4948800>.
- [5] Chen, S. and Rothstein, J.P. 2004. Flow of a Wormlike Micelle Solution Past a Falling Sphere. *Journal of Non-Newtonian Fluid Mechanics* **116** (2): 205-234. <https://doi.org/10.1016/j.jnnfm.2003.08.005>.
- [6] Fabris, D., Muller, S.J. and Liepmann, D. 1999. Wake Measurements for Flow around a Sphere in a Viscoelastic Fluid. *Physics of fluids* **11** (12): 3599-3612. <http://dx.doi.org/10.1063/1.870225>.
- [7] McKinley, G.H. 2002. Steady and Transient Motion of Spherical Particles in Viscoelastic Liquids. In *Transport Processes in Bubbles, Drops & Particles*, 2nd edition, ed. Chhabra, R. and De Kee, D., Chap. 14. New York: Talyor & Francis.
- [8] Mena, B., Manero, O. and Leal, L. 1987. The Influence of Rheological Properties on the Slow Flow Past Spheres. *Journal of Non-Newtonian Fluid Mechanics* **26** (2): 247-275. [https://doi.org/10.1016/0377-0257\(87\)80006-X](https://doi.org/10.1016/0377-0257(87)80006-X).
- [9] Mendoza-Fuentes, A.J., Manero, O. and Zenit, R. 2010. Evaluation of Drag Correction Factor for Spheres Settling in Associative Polymers. *Rheologica Acta* **49** (9): 979-984. <http://dx.doi.org/10.1007/s00397-010-0456-7>.
- [10] Solomon, M. and Muller, S. 1996. Flow Past a Sphere in Polystyrene-Based Boger Fluids: The Effect on the Drag Coefficient of Finite Extensibility, Solvent Quality and Polymer Molecular Weight. *Journal of Non-Newtonian Fluid Mechanics* **62** (1): 81-94. [https://doi.org/10.1016/0377-0257\(95\)01398-9](https://doi.org/10.1016/0377-0257(95)01398-9).
- [11] Jones, W.M., Price, A.H. and Walters, K. 1994. The Motion of a Sphere Falling under Gravity in a Constant-Viscosity Elastic Liquid. *Journal of Non-Newtonian Fluid Mechanics* **53**: 175-196. [http://dx.doi.org/10.1016/0377-0257\(94\)85048-8](http://dx.doi.org/10.1016/0377-0257(94)85048-8).

- [12] Arigo, M., Rajagopalan, D., Shapley, N. and McKinley, G.H. 1995. The Sedimentation of a Sphere through an Elastic Fluid. Part 1. Steady Motion. *Journal of Non-Newtonian Fluid Mechanics* **60** (2-3): 225-257. [https://doi.org/10.1016/0377-0257\(95\)01379-6](https://doi.org/10.1016/0377-0257(95)01379-6).
- [13] Walters, K. and Tanner, R. 1992. The Motion of a Sphere through an Elastic Fluid. In *Transport Processes in Bubbles, Drops and Particles*, ed. Chhabra, R. and De Kee, D., Chap. 3. New York: Hemisphere.

## **CHAPTER 7: CONCLUSIONS AND RECOMMENDATIONS FOR FUTURE WORK**

This chapter summarizes the results of the current experimental study and provides the recommendations for future studies in this area of research.

## 7.1 CONCLUSIONS

The first phase of the experimental study was performed to determine how the fluid shear viscosity and the elasticity would influence the particle settling velocity and even more so to answer the question of which one of these two rheological properties is more dominant in controlling the particle settling velocity when viscoelastic drilling fluids are used. The results of experimental investigation of settling velocities of spherical particles in viscoelastic fluids are summarized and following conclusions are made.

- Two groups (Group-A & Group-B) of test fluids of the HPAM polymer were formulated in this study. The test fluids of Group-A were used to investigate the effect of the fluid elasticity on the settling velocity of particles in viscoelastic fluids, and the test fluids of Group-B were used to identify the most influential factor between the fluid elasticity and the shear viscosity for reducing the settling velocity of the particles in viscoelastic fluids.
- The effect of the elasticity was decoupled from the effect of the shear viscosity by performing the settling velocity measurements in the test fluids of the HPAM polymer that possessed almost identical shear thinning viscosity but significantly different elastic properties.
- The test fluids of Group-A were formulated by mixing three different molecular weights of HPAM polymer in such a way that they maintained constant average molecular weight but varied molecular weight distribution. The results of the rheological measurements such as the shear viscosity and the oscillatory frequency sweep demonstrated that the

test fluids of Group-A had almost identical shear thinning viscosity behavior but different elasticity that was quantified in terms of the longest relaxation times.

- The Group-B comprised of Set-I and Set-II test fluids. The Set-I test fluids were formulated by mixing three different molecular weights of HPAM polymer in such a way that they maintained constant average molecular weight but varied molecular weight distribution. The Set-II test fluids were formulated using HPAM polymer of constant molecular weight but at different polymer concentration levels. The results of rheological measurements indicated that Set-I test fluids had almost identical shear viscosity, but significantly different elasticity properties and Set-II fluids had similar elasticity but different shear viscosities.
- The settling velocity measurements in the test fluids were performed using the particle image shadowgraph (PIS) technique. The results of settling velocity measurements of 2mm spherical particles in the test fluids of Group-A confirmed that the settling velocity of the particles was strongly influenced by the elastic properties of the fluids. Moreover, the longest relaxation time of the fluid can be used to quantify such effect.
- The results of the settling velocity measurements in Group-B (Set-I & Set-II) test fluids confirmed that: (i) When the fluids having similar shear viscosity profile were used, the settling velocity of spherical particles decreased significantly with the increasing fluid elasticity; (ii) At constant elasticity, the settling velocity of spherical particles also decreased significantly when the fluid shear viscosity was increased; (iii) The spherical particles settling velocity increased pronouncedly as their diameter increased from 1.18mm to 3mm. But the magnitude of the increase in settling velocity with the increasing particle diameter is less for the samples having higher elasticity and similar

shear viscosity characteristics. The fluid shear viscosity and the elasticity both seem to have significant effect on the particle settling velocity

- From the field operational point of view, fluids with high shear viscosity values may not always be practical to use as the high shear viscosity values increase the parasitic pressure losses. Therefore, in such cases, increasing the fluid elasticity may help to reduce the particle settling velocity even when using fluids with low shear viscosity values, especially when large size drill cuttings need to be transported.
- The impact of the elasticity on the settling velocity was quantified by comparing the experimentally measured settling velocities to the values calculated by using the model developed for predicting settling velocity of spherical particles in power law (visco-inelastic) fluids. It was observed that within the range of the tests conducted in this study if the influence of elasticity were not taken into consideration, the settling velocities would have been significantly (up to 50 times) overpredicted.
- The dimensionless parameters such as Weissenberg number ( $Wi$ ), Reynolds number ( $Re$ ), drag coefficients ( $C_D$ ) and drag correction factors ( $K$ ) were calculated and analyzed from experimental values of settling velocities.
- It was recognized that the effect of parameters such as elasticity, shear viscosity and particle sizes on the settling velocity and the drag coefficients could be analyzed collectively by determining  $Wi/Re$  ratio. The higher the  $Wi/Re$  ratio, the lower the settling velocity and the higher the drag on the settling particle.
- The drag correction factor was also determined to analyze the drag deviation from its Newtonian value. It was found that the drag correction factor was highly dependent on

the Weissenberg number. The deviation in the drag noticed to be augmenting with the increase of the Weissenberg number.

Results from the first phase of the study have shown that the settling velocity of particles in viscoelastic fluids decreased significantly with the increasing elasticity of the fluids. However, our understanding of why the change in fluid elasticity influences the particle settling velocity was very limited at this point. A follow up experimental study has, therefore, been conducted to understand the reasons behind why the settling velocity of the particles decrease with the increasing fluid elasticity.

The second phase of the experimental study was performed (i) to investigate the fluid flow field behind the settling particle by using particle image velocity (PIV) technique; (ii) to understand the changes caused by the elasticity of the fluid on the flow field past the settling particle; (iii) more specifically, to determine how the fluid velocity profile and the resultant drag forces acting on the settling particle change with the increasing fluid elasticity. The results of the experimental study are summarized and following conclusions are made.

- Two test fluids of HPAM were formulated by mixing three different molecular weights of HPAM polymer in such a way that they maintain constant average molecular weight but varied molecular weight distribution.
- The results of the rheological measurements demonstrated that the two test fluids had almost identical shear thinning viscosity behavior but different elasticity.
- The flow field past the settling particle in these two test fluids was observed using particle image velocimetry (PIV) technique. The results of PIV measurements demonstrated that negative wake was present in the flow fields behind the settling particle in viscoelastic fluids. However, the stagnant point (the point at which fluid

velocity becomes zero and beyond which the fluid starts moving in opposite direction to the particle movement) was closer to the particle settling in the fluid with higher elasticity than that in the fluid with lower elasticity.

- The velocity of the fluid in the recirculation region was higher for the fluid with the higher elasticity than for the fluid with the lower elasticity. Therefore, the presence of negative wake having fast moving fluid in reverse direction nearer to the settling particle could possibly create higher drag forces (acting in the direction against the particle movement), which would affect the settling velocity of the particle.

## **7.2 RECOMMENDATIONS FOR FUTURE WORK**

This study involved many aspects of experimentation to understand the particle settling in viscoelastic fluids including the investigation of the effect of fluid elasticity on the settling velocity of particles, the examination of flow field past the settling particle and the analyses of dimensionless parameters affecting the particle settling velocities etc. However, there are few aspects remained to be explored further. Hence, the recommendations for the future research work in this area are mentioned below:

- Further experimentation needs to be done with different sized particles in fluids having different levels of viscosities, elasticities to validate these observations at a wide range of flow regimes and Weissenberg numbers and to develop a generalized correlation for settling velocity of particles in viscoelastic fluids.
- Based on the above experimental results, it was concluded that increasing the fluid elasticity (rather than the fluid shear viscosity) would rather be more effective way of controlling the particle settling velocity when dealing with large size drilled cuttings. However, consequential effects of increasing fluid elasticity on the other operational

parameters (such as frictional pressure losses) are still uncertain and yet to be investigated.

- Experiments need to be conducted in horizontal & vertical flow loops to investigate the influence of fluid elasticity on the frictional pressure losses and cutting transportation.
- Experiments need to be conducted to investigate the effect of elasticity on settling velocity of particles in yield power law (YPL) fluids as most of the fluids encountered in industries also possess yielding behavior along with viscoelasticity.

## BIBLIOGRAPHY

- Acharya, A., Mashelkar, R.A. and Ulbrecht, J. 1976. Flow of Inelastic and Viscoelastic Fluids Past a Sphere. Part I. Drag Coefficient in Creeping and Boundary-Layer Flows. *Rheologica Acta* **15** (9): 454-470. <http://dx.doi.org/10.1007/bf01530348>.
- Acharya, A., Mashelkar, R.A. and Ulbrecht, J. 1976. Flow of Inelastic and Viscoelastic Fluids Past a Sphere. Part II: Anomalous Separation in the Viscoelastic Fluid Flow. *Rheologica Acta* **15** (9): 471-478. <http://dx.doi.org/10.1007/bf01530349>.
- Acharya, A.R. 1986. Particle Transport in Viscous and Viscoelastic Fracturing Fluids. *SPE Production Engineering* **1** (02). SPE-13179-PA. <http://dx.doi.org/10.2118/13179-PA>.
- Acharya, A.R. 1988. Viscoelasticity of Crosslinked Fracturing Fluids and Proppant Transport. *SPE Production Engineering* **3**: 483-488. SPE-15937-PA. <http://dx.doi.org/10.2118/15937-PA>.
- Adrian, R.J. 2005. Twenty Years of Particle Image Velocimetry. *Experiments in Fluids* **39** (2): 159-169. <http://dx.doi.org/10.1007/s00348-005-0991-7>.
- Arigo, M., Rajagopalan, D., Shapley, N. and McKinley, G.H. 1995. The Sedimentation of a Sphere through an Elastic Fluid. Part 1. Steady Motion. *Journal of Non-Newtonian Fluid Mechanics* **60** (2-3): 225-257. [https://doi.org/10.1016/0377-0257\(95\)01379-6](https://doi.org/10.1016/0377-0257(95)01379-6).
- Arigo, M.T. and McKinley, G.H. 1998. An Experimental Investigation of Negative Wakes Behind Spheres Settling in a Shear-Thinning Viscoelastic Fluid. *Rheologica Acta* **37** (4): 307-327. <http://dx.doi.org/10.1007/s003970050118>.
- Barnes, H.A. 2000. *A Handbook of Elementary Rheology*, Aberystwyth: University of Wales, Institute of Non-Newtonian Fluid Mechanics (Reprint).

- Barnes, H.A., Hutton, J.F. and Walters, K. 1989. *An Introduction to Rheology*, Amsterdam: Elsevier (Reprint).
- Bizhani, M. 2013. *Solids Transport with Turbulent Flow of Non-Newtonian Fluid in the Horizontal Annuli*. Masters Thesis, University of Alberta, Edmonton, Canada (25th Sep 2013).
- Bizhani, M., Corredor, F.E.R. and Kuru, E. 2015. An Experimental Study of Turbulent Non-Newtonian Fluid Flow in Concentric Annuli Using Particle Image Velocimetry Technique. *Flow, Turbulence and Combustion* **94** (3): 527-554. <http://dx.doi.org/10.1007/s10494-014-9589-6>.
- Boger, D.V. 1977. A Highly Elastic Constant-Viscosity Fluid. *Journal of Non-Newtonian Fluid Mechanics* **3** (1): 87-91. [http://dx.doi.org/10.1016/0377-0257\(77\)80014-1](http://dx.doi.org/10.1016/0377-0257(77)80014-1).
- Broadbent, J.M. and Mena, B. 1974. Slow Flow of an Elastico-Viscous Fluid Past Cylinders and Spheres. *The Chemical Engineering Journal* **8** (1): 11-19. [http://dx.doi.org/10.1016/0300-9467\(74\)80014-6](http://dx.doi.org/10.1016/0300-9467(74)80014-6).
- Bui, B., Saasen, A., Maxey, J., Ozbayoglu, M.E., Miska, S.Z., Yu, M. and Takach, N.E. 2012. Viscoelastic Properties of Oil-Based Drilling Fluids. *Annual Transactions of the Nordic Rheology Society* **20**: 33-48.
- Caenn, R., Darley, H.C.H. and Gray, G.R. 2011. Introduction to Drilling Fluids. In *Composition and Properties of Drilling and Completion Fluids*, 6th edition, Chap. 1, 1-37. Boston: Gulf Professional Publishing.
- Castrejón-García, R., Castrejón-Pita, J.R., Martin, G.D. and Hutchings, I.M. 2011. The Shadowgraph Imaging Technique and Its Modern Application to Fluid Jets and Drops. *Revista Mexicana de Física* **57** (3): 266-275.

- Chen, S. and Rothstein, J.P. 2004. Flow of a Wormlike Micelle Solution Past a Falling Sphere. *Journal of Non-Newtonian Fluid Mechanics* **116** (2): 205-234. <https://doi.org/10.1016/j.jnnfm.2003.08.005>.
- Chhabra, R.P. 1990. Motion of Spheres in Power Law (Viscoelastic) Fluids at Intermediate Reynolds Numbers: A Unified Approach. *Chemical Engineering and Processing: Process Intensification* **28** (2): 89-94. [http://dx.doi.org/10.1016/0255-2701\(90\)80004-O](http://dx.doi.org/10.1016/0255-2701(90)80004-O).
- Chhabra, R.P. 2007. *Bubbles, Drops, and Particles in Non-Newtonian Fluids, Second Edition*: CRC Press, Taylor & Francis Group (Reprint).
- Chhabra, R.P., Uhlherr, P.H.T. and Boger, D.V. 1980. The Influence of Fluid Elasticity on the Drag Coefficient for Creeping Flow around a Sphere. *Journal of Non-Newtonian Fluid Mechanics* **6** (3): 187-199. [http://dx.doi.org/10.1016/0377-0257\(80\)80002-4](http://dx.doi.org/10.1016/0377-0257(80)80002-4).
- Chien, S.F. 1972. Annular Velocity for Rotary Drilling Operations. *International Journal of Rock Mechanics and Mining Sciences & Geomechanics Abstracts* **9** (3): 403-416. [http://dx.doi.org/10.1016/0148-9062\(72\)90005-8](http://dx.doi.org/10.1016/0148-9062(72)90005-8).
- Chmielewski, C., Nichols, K.L. and Jayaraman, K. 1990. A Comparison of the Drag Coefficients of Spheres Translating in Corn-Syrup-Based and Polybutene-Based Boger Fluids. *Journal of Non-Newtonian Fluid Mechanics* **35** (1): 37-49. [http://dx.doi.org/10.1016/0377-0257\(90\)85071-6](http://dx.doi.org/10.1016/0377-0257(90)85071-6).
- Choi, S.K. 2008. *pH Sensitive Polymers for Novel Conformance Control and Polymer Flooding Applications*. PhD Thesis, University of Texas, , Austin.
- Clift, R., Grace, J. and Weber, M. 1978. *Bubbles, Drops and Particles*, Academic Press, New York (Reprint).

- Cross, M.M. 1965. Rheology of Non-Newtonian Fluids: A New Flow Equation for Pseudoplastic Systems. *Journal of colloid science* **20** (5): 417-437.
- Dallon, D.S. 1967. *A Drag-Coefficient Correlation for Spheres Settling in Ellis Fluids*. Ph. D Thesis, University of Utah, Salt Lake City, UT.
- Degand, E. and Walters, K. 1995. On the Motion of a Sphere Falling through an Elastic Liquid Contained in a Tightly-Fitting Cylindrical Container. *Journal of Non-Newtonian Fluid Mechanics* **57** (1): 103-115. [http://dx.doi.org/10.1016/0377-0257\(94\)01298-V](http://dx.doi.org/10.1016/0377-0257(94)01298-V).
- Dehghanpour, H. and Kuru, E. 2011. Effect of Viscoelasticity on the Filtration Loss Characteristics of Aqueous Polymer Solutions. *Journal of Petroleum Science and Engineering* **76** (1–2): 12-20. <http://dx.doi.org/10.1016/j.petrol.2010.12.005>.
- Dehghanpour Hossein Abadi, H. 2008. *Investigation of Viscoelastic Properties of Polymer Based Fluids as a Possible Mechanism of Internal Filter Cake Formation*. Masters, University of Alberta, Edmonton, Canada (Fall 2008).
- Doda, A. 2014. *Effect of Viscoelasticity and Alkali on Heavy Oil Eor Performance Using Hpam, 'Aa-Nvp' Co- and Cross-Linked Polymers*. Masters Thesis, University of Alberta, Edmonton, Canada (Spring 2014).
- Fabris, D., Muller, S.J. and Liepmann, D. 1999. Wake Measurements for Flow around a Sphere in a Viscoelastic Fluid. *Physics of fluids* **11** (12): 3599-3612. <http://dx.doi.org/10.1063/1.870225>.
- Ferry, J.D. 1980. *Viscoelastic Properties of Polymers*, 3rd. edition, New York: Wiley (Reprint).
- Fink, J.K. 2015. Drilling Fluids In *Water-Based Chemicals and Technology for Drilling, Completion, and Workover Fluids*, Chap. 2, 5-114. Boston: Gulf Professional Publishing.

- Flemmer, R.L.C. and Banks, C.L. 1986. On the Drag Coefficient of a Sphere. *Powder Technology* **48** (3): 217-221. [http://dx.doi.org/10.1016/0032-5910\(86\)80044-4](http://dx.doi.org/10.1016/0032-5910(86)80044-4).
- Foshee, W.C., Jennings, R.R. and West, T.J. 1976. Preparation and Testing of Partially Hydrolyzed Polyacrylamide Solutions. Presented at SPE Annual Fall Technical Conference and Exhibition, New Orleans, Louisiana, USA, 3-6 October. SPE-6202-MS. <https://doi.org/10.2118/6202-MS>.
- Fountain, M.S., Blanchard, J., Erikson, R.L., Kurath, D.E., Howe, D.T., Adkins, H. and Jenks, J. 2012. Design of a Particle Shadowgraph Velocimetry and Size (PSVS) System to Determine Particle Size and Density Distributions in Hanford Nuclear Tank Wastes - 12280. Presented at Waste Management-Tucson, Phoenix, Arizona, USA.
- Frank, X., Dietrich, N. and Li, H.Z. 2014. A Damping Phenomenon in Viscoelastic Fluids. *EPL (Europhysics Letters)* **105** (5).
- Frank, X. and Li, H.Z. 2006. Negative Wake Behind a Sphere Rising in Viscoelastic Fluids: A Lattice Boltzmann Investigation. *Physical Review E* **74** (5): 056307.
- Gomaa, A.M., Gupta, D.V.S.V. and Carman, P.S. 2015. Proppant Transport? Viscosity Is Not All It's Cracked up to Be. Presented at SPE Hydraulic Fracturing Technology Conference, 3-5 February., The Woodlands, Texas, USA., 2015/2/3/. SPE-173323-MS. <http://dx.doi.org/10.2118/173323-MS>.
- Haider, A. and Levenspiel, O. 1989. Drag Coefficient and Terminal Velocity of Spherical and Nonspherical Particles. *Powder Technology* **58** (1): 63-70. [http://dx.doi.org/10.1016/0032-5910\(89\)80008-7](http://dx.doi.org/10.1016/0032-5910(89)80008-7).

- Harlen, O.G. 2002. The Negative Wake Behind a Sphere Sedimenting through a Viscoelastic Fluid. *Journal of Non-Newtonian Fluid Mechanics* **108** (1): 411-430. [http://dx.doi.org/10.1016/S0377-0257\(02\)00139-8](http://dx.doi.org/10.1016/S0377-0257(02)00139-8).
- Hassager, O. 1979. Negative Wake Behind Bubbles in Non-Newtonian Liquids. *Nature* **279** (5712): 402-403. <http://dx.doi.org/10.1038/279402a0>.
- Hu, Y.T., Chung, H. and Maxey, J.E. 2015. What is More Important for Proppant Transport, Viscosity or Elasticity? Presented at SPE Hydraulic Fracturing Technology Conference, 3-5 February., The Woodlands, Texas, USA 2015/2/3/. SPE-173339-MS. <http://dx.doi.org/10.2118/173339-MS>.
- Hubner, T., Will, S. and Leipertz, A. 2001. Sedimentation Image Analysis (SIA) for the Simultaneous Determination of Particle Mass Density and Particle Size. *Particle & Particle Systems Characterization* **18** (2): 70-78
- Jones, W.M., Price, A.H. and Walters, K. 1994. The Motion of a Sphere Falling under Gravity in a Constant-Viscosity Elastic Liquid. *Journal of Non-Newtonian Fluid Mechanics* **53**: 175-196. [http://dx.doi.org/10.1016/0377-0257\(94\)85048-8](http://dx.doi.org/10.1016/0377-0257(94)85048-8).
- Kelessidis, V.C. and Mpandelis, G. 2004. Measurements and Prediction of Terminal Velocity of Solid Spheres Falling through Stagnant Pseudoplastic Liquids. *Powder Technology* **147** (1-3): 117-125. <http://dx.doi.org/10.1016/j.powtec.2004.09.034>.
- Khan, A.R. and Richardson, J.F. 1987. The Resistance to Motion of a Solid Sphere in a Fluid. *Chemical Engineering Communications* **62** (1-6): 135-150. <http://dx.doi.org/10.1080/00986448708912056>.
- Lali, A.M., Khare, A.S., Joshi, J.B. and Nigam, K.D.P. 1989. Behaviour of Solid Particles in Viscous Non-Newtonian Solutions: Settling Velocity, Wall Effects and Bed Expansion in

- Solid-Liquid Fluidized Beds. *Powder Technology* **57** (1): 39-50.  
[http://dx.doi.org/10.1016/0032-5910\(89\)80102-0](http://dx.doi.org/10.1016/0032-5910(89)80102-0).
- Larson, R.G. 1998. *The Structure and Rheology of Complex Fluids*, New York: Oxford University Press (Reprint).
- LaVision. 2006. *Flow Master, Product Manual* (Reprint).
- LaVision. 2006. *Image Intense, Product Catalogue* (Reprint).
- LaVision. 2007. *Product Manual for Double Pulsed Nd:Yag Laser* (Reprint).
- LaVision. 2008. *Product Manual for Diffuser* (Reprint).
- LaVision. 2015. *Davis 8.3, Product Manual* (Reprint).
- LaVision. 2016. *Flow Master, Advanced PIV/PTV Systems for Quantitative Flow Field Analysis Product Manual* (Reprint).
- Liu, Y., Shaw, M.T. and Tuminello, W.H. 1998. Obtaining Molecular-Weight Distribution Information from the Viscosity Data of Linear Polymer Melts. *Journal of Rheology* **42** (3): 453-476. <http://dx.doi.org/10.1122/1.550951>.
- Maalouf, A. and Sigli, D. 1984. Effects of Body Shape and Viscoelasticity on the Slow Flow around an Obstacle. *Rheologica Acta* **23** (5): 497-507.  
<http://dx.doi.org/10.1007/bf01329282>.
- Macosko, C. 1994. *Rheology: Principles, Measurements and Applications*, New York: Wiley-VCH (Reprint).
- Malhotra, S. and Sharma, M.M. 2012. Settling of Spherical Particles in Unbounded and Confined Surfactant-Based Shear Thinning Viscoelastic Fluids: An Experimental Study. *Chemical Engineering Science* **84**: 646-655. <http://dx.doi.org/10.1016/j.ces.2012.09.010>.

- Mantovanelli, A. and Ridd, P.V. 2006. Devices to Measure Settling Velocities of Cohesive Sediment Aggregates: A Review of the in Situ Technology. *Journal of Sea Research* **56** (3): 199-226. <http://dx.doi.org/10.1016/j.seares.2006.05.002>.
- McCabe, W.L., Smith, J.C. and Harriott, P. 2004. *Unit Operations of Chemical Engineering*, New York: McGraw-Hill (Reprint).
- McKinley, G.H. 2002. Steady and Transient Motion of Spherical Particles in Viscoelastic Liquids. In *Transport Processes in Bubbles, Drops & Particles*, 2nd edition, ed. Chhabra, R. and De Kee, D., Chap. 14. New York: Talyor & Francis.
- Melling, A. 1997. Tracer Particles and Seeding for Particle Image Velocimetry. *Measurement Science and Technology* **8** (12): 1406.
- Mena, B., Manero, O. and Leal, L. 1987. The Influence of Rheological Properties on the Slow Flow Past Spheres. *Journal of Non-Newtonian Fluid Mechanics* **26** (2): 247-275. [https://doi.org/10.1016/0377-0257\(87\)80006-X](https://doi.org/10.1016/0377-0257(87)80006-X).
- Mendoza-Fuentes, A.J., Manero, O. and Zenit, R. 2010. Evaluation of Drag Correction Factor for Spheres Settling in Associative Polymers. *Rheologica Acta* **49** (9): 979-984. <http://dx.doi.org/10.1007/s00397-010-0456-7>.
- Mendoza-Fuentes, A.J., Montiel, R., Zenit, R. and Manero, O. 2009. On the Flow of Associative Polymers Past a Sphere: Evaluation of Negative Wake Criteria. *Physics of fluids* **21** (3). <http://dx.doi.org/10.1063/1.3090180>.
- Merzkirch, W. 2017. Shadowgraph Technique, <http://www.thermopedia.com/content/1117/> (accessed on 28th June 2017).
- Miura, H., Takahashi, T., Ichikawa, J. and Kawase, Y. 2001. Bed Expansion in Liquid–Solid Two-Phase Fluidized Beds with Newtonian and Non-Newtonian Fluids over the Wide Range of

- Reynolds Numbers. *Powder Technology* **117** (3): 239-246.  
[http://dx.doi.org/10.1016/S0032-5910\(00\)00375-2](http://dx.doi.org/10.1016/S0032-5910(00)00375-2).
- Mohammadigoushki, H. and Muller, S.J. 2016. Sedimentation of a Sphere in Wormlike Micellar Fluids. *Journal of Rheology* **60** (4): 587-601. <http://dx.doi.org/10.1122/1.4948800>.
- Moore, P.L. 1974. *Drilling Practices Manual*, Tulsa, Oklahoma, USA: Petroleum Publishing Company (Reprint).
- Morrison, F.A. 2013. Data Correlation for Drag Coefficient for Sphere. *Department of Chemical Engineering, Michigan Technological University, Houghton, MI*.  
[www.chem.mtu.edu/~fmorriso/DataCorrelationForSphereDrag2013.pdf](http://www.chem.mtu.edu/~fmorriso/DataCorrelationForSphereDrag2013.pdf).
- Nezu, I. and Sanjou, M. 2011. PIV and PTV Measurements in Hydro-Sciences with Focus on Turbulent Open-Channel Flows. *Journal of hydro-environment research* **5** (4): 215-230.
- Nobbs, D., Tang, P. and Raper, J.A. 2002. The Design, Construction and Commissioning of a Low-Cost Optical Particle Size Analyser Specifically for Measurement of Settling Velocities and Size of Flocs (in English). *Measurement Science and Technology* **13**: 297-302.
- Peden, J.M. and Luo, Y. 1987. Settling Velocity of Various Shaped Particles in Drilling and Fracturing Fluids. *SPE Drilling Engineering* **2** (04): 337-343.
- Pimentel, R.G. 2006. *Measurement and Predictions of Droplet Size Distributions in Sprays*. PhD Thesis, University Laval, Quebec.
- Prakash, S. 1983. Experimental Evaluation of Terminal Velocity in Non-Newtonian Fluids in the Turbulent Region. *Chem. Eng* **25**: 1-4.
- Raffel, M., Willert, C.E., Wereley, S.T. and Kompenhans, J. 2007. *Particle Image Velocimetry: A Practical Guide*, 2nd edition, Berlin Heidelberg: Springer (Reprint).

- Remondino, F. and Fraser, C. 2006. Digital Camera Calibration Methods: Considerations and Comparisons. *International Archives of Photogrammetry, Remote Sensing and Spatial Information Sciences* **36** (5): 266-272.
- RheoSense. 2017. Viscosity of Newtonian and Non-Newtonian Fluids, <http://www.rheosense.com/applications/viscosity/newtonian-non-newtonian> (downloaded 20th June 2017).
- Rouse Jr, P.E. 1953. A Theory of the Linear Viscoelastic Properties of Dilute Solutions of Coiling Polymers. *The Journal of Chemical Physics* **21** (7): 1272-1280. <http://dx.doi.org/10.1063/1.1699180>.
- Settles, G.S. 2001. Shadowgraph Techniques. In *Schlieren and Shadowgraph Techniques: Visualizing Phenomena in Transparent Media*, Chap. 6, 143-163. Berlin, Heidelberg: Springer Berlin Heidelberg.
- Shah, S.N., El Fadili, Y. and Chhabra, R.P. 2007. New Model for Single Spherical Particle Settling Velocity in Power Law (Visco-Inelastic) Fluids. *International Journal of Multiphase Flow* **33** (1): 51-66. <http://dx.doi.org/10.1016/j.ijmultiphaseflow.2006.06.006>.
- Shahi, S. 2014. *An Experimental Investigation of Settling Velocity of Spherical and Industrial Sand Particles in Newtonian and Non Newtonian Fluids Using Particle Image Shadowgraph*. Master of Science Thesis, University of Alberta Edmonton, Canada (23rd June 2014).
- Shahi, S. and Kuru, E. 2015. An Experimental Investigation of Settling Velocity of Natural Sands in Water Using Particle Image Shadowgraph. *Powder Technology* **281**: 184-192. <http://dx.doi.org/10.1016/j.powtec.2015.04.065>.
- Shahi, S. and Kuru, E. 2016. Experimental Investigation of the Settling Velocity of Spherical Particles in Power-Law Fluids Using Particle Image Shadowgraph Technique.

- International Journal of Mineral Processing* **153**: 60-65.  
<http://dx.doi.org/10.1016/j.minpro.2016.06.002>.
- Shaw, M.T. and Tuminello, W.H. 1994. A Closer Look at the MWD-Viscosity Transform.  
*Polymer Engineering & Science* **34** (2): 159-165.  
<http://dx.doi.org/10.1002/pen.760340213>.
- Sigli, D. and Coutanceau, M. 1977. Effect of Finite Boundaries on the Slow Laminar Isothermal Flow of a Viscoelastic Fluid around a Spherical Obstacle. *Journal of Non-Newtonian Fluid Mechanics* **2** (1): 1-21. [http://dx.doi.org/10.1016/0377-0257\(77\)80029-3](http://dx.doi.org/10.1016/0377-0257(77)80029-3).
- Sisko, A. 1958. The Flow of Lubricating Greases. *Industrial & Engineering Chemistry* **50** (12): 1789-1792.
- Solomon, M. and Muller, S. 1996. Flow Past a Sphere in Polystyrene-Based Boger Fluids: The Effect on the Drag Coefficient of Finite Extensibility, Solvent Quality and Polymer Molecular Weight. *Journal of Non-Newtonian Fluid Mechanics* **62** (1): 81-94.  
[https://doi.org/10.1016/0377-0257\(95\)01398-9](https://doi.org/10.1016/0377-0257(95)01398-9).
- SoloPIV. 2003. Nd:Yag Laser System Operator's Manual.
- Sorbie, K.S. 1991. *Polymer-Improved Oil Recovery*, Glasgow: Blackie and Son Ltd (Reprint).
- Spectral Instruments, Inc. What Is a CCD?, [http://www.specinst.com/What\\_Is\\_A\\_CCD.html](http://www.specinst.com/What_Is_A_CCD.html) (accessed on 28th June 2017).
- Stokes, G.G. 1851. *On the Effect of the Internal Friction of Fluids on the Motion of Pendulums*: Pitt Press (Reprint).
- Sunthar, P. 2010. Polymer Rheology. In *Rheology of Complex Fluids*, 171-191. Springer New York.

- Tang, P., Greenwood, J. and Raper, J.A. 2002. A Model to Describe the Settling Behavior of Fractal Aggregates. *Journal of Colloid and Interface Science* **247** (1): 210-219. <http://dx.doi.org/10.1006/jcis.2001.8028>.
- Tirtaatmadja, V., Uhlherr, P.H.T. and Sridhar, T. 1990. Creeping Motion of Spheres in Fluid M1. *Journal of Non-Newtonian Fluid Mechanics* **35** (2): 327-337. [http://dx.doi.org/10.1016/0377-0257\(90\)85057-6](http://dx.doi.org/10.1016/0377-0257(90)85057-6).
- Turton, R. and Levenspiel, O. 1986. A Short Note on the Drag Correlation for Spheres. *Powder Technology* **47** (1): 83-86. [http://dx.doi.org/10.1016/0032-5910\(86\)80012-2](http://dx.doi.org/10.1016/0032-5910(86)80012-2).
- Urbissinova, T. 2010. *Experimental Investigation of the Effect of Elasticity on the Sweep Efficiency in Viscoelastic Polymer Flooding Operations*. Masters Thesis, University of Alberta, Edmonton, Canada (Fall 2010).
- Urbissinova, T.S., Trivedi, J. and Kuru, E. 2010. Effect of Elasticity During Viscoelastic Polymer Flooding: A Possible Mechanism of Increasing the Sweep Efficiency. *Journal of Canadian Petroleum Technology* **49** (12): 49-56. SPE-133471-PA. <http://dx.doi.org/10.2118/133471-PA>.
- Van den Brule, B.H.A.A. and Gheissary, G. 1993. Effects of Fluid Elasticity on the Static and Dynamic Settling of a Spherical Particle. *Journal of Non-Newtonian Fluid Mechanics* **49** (1): 123-132. [http://dx.doi.org/10.1016/0377-0257\(93\)85026-7](http://dx.doi.org/10.1016/0377-0257(93)85026-7).
- Veerabhadrapa, S.K. 2012. *Study of Effects of Polymer Elasticity on Enhanced Oil Recovery by Core Flooding and Visualization Experiments*. Masters Thesis, University of Alberta, Edmonton, Canada (Fall 2012).

- Veerabhadrapa, S.K., Doda, A., Trivedi, J.J. and Kuru, E. 2013. On the Effect of Polymer Elasticity on Secondary and Tertiary Oil Recovery. *Industrial & Engineering Chemistry Research* **52** (51): 18421-18428. <http://dx.doi.org/10.1021/ie4026456>.
- Veerabhadrapa, S.K., Trivedi, J.J. and Kuru, E. 2013. Visual Confirmation of the Elasticity Dependence of Unstable Secondary Polymer Floods. *Industrial & Engineering Chemistry Research* **52** (18): 6234-6241. <http://dx.doi.org/10.1021/ie303241b>.
- Walters, K. and Tanner, R. 1992. The Motion of a Sphere through an Elastic Fluid. In *Transport Processes in Bubbles, Drops and Particles*, ed. Chhabra, R. and De Kee, D., Chap. 3. New York: Hemisphere.
- WEE-Solve. 2017. Oscillatory Test: Frequency Sweep, <http://www.wee-solve.de/en/frequency-sweep.html> (downloaded 20th June 2017).
- Wieneke, B. 2005. Stereo-PIV Using Self-Calibration on Particle Images. *Experiments in Fluids* **39** (2): 267-280. <http://dx.doi.org/10.1007/s00348-005-0962-z>.
- Wilton, R.R. 2015. *Rheology and Flow Behaviour of Non-Newtonian, Polymeric Fluids in Capillary and Porous Media: Aspects Related to Polymer Flooding for Enhanced Recovery of Heavy Oil*. PhD thesis, University of Regina, Regina, Saskatchewan (Dec 2015).
- Wulf, K. 1987. Fließverhalten Von Stoffen Und Stoffgemischen. Hg. Von W.-M. Kulicke. Isbn 3-85738-115-4. Basel/Heidelberg/New York: Hüthig Und Wepf Verlag 1986. 487 S., Geb. Dm 168,-. *Acta Polymerica* **38** (8): 507-507. <http://dx.doi.org/10.1002/actp.1987.010380817>.

- Yamanaka, A., Yuki, T. and Mitsuishi, N. 1976. Drag Coefficient of a Moving Sphere in Viscoelastic Fluids. *KAGAKU KOGAKU RONBUNSHU* **2** (3): 222-227.  
<http://dx.doi.org/10.1252/kakoronbunshu.2.222>.
- Zang, Y.H., Muller, R. and Froelich, D. 1987. Influence of Molecular Weight Distribution on Viscoelastic Constants of Polymer Melts in the Terminal Zone. New Blending Law and Comparison with Experimental Data. *Polymer* **28** (9): 1577-1582.  
[http://dx.doi.org/10.1016/0032-3861\(87\)90362-4](http://dx.doi.org/10.1016/0032-3861(87)90362-4).
- Zheng, R., Phan-Thien, N. and Tanner, R.I. 1991. The Flow Past a Sphere in a Cylindrical Tube: Effects of Inertia, Shear-Thinning and Elasticity. *Rheologica Acta* **30** (6): 499-510.  
<http://dx.doi.org/10.1007/bf00444368>.
- Zimm, B.H. 1956. Dynamics of Polymer Molecules in Dilute Solution: Viscoelasticity, Flow Birefringence and Dielectric Loss. *The Journal of Chemical Physics* **24** (2): 269-278.  
<http://dx.doi.org/10.1063/1.1742462>.